THE GEOLOGICAL SOCIETY OF AMERICA®

Multicyclic Phanerozoic orogeny recorded in the Qaidam continent, northern Tibet: Implications for the tectonic evolution of the Tethyan orogenic system

Chen Wu[1,†], Yonghui Zhao[1,2], Jie Li[3], Wenyou Liu[4], Andrew V. Zuza[5], Peter J. Haproff[6], and Lin Ding[1]

[1]*State Key Laboratory of Tibetan Plateau Earth System and Resources Environment (TPESRE), Institute of Tibetan Plateau Research, Chinese Academy of Sciences, Beijing 100101, China*

[2]*University of Chinese Academy of Sciences, Beijing 100049, China*

[3]*Chongqing Key Laboratory of Complex Oil and Gas Field Exploration and Development, Chongqing University of Science and Technology, Chongqing 401331, China*

[4]*School of Earth Sciences and Resources, China University of Geosciences (Beijing), Beijing 100083, China*

[5]*Nevada Bureau of Mines and Geology, Nevada Geosciences, University of Nevada, Reno, Nevada 89557, USA*

[6]*Department of Earth and Ocean Sciences, University of North Carolina, Wilmington, North Carolina 28403, USA*

ABSTRACT

The growth and evolution of the Eurasian continent involved the progressive closure of major ocean basins during the Phanerozoic, including the Tethyan and Paleo-Asian oceanic realms. Unraveling this complicated history requires interpreting multiple overprinted episodes of subduction-related magmatism and collisional orogeny, the products of which were later affected by the Cenozoic construction of the Himalayan-Tibetan orogen due to the India-Asia collision. In particular, the tectonic evolution of northern Tibet surrounding the Cenozoic Qaidam Basin is poorly resolved due to several phases of Phanerozoic orogeny that have been reactivated during the Cenozoic deformation. In this study, we investigated the geology of the northern Qaidam continent, which experienced Paleozoic–Mesozoic tectonic activity associated with the development of the Eastern Kunlun orogen to the south and the Qilian orogen to the north. We combined new and published field observations, geochronologic and thermochronologic ages, and geochemical data to construct regional tectonostratigraphic sections and bracket phases of Paleozoic–Mesozoic magmatism associated with oceanic subduction and continental collision. Results suggest that the Qaidam continent experienced two major phases of subduction magmatism and collision. First, a Cambrian–Ordovician magmatic arc developed in the northern Qaidam continent due to south-dipping subduction. This phase was followed by the closure of the Qilian Ocean and the collision of the North China craton and Qaidam continent, resulting in Silurian–Devonian orogeny and the development of a regional unconformity across northern Tibet. A subsequent Permian–Triassic magmatic arc developed across the northern Qaidam continent due to north-dipping subduction. This phase was followed by the closure of the Neo-Kunlun Ocean and the collision of the Songpan Ganzi terrane in the south and Qaidam continent. These interpretations are incorporated into a new and comprehensive model for the Phanerozoic formation of northern Tibet and the Eurasia continent.

1. INTRODUCTION

Eurasia is the only major continent assembled during the Phanerozoic (e.g., Şengör and Natal'in, 1996; Yin and Nie, 1996), and understanding its formation and evolution greatly impacts our knowledge of continental tectonics and crustal growth (e.g., Molnar, 1988; Scotese and McKerrow, 1990; Yin and Nie, 1996; Şengör and Natal'in, 1996; Yin and Harrison, 2000; Wu et al., 2016). The construction of Eurasia was accomplished by several continental collisions associated with the closure of the Paleo-Asian and Tethyan oceanic domains in north-central and southern Asia, respectively (e.g., Zonenshain et al., 1990; Yin and Nie, 1996; Şengör and Natal'in, 1996; Şengör et al., 1988; Heubeck, 2001; Badarch et al., 2002; Stampfli and Borel, 2002; Biske and Seltmann, 2010; Dong et al., 2018; Wu et al., 2016; Zuza and Yin, 2017; Li et al., 2018; Allen et al., 2023). A key region of the Eurasian continent is northern Tibet (Fig. 1), which is composed of several orogenic belts that formed via repeated episodes of ocean closure, craton/terrane collision, and intracontinental deformation spanning the development of the early Neoproterozoic Rodinia supercontinent to the Cenozoic Tibetan Plateau (e.g., Xiao et al., 2009; Pan et al., 2012; Song et al., 2013, 2014a; Wu et al., 2016, 2021; Zhang et al., 2019b; Zuza et al., 2018; Yin et al., 2007a, 2008a, 2008b).

Northern Tibet is located at the junction of multiple continental blocks (Fig. 1), making the region ideal for examining orogenic and mountain-building processes. Northern Tibet experienced a protracted tectonic history that spans early Neoproterozoic subduction and late Neoproterozoic continental rifting, Paleozoic–early Mesozoic subduction and continental collision, Mesozoic extension, and Cenozoic intracontinental deformation related to the India-Asia collision (e.g., Hsü et al., 1995; Yin and Harrison, 2000; Sun et al., 2006, 2022; Xiao et al., 2009; Song et al., 2013, 2014a; Wu et al., 2016; Zhang et al., 2019b; Zuza et al., 2018; Yin et al., 2007a, 2008a, 2008b; Yin, 2010; Qian et al., 2021a). Continental blocks within northern Tibet are bounded by suture zones that contain dismembered ophiolitic mélanges and marine sedimentary sequences. These suture zones have been overprinted by younger deformation (Fig. 1;

Chen Wu https://orcid.org/0000-0003-0647-3530

[†]wuchen@itpcas.ac.cn

GSA Bulletin; March/April 2025; v. 137; no. 3/4; p. 1553–1581; https://doi.org/10.1130/B37906.1.
Published online 30 October 2024

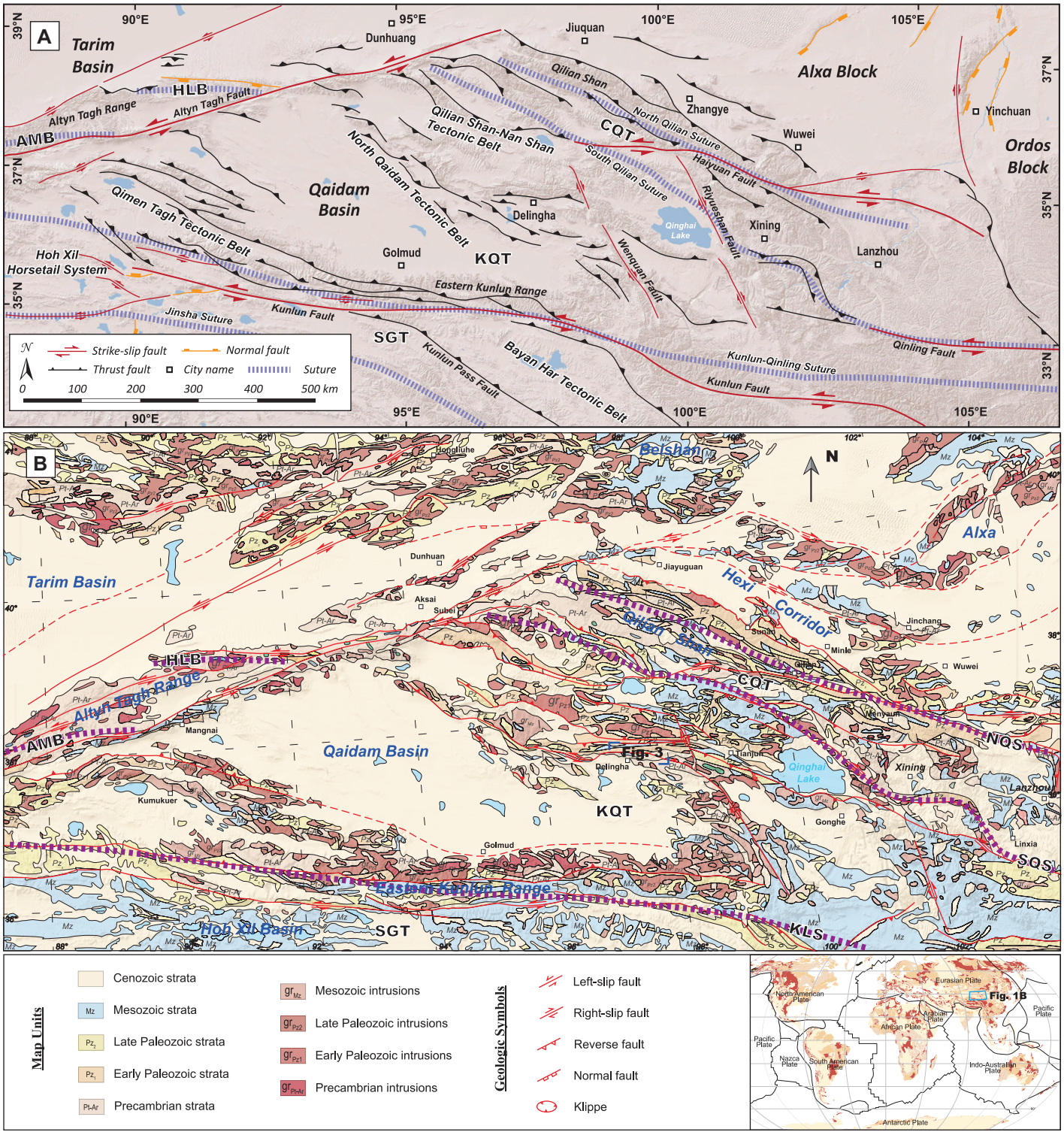

Figure 1. (A) Tectonic map of northern Tibet showing major tectonic units, suture zones, and Cenozoic structures based on Yin and Harrison (2000), Wu et al. (2016, 2020, 2022a), and Zuza et al. (2018). (B) Simplified geologic map of northern Tibet modified from Pan et al. (2004), Wang et al. (2013), and this study. The location of Figure 3 in the southern Zongwulong Shan is shown. Bottom-right inset shows the location of Figure 1B in the context of the globe. KLS—Kunlun suture; SQS—South Qilian suture; NQS—North Qilian suture; HLB—Hongliugou-Lapeiquan ophiolitic mélange belt; AMB—Apa-Mangai ophiolitic mélange belt; SGT—Songpan-Ganzi terrane; KQT—Kunlun-Qaidam terrane; CQT—Central Qilian terrane.

e.g., Yin and Harrison, 2000; Yang et al., 1996; Yin et al., 2007b; Li et al., 2024; Wu et al., 2016; Zuza et al., 2018; Zuza and Yin, 2017; Song et al., 2019; Allen et al., 2023).

The Qaidam continent of northern Tibet mainly consists of Precambrian basement metamorphic rocks, early Paleozoic magmatic arc rocks, late Paleozoic–Mesozoic shallow-marine limestone, and clastic and volcanic rocks, mostly exposed along the margins of the present-day Qaidam Basin (Fig. 1; e.g., Yin et al., 2007a, 2007b, 2008a, 2008b; Chen et al., 2012b, 2015; Wu et al., 2016; Zhang et al., 2019b; Qian et al., 2021a; Sun et al., 2022). The northern portion of the Qaidam continent is composed of Precambrian basement metamorphic rocks, Cambrian shallow-marine strata, and Ordovician–Silurian magmatic arc rocks (Fig. 1; e.g., Yin and Harrison, 2000; Pan et al., 2004, 2012; Lu et al., 2002; Wu et al., 2016; Sun et al., 2022). The southern portion of the Qaidam continent is best exposed in the Eastern Kunlun Range, which is bounded by the present-day Qaidam Basin in the north and the active left-slip Kunlun fault in the south, the latter of which follows the Triassic Anyimaqen-Kunlun-Muztagh suture zone (Fig. 1; e.g., Jiang et al., 1992; Yang et al., 1996; Yin and Harrison, 2000; Yin et al., 2008a, 2008b; Wu et al., 2016, 2019a; Dong et al., 2018). End-member models for the tectonic development of the Eastern Kunlun orogen and Qilian orogen to the north (Fig. 1) differ primarily based on their numbers of magmatic arcs and the basement rocks upon which the arc(s) was (were) constructed, in addition to subduction polarities, timings of collision, and processes responsible for ultrahigh-pressure metamorphism and exhumation (e.g., Wu et al., 2016; Zuza et al., 2018; Allen et al., 2023). The role the Qaidam continent played during the evolution of northern Tibet remains controversial.

In this contribution, we investigated the Phanerozoic tectonic evolution of northern Tibet recorded in the Qaidam continent, located at the intersection of the Kunlun-Qaidam-Qilian, Tarim–North China, and Songpan-Ganzi continents, based on new and existing field observations, geochronologic and thermochronologic results, and geochemical data. Our findings allowed us to construct regional tectonostratigraphic sections, assign detrital provenance, and constrain the spatial and temporal extents of arc magmatism associated with Paleozoic Wilson cycles and Mesozoic–Cenozoic intracontinental deformation. This work provides a new, comprehensive view of the Phanerozoic formation of northern Tibet and Eurasia.

2. PHANEROZOIC OROGENS OF NORTHERN TIBET

2.1. Early Paleozoic Qilian Orogen

The early Paleozoic Qilian orogen, exposed in the Qilian Shan, contains several subparallel ophiolitic mélange belts of the North and South Qilian suture zones located between the Qaidam continent in the south and the combined North Tarim–North China craton in the north (Fig. 1A; e.g., Xiao et al., 2009; Song et al., 2013; Zuza and Yin, 2017; Wu et al., 2016; Allen et al., 2023). In general, the primary tectonic domains of the early Paleozoic Qilian orogen from north to south consist of (1) the southern margin of the North China craton, including Paleoproterozoic basement metamorphic rocks overlain by Mesoproterozoic sedimentary rocks and Neoproterozoic passive-margin strata and postcollisional intrusions; (2) the North Qilian suture zone, composed of discontinuously exposed, blueschist-facies ophiolitic rocks; (3) the Central Qilian terrane, composed of Precambrian basement rocks and early Neoproterozoic plutons (ca. 1100–900 Ma); (4) the South Qilian suture zone (i.e., Danghe Nanshan–Laji Shan ophiolitic mélange), composed of weakly metamorphosed ophiolitic rocks; (5) widely exposed Qilian volcanic and magmatic arc rocks, which overlie and/or intrude amphibolite-facies rocks; and (6) the northern Qaidam continent, composed of ultrahigh-pressure metamorphic rocks and the Zongwulong ophiolitic complex (Fig. 1B; e.g., Yin and Harrison, 2000; Pan et al., 2004, 2012; Zuza et al., 2018; Wu et al., 2022a).

The key reported geologic relationships and geochronologic ages of the North, Central, and South Qilian Shan are summarized in four simplified tectonostratigraphic columns and regional-scale geologic maps in Figure 2 (Wu et al., 2022a). Here, we summarize the tectonostratigraphic evolution of the early Paleozoic Qilian orogen based on its major divisions, including the North Qilian orogen, Central Qilian terrane, South Qilian orogen, and North Qaidam tectonic zone or metamorphic belt (Fig. 2).

The North Qilian orogen consists of Paleoproterozoic (ca. 2300–1800 Ma) basement metamorphic rocks, which are overlain by Mesoproterozoic sedimentary rocks along an unconformity. Paleoproterozoic rocks experienced amphibolite-facies regional metamorphism. In contrast, the Mesoproterozoic sedimentary rocks consist of weakly metamorphosed siliciclastic and carbonate rocks. Neoproterozoic passive-margin strata consist of rift-related siliciclastic rocks, limestone, mafic rocks, and glacial deposits, which are intruded by postorogenic early Paleozoic granitoids (Fig. 2A). Cambrian–Ordovician marine strata of the North Qilian orogen probably represent a complex mélange of forearc, accretionary wedge, and foreland basin strata. Silurian strata are considered to have been deposited in a flysch basin that transitions into molasse (Fig. 2). The North Qilian suture zone contains discontinuously exposed, ophiolitic rocks that locally experienced blueschist-facies metamorphism. These ophiolitic rocks include the ca. 490–445 Ma back-arc Sunan-Laohushan ophiolitic mélange and the ca. 517–487 Ma forearc Yushigou-Yieniugou-Qingshuigou ophiolitic mélange located north of the Tuolai Shan (e.g., Shi et al., 2004; Song et al., 2013, 2019; Fu et al., 2020a, 2020b). The oldest ophiolites representing the North Qilian oceanic crust are ca. 550 Ma (e.g., Shi et al., 2004). Silurian and Devonian strata are divided by a regional unconformity marked by conglomerate (Fig. 2A). Carboniferous strata overlie early Paleozoic rocks along a regional angular unconformity, which was deformed along shaley coal-bearing shale beds (Fig. 2A). Carboniferous and early Paleozoic rocks are overlain by Triassic strata. Overlying Jurassic strata are generally parallel to Triassic strata along a regional disconformity (Fig. 2A). Cretaceous strata are widespread in the North Qilian orogen and consist of polymictic conglomerate and red-colored, coarse-grained sandstone (Fig. 2A; Wu et al., 2021; Wang et al., 2022). Sandstone beds commonly exhibit growth strata and are interpreted to have been deposited in extensional basins (Wang et al., 2022). Cenozoic rocks are predominantly Miocene–Pliocene and consist of red-colored, gypsum-bearing fluvial and lacustrine strata (Wu et al., 2017, 2021; Zuza et al., 2018; Wang et al., 2022). Quaternary rocks consist of alluvial, fluvial, and glaciofluvial strata (Wu et al., 2017; Zuza et al., 2018).

The oldest basement metamorphic rocks exposed in the Central Qilian terrane are gneisses, dolomitic schists, marbles, and amphibolites of the Tuolai and Huangyuan Groups, which are mainly exposed in the Tuolai Mountains, Tuolai Nanshan Mountains, and Huangyuan region (Wu et al., 2017; Liu et al., 2018; Zuza et al., 2018). These rocks have been interpreted as part of a Proterozoic passive margin (Gehrels et al., 2003a, 2003b, 2011; Wu et al., 2017). The metasedimentary portion of the Tuolai and Huangyuan Groups yielded ca. 1800 Ma detrital zircon ages (Tung et al., 2007), and it has been interpreted to have been deposited in a passive-margin (Tung et al., 2007) or magmatic arc setting (Wan et al., 2001; Smith, 2006). Zuza et al. (2018) reported that the three youngest zircon grains from a biotite-plagioclase paragneiss of the Tuolai Group gave a weighted

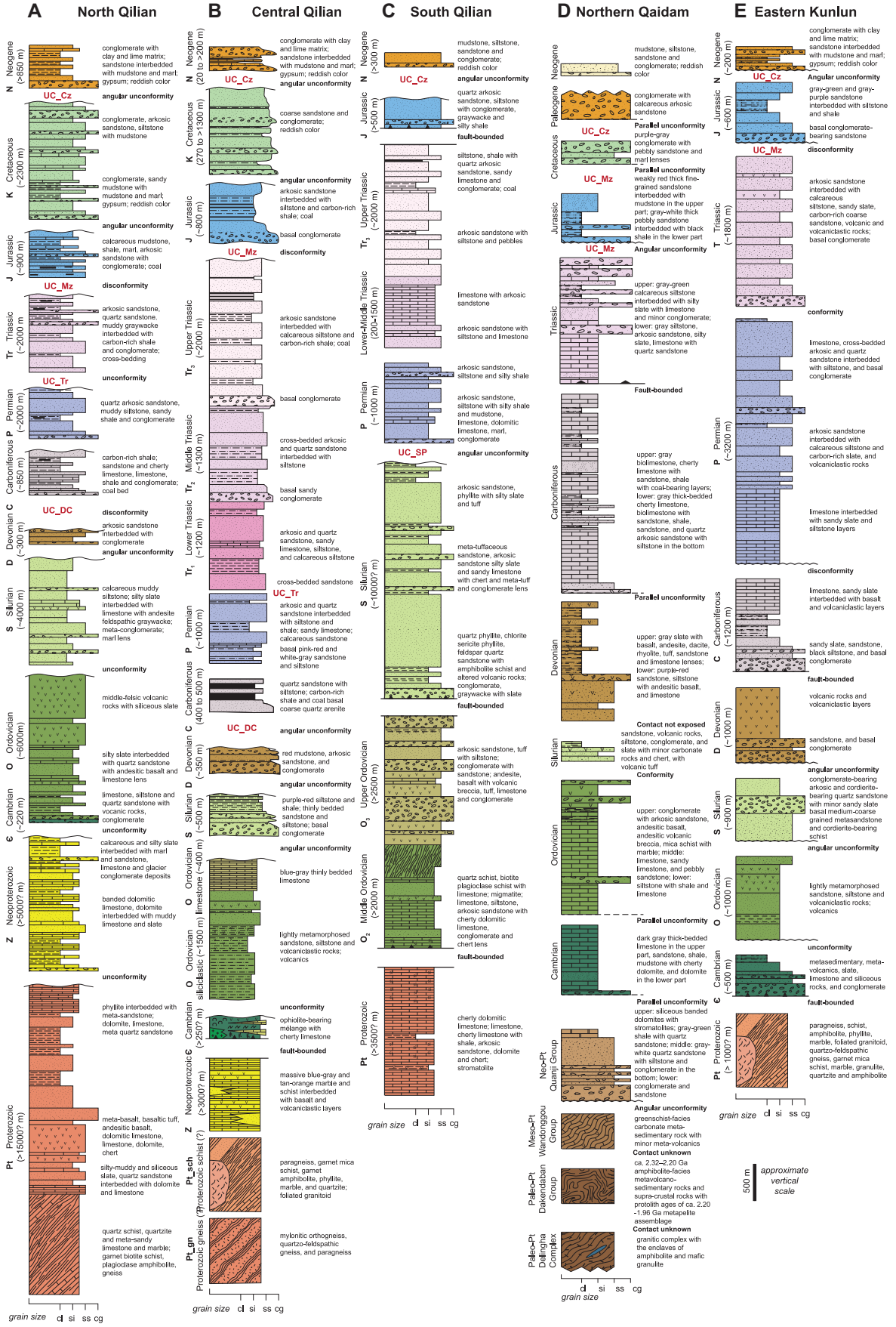

Figure 2. Lithostratigraphy of the (A) North, (B) Central, and (C) South Qilian Shan, (D) northern Qaidam, and (E) Eastern Kunlun Range, northern Tibet. Ages are compiled from Qinghai BGMR (1997), Pan et al. (2004), Wang et al. (2013), Wu et al. (2022a), and this study. cl—clay; si—silt; ss—sand cg—conglomerate; Pt—Proterozoic.

mean age of ca. 1500 Ma, which reflects deposition in the Mesoproterozoic. Basement rocks of the Central Qilian terrane are overlain by massive limestone and dolostone of the Tuolai Nanshan Group, which have been commonly metamorphosed to marble and are interbedded with low-grade meta-basalt and meta-volcaniclastic layers (Fig. 2B). The regional geologic map of Pan et al. (2004) assigned a Changchengian age for this unit (i.e., Paleoproterozoic or Mesoproterozoic) based on an older regional geologic survey (Gansu Bureau of Geology and Mineral Resources, 1974). However, Wu et al. (2017) and Zuza et al. (2018) reassigned a Neoproterozoic age for this unit based on more recent geochronology of widespread meta-basalt (zircon U-Pb ages of ca. 600–580 Ma; Xu et al., 2015) interbedded with carbonate strata (Mao et al., 1998; Xia et al., 1999).

Cambrian strata are sporadically exposed in the Datong region of the Central Qilian terrane and mainly consist of limestone and slate with basic volcanic rocks (Fig. 2B). Ordovician strata consist of low-grade meta-sandstone, meta-siltstone, and meta-limestone with minor metavolcanic and meta-volcaniclastic rocks (Fig. 2B; Zuza et al., 2018). Lowermost Ordovician strata are intruded by granitoids and intermediate to mafic dikes (Fig. 2B). Ordovician strata are variably deformed, and their original sedimentary structures are obscured (Zuza et al., 2018; Wu et al., 2024). Silurian strata in the Central Qilian terrane are a widely distributed, thick sequence of continental-margin clastic rocks, which unconformably overlie Ordovician strata and often form isoclinal folds with transposed bedding (Fig. 2B). Silurian strata include flysch that transitions upward to molasse (Du et al., 2003).

Devonian strata are mostly absent from the Central Qilian terrane except for sporadic outcrops in the north and south. There, Devonian strata unconformably overlie deformed Proterozoic–early Paleozoic strata and are disconformably overlain by younger strata (Fig. 2B; Wu et al., 2022a). The Devonian sequence does not exceed ~300 m in thickness and consists of terrestrial conglomerate, sandstone, mudstone, and minor volcanic rocks (Qinghai BGMR, 1991). This sequence is interpreted to be molasse deposited in intermontane and/or foreland basins during the Qilian orogeny (e.g., Xia et al., 2003; Yan et al., 2007).

Carboniferous strata overlie Ordovician–Devonian strata and other nonsedimentary rocks along a regional angular unconformity. Carboniferous strata consist of quartz sandstone, siltstone, shale, and sandy limestone interbedded with coal and gypsum beds (Fig. 2B; Zuza et al., 2018). The Lower Permian section of the Central Qilian terrane consists of distinctive pink-red– and white-gray–colored, coarse-grained sandstone and siltstone. The Upper Permian section is composed of arkosic and quartz sandstone interbedded with siltstone and shale and sandy limestone (Fig. 2B; Zuza et al., 2018). The conformably overlying Triassic section is >4 km thick and divided into Lower, Middle, and Upper Triassic sections. The Lower Triassic section consists of massive, cross-bedded, gray-colored sandstone overlain by arkosic and quartz sandstone, sandy limestone, siltstone, and calcareous siltstone (Fig. 2B; Zuza et al., 2018). The Middle Triassic section is dominated by sandy conglomerate at its base and overlying cross-bedded arkosic and quartz sandstone with minor siltstone. The Upper Triassic section consists of a basal conglomerate and overlying arkosic sandstone interbedded with calcareous siltstone, organic-rich shale, and distinctive coal layers. Overlying Jurassic strata are generally parallel to Upper Triassic strata along a regional disconformity (Fig. 2B; Yin et al., 2008b). Jurassic strata are ~800 m thick and consist of a basal conglomerate overlain by arkosic sandstone interbedded with siltstone, organic-rich shale, and numerous coal beds. Jurassic strata are generally restricted to valleys in the central Qilian Shan (Fig. 2B; Zuza et al., 2018). Cretaceous strata consist of polymictic conglomerate and red-colored, coarse-grained sandstone (Wu et al., 2021; Wang et al., 2022) exposed on both sides of the Tuo Lai Shan. Map-view relationships require the Cretaceous section to be >270 m thick (Fig. 2B). In the Hexi Corridor, the Cretaceous section is >3 km thick (Zhiyi and Dean, 1996; Zuza et al., 2016; Wang et al., 2022). These strata often exhibit growth strata and are interpreted to have been deposited in an extensional setting (Yin et al., 2008b). Cenozoic strata are predominantly Miocene–Pliocene (Qinghai BGMR, 1991; Zhiyi and Dean, 1996; Bovet et al., 2009), although the southernmost strata may be Oligocene (e.g., Zhuang et al., 2011). Cenozoic strata consist of red-colored fluvial and lacustrine strata and conglomerate, sandstone, and mudstone. These strata have a clay, marl, or limestone matrix, and gypsum layers are prevalent (Fig. 2B; Wu et al., 2021; Wang et al., 2022). Quaternary rocks consist of alluvial, fluvial, and glaciofluvial strata (Li and Yang, 1998), which are distinguished in the central Qilian Shan as active axial river deposits, active alluvial deposits, and inactive alluvial deposits (Wu et al., 2017; Zuza et al., 2018).

The South Qilian orogen is bounded by the Central Qilian terrane to the north and Qaidam Basin to the south along the Southern Central Qilian fault and Northern Qaidam fault, respectively (Fig. 1). Basement metamorphic rocks of the South Qilian orogen (i.e., Neoproterozoic Hualong Group/Complex) are only exposed at its eastern end and consist of mafic to felsic plutons, chert, and turbiditic strata, some of which experienced amphibolite-facies metamorphism (Fig. 2C; e.g., Yan et al., 2015). The Cambrian Lajishan ophiolite complex is exposed along the southern margin of the South Qilian Shan (Fig. 2C; e.g., Fu et al., 2018, 2022a). The oldest sedimentary rocks of the South Qilian orogen are a >4-km-thick section of Ordovician pyroclastic rocks and volcanic rocks, which are mainly distributed near the bounding faults (Fig. 2C; Yang, 1983). Overlying Silurian phyllite, sandstone, and slate are widely distributed in the South Qilian orogen (Fig. 2C; Xie et al., 2014) and interpreted to be marine flysch deposits (Xu et al., 2006; Song et al., 2013). Devonian strata are generally absent in the South Qilian orogen. Minor Carboniferous strata occur along the northern margin of the South Qilian orogen. The Lower Carboniferous section consists of a basal conglomerate and sandstone. The Upper Carboniferous section is composed of feldspar quartz sandstone (Fig. 2C; Yan et al., 2019). Carboniferous strata exposed in the Zongwulong Shan along the southern margin of South Qilian orogen are mainly composed of marine volcanic sedimentary rocks with thin siliceous beds (Guo et al., 2009). Overlying Permian rocks are composed of clastic and carbonate strata. Triassic rocks consist of clastic and carbonate strata interbedded with lacustrine carbonaceous shale and coal beds (Fig. 2C; e.g., Yan et al., 2019; Fu et al., 2022a). Jurassic continental, coal-bearing strata and Cenozoic clastic strata occur in the South Qilian orogen (e.g., Yan et al., 2019).

2.2. Altyn Tagh Orogen

The Altyn Tagh orogen is exposed in the ~600-km-long northeast-trending Altyn-Tagh Range, located between the Tarim Basin to the

west and Qaidam Basin and Kunlun Range to the east (Fig. 1). The main tectonic units of the Altyn Tagh orogen from north to south include (1) Archean basement metamorphic rocks, which are commonly combined with an Archean–Paleoproterozoic complex of the northern Altyn-Tagh Range; (2) the early–middle Cambrian to early Silurian Hongliugou-Lapeiquan ophiolitic mélange, which is bounded by Archean basement metamorphic rocks to the north and Mesoproterozoic to Neoproterozoic rocks to the south; (3) Mesoproterozoic to Neoproterozoic, stromatolite-bearing quartzite and cherty limestone exposed in the central and eastern Altyn Tagh; and (4) the early Paleozoic Apa-Mangai ophiolitic mélange, which is mainly exposed in the southwestern Altyn Tagh and extending ~250–300 km west of Mangai to south of Qiemo (e.g., Xinjiang BGMR, 2003; Che and Sun, 1996; Liu et al., 1998; Cowgill et al., 2003; Chen et al., 2003; Zhang et al., 2005). The Archean basement rocks consist of ca. 2800–2500 Ma tonalite-trondhjemite-granodiorite, granulite, amphibolite, and paragneiss that experienced amphibolite-facies metamorphism (e.g., Zhang et al., 2011a; Long et al., 2014; Wang et al., 2020). These Archean rocks are considered to be the basement of the Tarim craton (Zhang et al., 2011a; Wang et al., 2020).

Early Paleozoic volcanic and marine sediments are exclusively exposed in the eastern Altyn-Tagh Range (Xinjiang BGMR, 1993; Cowgill et al., 2003; Chen et al., 2003) and are composed of the Ordovician Erantag and Huanxingshan Formations (Xinjiang BGMR, 2003). Jurassic coal-bearing terrestrial strata are widespread in the eastern Altyn-Tagh Range, whereas Cretaceous strata are only exposed along the southwestern edge of the range (Cowgill et al., 2003; Chen et al., 2003). The Hongliugou-Lapeiquan ophiolitic mélange is composed of ultramafic and mafic rocks, serpentinite, pillow lavas, plagiogranite, chert, and mafic dikes. These rocks yield enriched mid-ocean-ridge basalt (E-MORB)–type geochemistry and ca. 521–449 Ma ages (e.g., Liu et al., 1998, 2021; Zhang et al., 2005; Gao et al., 2011). The Apa-Mangai ophiolitic mélange mainly consists of serpentinite, gabbro, basalt, plagiogranite, diabase, and chert blocks (Zhang et al., 2009a) with ca. 510–445 Ma ages (e.g., Liu et al., 1998; Yao et al., 2021). These ophiolitic mélange rocks have been interpreted to have been generated in a continental rift (Ma et al., 2009; Guo et al., 2014), mid-ocean ridge (Liu et al., 1998; Zhang et al., 2009b; Liu et al., 2024a), or oceanic subduction zone (Yao et al., 2021).

Early Paleozoic granitoid plutons are exposed throughout the northern Altyn-Tagh Range. These plutons have ca. 500–405 Ma ages and are thought to have been emplaced during three distinct episodes: (1) ca. 500–480 Ma island-arc magmatism related to subduction (e.g., Qi et al., 2005; Wu et al., 2006b, 2009b; Kang et al., 2011); (2) ca. 475–445 Ma syncollisional magmatism (e.g., Wu et al., 2006b, 2009b; Hao et al., 2006), except for subduction-related emplacement of a ca. 443 Ma porphyritic granite pluton (Chen et al., 2003); and (3) ca. 435–405 Ma calc-alkaline magmatism related to postcollisional extension (e.g., Qi et al., 2005; Wu et al., 2006b, 2009b). Late Cambrian–Silurian granitic plutons (ca. 491–414 Ma) sporadically occur in the southern Altyn-Tagh Range (e.g., Xinjiang BGMR, 2003; Sobel and Arnaud, 1999; Cowgill et al., 2003; Gehrels et al., 2003a; Dong et al., 2011b). The reported absence of Neoproterozoic and late Paleozoic granitoids in the southern Altyn-Tagh Range is most likely the result of limited geologic studies.

2.3. Eastern Kunlun Orogen

The Eastern Kunlun orogen is exposed in the Eastern Kunlun Range, located between the Qaidam Basin to the north and active left-slip Kunlun fault to the south (Fig. 1). The Eastern Kunlun orogen mainly comprises three tectonic units from north to south: (1) Paleoproterozoic basement metamorphic rocks and Phanerozoic cover sequences along the southern margin of the Qaidam Basin; (2) a central zone of volcanic and plutonic rocks associated with the Kunlun magmatic arc(s) and intermittently exposed (ultra)mafic rocks and ophiolitic fragments that occur within Precambrian–early Paleozoic metamorphic complexes; and (3) the Triassic Anyimaqen-Kunlun-Muztagh suture zone, which separates the Kunlun magmatic arc(s) to the north and the South China craton and Songpan-Ganzi flysch complex to the south (e.g., Dewey et al., 1988; Yin and Harrison, 2000; Jiang et al., 1992; Yang et al., 1996; Konstantinovskaia et al., 2003; Bian et al., 2004; Ding et al., 2013; Wu et al., 2016, 2019a, 2022a; Tang et al., 2023). The Triassic Anyimaqen-Kunlun-Muztagh suture zone represents the northern margin of a triangular-shaped ocean basin situated between the composite Kunlun–Qaidam–North China craton to the north, South China block to the east, and Songpan-Ganzi and Qiangtang terranes to the southwest (Yin and Nie, 1996; Nie et al., 1994; Zhou and Graham, 1996; Yin and Harrison, 2000; She et al., 2006; Weislogel et al., 2006; Enkelmann et al., 2007; Weislogel, 2008).

The oldest metamorphosed basement rocks exposed in the Eastern Kunlun Range are gneiss, metavolcanics, and schist of the Paleoproterozoic Kuhai and Baishahe Groups (Fig. 2D). The gneiss unit is the oldest unit, and it is composed of quartzofeldspathic gneiss, mylonitic biotite orthogneiss with migmatite layers, and paragneiss. A ca. 1441 Ma fine-grained gneissic intrusion occurs within the Kuhai Group (Liu et al., 2005). The metavolcanic unit consists of metamorphosed (ultra)mafic rocks and foliated amphibolite. The schist unit is characterized by mica garnet schist, quartzite, and marble, and local dolomite/limestone, phyllite, and slate. The Mesoproterozoic Xiaomiao Formation, exposed along the southern margin of the Qaidam Basin, is composed of gneiss, quartz schist, marble, and plagioclase amphibolite (Fig. 2D). U-Pb detrital zircon ages of the Xiaomiao Formation suggest a ca. 1683–1554 Ma maximum depositional age (Chen et al., 2011). The oldest sedimentary strata exposed in the Eastern Kunlun Range are greenschist-facies, massive limestone, schistose quartz sandstone, and intermediate to basic volcanic rocks of the Neoproterozoic Wanbaogou Formation, which are thought to be a passive-margin sequence (Fig. 2D; Jiang et al., 1992; Wang et al., 2013). Neoproterozoic granite and mafic dikes intruded Proterozoic basement metamorphic rocks and experienced amphibolite- to granulite-facies metamorphism (e.g., Ren et al., 2010).

Precambrian metamorphic rocks of the Eastern Kunlun orogen are unconformably overlain by Cambrian–Ordovician, shallow- and deep-water marine sedimentary rocks (Fig. 2D). Cambrian strata are divided into a lower metavolcanic section and an upper metasedimentary section composed of quartz schist, biotite granulite, marble, limestone, and siliceous rocks (Fig. 2D). The Cambrian strata were deposited between ca. 533–526 Ma and ca. 443 Ma based on detrital zircon ages and an early Paleozoic intrusion (Wu et al., 2019a). The Ordovician–Silurian Naij Tal Group includes shallow- and deep-water marine clastic strata, carbonate, volcanic rocks, and volcaniclastic rocks (Wang et al., 2013), which may represent a magmatic arc sequence. Wu et al. (2019a) suggested that the deep-water marine clastic strata of the Naij Tal Group were deposited between ca. 447 Ma and 440 Ma, based on detrital zircon ages and intrusive relationships with Late Ordovician to early Silurian granitoids. The Silurian Saishenteng Formation conformably overlies these rocks and is dominated by basal medium- to coarse-grained, weakly metamorphosed sandstone and cordierite-bearing schist, meta-conglomerate, and meta-sandstone with minor sandy slate (Fig. 2D). The Devonian Maoniushan Formation overlies these rocks along an angular unconformity (Fig. 2D) and consists of gray-purple–colored, medium- to coarse-grained, massive conglomerate, sandstone, ca.

388–368 Ma andesite, trachyandesite, ca. 423–399 Ma dacite and rhyolite, and lava breccia (e.g., Qinghai BGMR, 1997; Feng et al., 2015; Lu et al., 2010; Zhang et al., 2010, 2019a; Xiang et al., 2014). Wu et al. (2019a) reported that the clastic strata of the Maoniushan Formation were deposited between ca. 393 Ma and 389 Ma, based on detrital zircon ages and an undeformed Devonian intrusion. Devonian strata only occur in the northeastern part of the Eastern Kunlun Range (Wang et al., 2013; Wu et al., 2016, 2019a). Overlying Carboniferous strata consist of basal sandy conglomerate overlain by arkosic sandstone, massive limestone interbedded with carbonaceous shale, and siltstone interbedded with volcanic rocks (Fig. 2D). Clastic strata contain dominantly volcanic and granitic gneiss clasts. Most of the mapped sedimentary sections are interpreted to be turbidite sequences with interfingering conglomerate beds. A ca. 357 Ma volcanic tuff occurs within the Lower Carboniferous section (Wu et al., 2020).

Lower to Middle Permian strata are dominated by basal breccia and massive limestone and do not exceed 1 km in total thickness (Fig. 2D). The overlying Permian Marerzheng Formation consists of basalt, arkosic and quartz sandstone, and sandy slate (e.g., Qinghai BGMR, 1997; Ren et al., 2012; Zhao et al., 2016). Conformably overlying these rocks, there are Triassic strata, which are mainly composed of synorogenic conglomerate and coarse-grained lithic sandstone interbedded with limestone (Fig. 2D; e.g., Ding et al., 2013; Wang et al., 2013; Wu et al., 2019a). Lower Triassic strata are composed of massive arkosic and quartz sandstone overlain by conglomerate-bearing sandstone and calcareous slate interbedded with limestone and siltstone. Middle Triassic strata are dominated by basal conglomerate-bearing sandstone interbedded with limestone, cross-bedded arkosic and quartz sandstone, and minor siltstone. Upper Triassic rocks consist of basal conglomerate and overlying arkosic sandstone interbedded with calcareous siltstone, andesite, and feldspar sandstone. Calc-alkaline volcanic rocks of island-arc affinity occur within the Upper Triassic strata. Triassic strata are unconformably overlain by Upper Jurassic terrestrial, coal-bearing strata (Fig. 2D; e.g., Ding et al., 2013; Tong et al., 2004; Wu et al., 2010, 2016). Jurassic strata consist of basal sandy conglomerate overlain by cross-bedded arkosic and quartz sandstone and minor siltstone and shale, darker organic-rich shale, and distinctive coal beds (Fig. 2D; Wu et al., 2019b). Lower Cretaceous strata are only exposed in the northeastern part of the Eastern Kunlun Range as a northwest-trending ribbon (Qinghai BGMR, 1997). These strata include basal sandy conglomerate and red-colored, cross-bedded, fine-grained sandstone and siltstone interbedded with silty mudstone (Fig. 2D; Qinghai BGMR, 1997; Wu et al., 2019b). Cenozoic terrestrial clastic sediments are predominantly Paleocene–Pliocene and have been dated via magnetostratigraphy, palynology, and detrital zircon U-Pb geochronology (e.g., Liu and Wang, 2001; Bush et al., 2016; Cheng et al., 2016; Wang et al., 2017; Wu et al., 2019b). These strata consist of red-colored fluvial and lacustrine sediments, including conglomerate, sandstone, and mudstone with a clay, marl, or limestone matrix (Fig. 2D; Wu et al., 2019b).

3. FIELD OBSERVATIONS AND SAMPLING OF THE NORTH QAIDAM CONTINENT

The northern Qaidam continent exposes the Precambrian Delingha complex and Dakendaban Group metamorphic rocks, overlain by Neoproterozoic–Cambrian strata, ultrahigh-pressure metamorphic rocks, and Ordovician–Silurian metagraywacke and metavolcanic rocks. Unmetamorphosed rocks include Devonian continental strata, Carboniferous shallow-marine strata, Permian–Triassic continental sedimentary and volcanic rocks, and Mesozoic–Cenozoic lacustrine and fluvial strata (Fig. 2E). Detailed structural mapping by Yin et al. (2007b) indicated that high-grade metamorphic rocks are located at different structural positions along a regional detachment fault. The original bedding of both the high-grade metamorphic rocks of the Dakendaban Group and Ordovician–Silurian metasedimentary rocks is transposed by younger cleavage and gneissic foliation associated with isoclinal folding. In contrast, Devonian and younger strata are devoid of ductile deformation (Fig. 2E). The North Qaidam ultrahigh-pressure metamorphic belt is located along the southernmost Qilian orogen, which is bounded in the north and south by a Cenozoic north-dipping thrust (Yin et al., 2007b; Menold et al., 2009). The ultrahigh-pressure metamorphic rocks are mostly garnet-bearing quartzofeldspathic gneisses with entrained eclogite and garnet peridotite blocks (e.g., Yang et al., 2001; Zhang et al., 2005; Xu et al., 2006; Song et al., 2004, 2014a; Yu et al., 2019a). The Zongwulong ophiolitic complex consists of serpentinized peridotite, gabbro, sheeted dikes, and basalt, all of which are penetratively deformed and experienced epidote-amphibolite–facies metamorphism (e.g., Guo et al., 2009; Fu et al., 2022a). The detachment fault divided these ophiolitic rocks in its hanging wall from ultrahigh-pressure garnet peridotite in its footwall (Yang et al., 2001; Song et al., 2003, 2005). Results of whole-rock geochemistry suggest that the ophiolitic rocks formed in a marginal or back-arc setting (e.g., Guo et al., 2009; Fu et al., 2022a).

Detailed field observations for this study focused on the northern Qaidam continent, with the goal of constraining the Precambrian and early Paleozoic metamorphic and magmatic evolution of northern Tibet (Fig. 3). Stratigraphic age assignments of major lithologic units are primarily based on Pan et al. (2004) and Wang et al. (2013), whereas the more detailed framework used in this study is based on our field observations (Fig. 2E). Specifically, detailed geologic mapping and structural analyses were performed in the Zongwulong Shan and Qinghai Nanshan regions (Fig. 3). We observed widespread Precambrian and early Paleozoic metamorphic rocks and foliated/undeformed granitoid plutons (Fig. 3), which previous researchers grouped as a Paleoproterozoic basement metamorphic complex. Here, we mapped and divided these rocks based on detailed field observations and geochronology. Both the Paleoproterozoic basement rocks and Mesoproterozoic to Neoproterozoic, weakly metamorphosed sedimentary rocks experienced early Paleozoic amphibolite-facies metamorphism and were intruded by the early Paleozoic granitoids and gabbros (Fig. 3).

Paleoproterozoic medium- to high-grade basement rocks (labeled Pt_1 in Fig. 3; mixed with the Delingha complex and Dakendaban Group) are widespread in the northern Qaidam continent and are divided into a lowermost gneiss unit, a middle metavolcanic unit, and an uppermost schist unit. The gneiss unit is composed of quartzofeldspathic gneiss, mylonitic biotite orthogneiss, garnet-bearing syenogranite, and paragneiss. These rocks are inferred to be Paleoproterozoic in age based on previous age assignments. Mafic and leucocratic dikes occur within the gneiss unit (Fig. 3). The metavolcanic unit consists of gray-green–colored meta-mafic rocks and foliated garnet amphibolite. The schist unit is characterized by mica ± garnet schist, quartzite, marble, and local phyllite. These basement rocks are intruded by early Paleozoic, amphibolite-facies, weakly foliated granitoids. Mesoproterozoic and Neoproterozoic metasedimentary rocks (labeled Pt_2 and Pt_3 in Fig. 3, respectively) are scattered in the northern Qaidam continent. Silurian metasedimentary strata (labeled S in Fig. 3) consist of medium- to low-grade metasandstone, amphibolite schist, altered metavolcanic rocks, meta-siltstone, meta-conglomerate, and slate, with minor meta-limestone and chert. Minor metavolcanic tuff occurs in the uppermost section. Precambrian basement metamor-

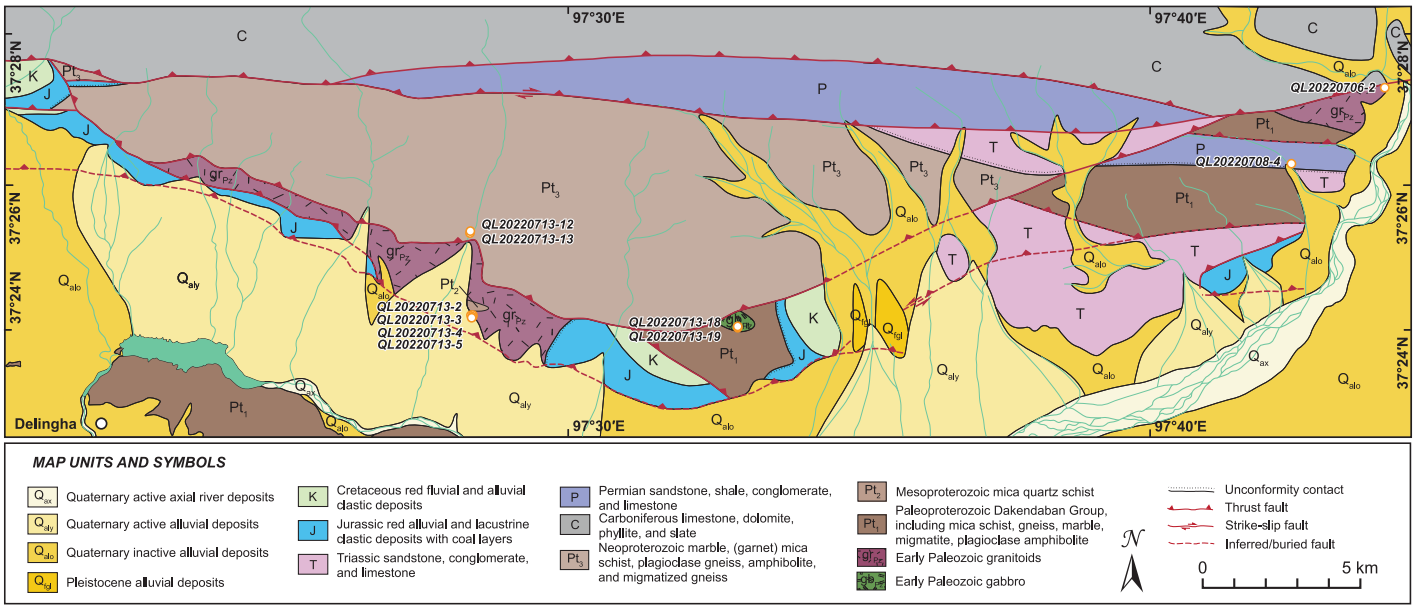

Figure 3. Geologic map of the southern Zongwulong Shan near Delingha city, northern Qaidam continent, based on Qinghai BGMR (1978) and this study. White lines are topographic contours in meters. Locations of samples are shown.

phic rocks are thrust over Silurian metasedimentary rocks. Carboniferous strata (labeled C in Fig. 3) are thrust over Precambrian and early Paleozoic rocks. Strong deformation of Carboniferous strata is localized along basal arkosic and quartz sandstone, slate, phyllite, and minor limestone beds. The Upper Carboniferous strata are composed of thickly bedded limestone and marble. Permian strata are mapped as a single unit (labeled P in Fig. 3) and consist of basal conglomerate, sandy limestone, and arkosic and quartz sandstone. Conformably overlying Triassic strata (labeled T in Fig. 3) are dominated by basal arkosic and quartz sandstone and overlying minor sandy limestone and calcareous siltstone. Overlying Jurassic strata (labeled J in Fig. 3) are generally parallel to Triassic strata along a regional disconformity (e.g., Yin et al., 2008b; Wu et al., 2017; Zuza et al., 2018; Fu et al., 2022a). Jurassic strata consist of a basal conglomerate overlain by interbedded arkosic sandstone and pink-colored siltstone, organic-rich shale, and coal beds (Fig. 2E). Overlying Cretaceous rocks (labeled K in Fig. 3) mainly consist of polymictic conglomerate and red-colored, coarse-grained sandstone.

We recognized seven distinct unconformities in the northern Qaidam continent, which are named for their overlying units (Fig. 2E). The oldest and most widespread unconformity divides the Neoproterozoic Quanji Group from underlying Paleoproterozoic basement metamorphic rocks and local Mesoproterozoic rocks. Two early Paleozoic parallel unconformities occur at the bases of Cambrian and Ordovician strata. The most widespread Phanerozoic unconformity divides Carboniferous strata from underlying Proterozoic basement rocks and early Paleozoic magmatic arc rocks. Two Mesozoic unconformities divide Proterozoic and Paleozoic strata from underlying Jurassic and/or Cretaceous strata, and these likely were related to the initiation of extension across northern Tibet (e.g., Li et al., 2024). The Jurassic unconformity is angular, whereas the Cretaceous unconformity is parallel to underlying strata. A parallel unconformity divides Jurassic and Cretaceous strata from overlying Cenozoic strata. This relationship indicates that prior to Cenozoic deformation, Mesozoic strata were not significantly tilted at the surface despite local Mesozoic deformation (e.g., Li et al., 2024). The development of this unconformity likely represents the initiation of Cenozoic deformation related to the Himalayan-Tibetan orogen.

Structures in the northern Qaidam continent generally trend northwest or north, including the trends of ranges, strikes of sedimentary strata, foliation within metamorphic rocks, and surface traces of faults (Fig. 3). We did not directly observe evidence of Mesozoic normal faulting, although previous field observations are consistent with Jurassic–Cretaceous synextensional sedimentation (Vincent and Allen, 1999; Chen et al., 2003; Yin et al., 2008b), including fining-upward sequences, growth strata, and normal faults in seismic profiles (e.g., Yu et al., 2023). We interpret that the observed contractional deformation of Carboniferous and younger strata occurred during the Cenozoic based on the following observations: (1) Most observed faults and folds in Carboniferous and younger strata merge with range-bounding thrusts; (2) these same faults truncate Cenozoic terrestrial strata and Quaternary alluvium along strike; (3) parallel Carboniferous–Triassic, shallow-marine, lacustrine, and continental-shelf strata are not associated with coeval structures; and (4) Jurassic–Cretaceous strata were deposited during extension (e.g., Vincent and Allen, 1999; Chen et al., 2003; Yin et al., 2008a, 2008b) (Fig. 3). These observations also imply that folding and duplication of the Carboniferous unconformity occurred in the Cenozoic (Fig. 3).

Early Paleozoic records of magmatism and metamorphism are widespread in Precambrian rocks of the northern Qaidam continent. For this study, we collected 10 samples of early Paleozoic rocks for geochronology and geochemistry (Fig. 4). Hornblende gabbro sample QL20220713-18 was collected from a gabbro intrusion within the Paleoproterozoic Dakendaban Group. This gabbro is intruded by ~10–100-cm-wide, pink-colored pegmatite dikes (sample QL20220713-19; Figs. 4A and 4B). Dark gray–colored, garnet-bearing plagioclase amphibolite samples QL20220713-12 and QL20220713-13 were collected from Neoproterozoic rocks, which consist of plagioclase amphibolite, garnet-bearing schist, marble, and garnet-bearing plagioclase amphibolite. These Neoproterozoic rocks experienced early Paleozoic amphibolite-facies metamorphism and were intruded by leucogranite dikes (Figs. 4B–4D). Pink-colored, altered granitoid sample

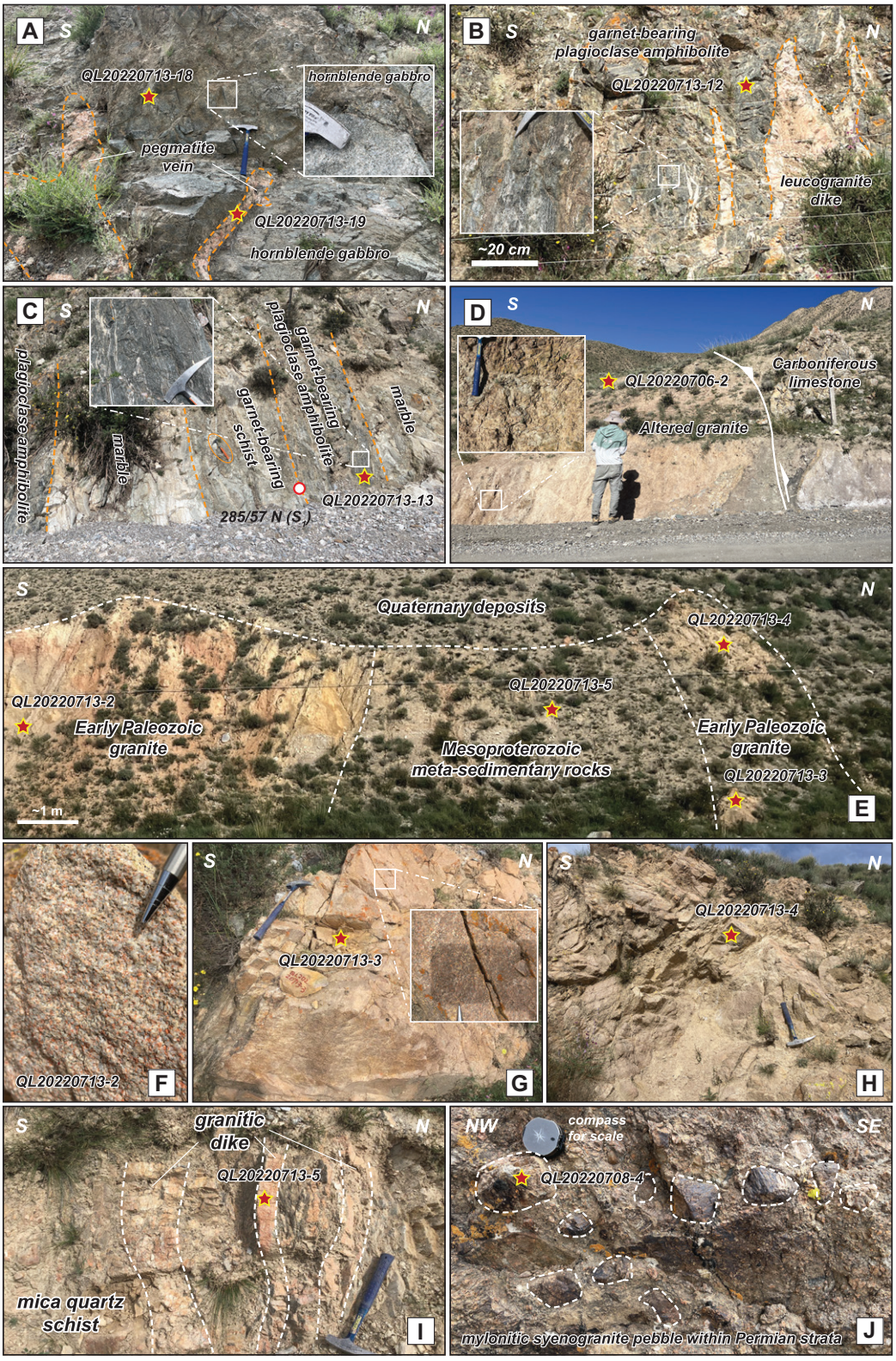

Figure 4. Field photographs from the northern Qaidam continent showing collected rock samples. (A) Hornblende gabbro (sample QL20220713-18) intruded by pink pegmatite veins (sample QL20220713-19). (B) Garnet-bearing plagioclase amphibolite (sample QL20220713-12) intruded by late Paleozoic leucogranite dikes. (C) Neoproterozoic metamorphic rocks including (garnet-)plagioclase amphibolite (sample QL20220713-13), garnet-bearing schist, and marble. (D) Road-cut exposure of a fault zone that places Carboniferous limestone over altered granitoid (sample QL20220706-2). (E–I) Mesoproterozoic metasedimentary rocks intruded by early Paleozoic granitoids (samples QL20220713-2, QL20220713-3, QL20220713-4, and QL20220713-5). (J) Mylonitic syenogranite pebbles within Permian strata (sample QL20220708-4).

QL20220706-2 was collected from an early Paleozoic granitoid, which intrudes the Paleoproterozoic Dakendaban Group (Fig. 3) and is exposed adjacent to a fault zone (Fig. 4D). Calcite veins occur along this fault zone (Fig. 4E). Mesoproterozoic mica quartz schist is intruded by early Paleozoic granitoids and dikes (samples QL20220713-2, QL20220713-3, QL20220713-4, and QL20220713-5; Figs. 4E–4I). Sample QL20220708-4 is a red-colored, mylonitic syenogranite pebble collected from Permian strata, which unconformably overlie Paleoproterozoic rocks (Fig. 4J). Photomicrographs of the collected samples are shown in Figure 5.

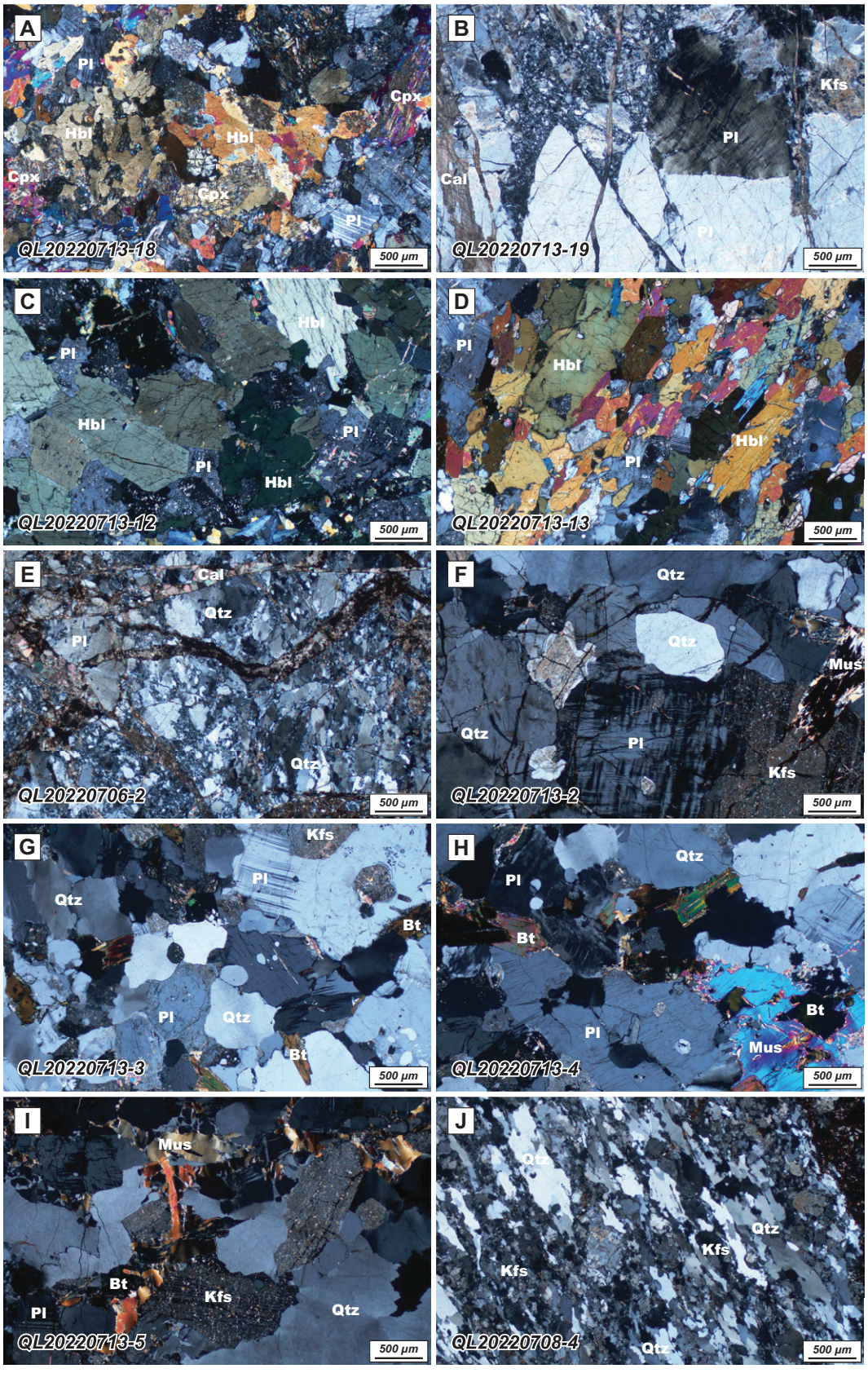

Figure 5. Photomicrographs in cross-polarized light of representative samples collected for this study. (A) Gabbro (sample QL20220713-18). (B) Pegmatite dike (sample QL20220713-19). (C, D) Garnet-bearing plagioclase amphibolite (samples QL20220713-12 and QL20220713-13). (E–I) Granite (samples QL20220706-2, QL20220713-2, QL20220713-3, QL20220713-4, and QL20220713-5). (J) Mylonitic syenogranite pebble (sample QL20220708-4). Bt—biotite; Cal—calcite; Cpx—clinopyroxene; Hbl—hornblende; Kfs—K-feldspar; Mus—muscovite; Pl—plagioclase; Qtz—quartz.

4. ANALYTICAL METHODS

In this study, we performed zircon U-Pb geochronology and Lu-Hf isotope analyses of 10 samples of early Paleozoic gabbro, garnet-bearing plagioclase amphibolite, migmatite and pegmatite dikes, and granitoid to constrain their crystallization histories. Seven samples, including the gabbro, pegmatite dike, and granitoid samples, were analyzed for their whole-rock major-oxide, trace-element, and Sr-Nd isotope compositions to determine the petrogenetic settings.

Zircon grains used for U-Pb geochronology and Lu-Hf isotope analyses were separated from whole-rock samples using traditional methods involving crushing, sieving, and magnetic and density separations. Individual zircon grains were picked under a binocular microscope and mounted in epoxy with standard zircon grains. Cathodoluminescence images of zircon grains were collected using a JXA-880 electron microscope with operating conditions of 20 kV and 20 nA at the Institute of Mineral Resources, Chinese Academy of Geological Sciences, Beijing, China. Zircon grains were analyzed via inductively coupled plasma–mass spectrometry (ICP-MS) using an Agilent 7500a instrument coupled with a New Wave Research UP193FX excimer laser-ablation system at the State Key Laboratory of Tibetan Plateau Earth System, Environment and Resources, Institute of Tibetan Plateau Research, Chinese Academy of Sciences, Beijing. Common Pb corrections were performed assuming an initial Pb composition from Stacey and Kramers (1975). The primary zircon standard used was GJ1 (Jackson et al., 2004). Secondary zircon standards included 91500 ($^{206}U/^{238}Pb$ age of 1065 Ma; Wiedenbeck et al., 1995) and Plešovice ($^{206}U/^{238}Pb$ age of 337 Ma; Sláma et al., 2008). Common-Pb corrections were made using the method of Andersen (2002). Reported U-Pb ages are $^{206}Pb^*/^{207}Pb^*$ ages for grains older than 1000 Ma and $^{206}Pb^*/^{238}U^*$ ages for grains younger than 1000 Ma. Crystallization ages were interpreted from analyses with <10% discordance. Concordia diagrams and weighted mean U-Pb ages were processed using Isoplot v.3 (Ludwig, 2003). Age data and concordia plots are reported with 2σ error. Uncertainties of weighted mean ages are presented at the 95% confidence level. Zircon Hf isotopes were measured in situ on a Nu Plasma II multicollector (MC) ICP-MS (Nu Instruments Ltd., UK), which was coupled to a 193 nm New Wave laser-ablation system. Analyses involved a beam diameter of ~45 μm, repetition rate of 6 Hz, and energy density of ~11.6 J/cm^2. Each measurement consisted of 10 s pre-ablation, 45 s ablation, and 30 s washout delay. Hf isotopes were calculated using Iolite v.4 (University of Melbourne). The measured Hf isotopic values were 0.282302 ± 19 for 91500, 0.281998 ± 15 for GJ-1, and 0.282475 ± 11 for Plešovice, consistent with recommended values. Sample locations and U-Pb zircon geochronology results are shown in Table 1. Details of geochronology and Lu-Hf isotope analyses are shown in Table S1 and Table S2,[1] respectively.

Seven early Paleozoic rock samples were analyzed for their geochemistry at the Wuhan Sample Solution Analytical Technology Co., Ltd., in Hubei, China. Before analysis, weathered sample surfaces were removed. Samples were then crushed and ground into powder (>200 mesh) using a ball mill. Major-element compositions were determined via X-ray fluorescence spectrometry with analytical accuracy better than 2%. Trace-element compositions were measured via ICP-MS with an analytical accuracy better than 5%. Sr-Nd isotopes were measured using a Neptune Plus MC-ICP-MS with spectral analysis accuracy better than 0.002%. Sample dissolution was performed using acid digestion ($HF + HCLO_4 + HNO_3$). Background isotope measurements were conducted within the error range. Aliquots of NIST SRM 987, JNDI-1, and JMC international standard solutions were regularly used to evaluate instrumental reproducibility and accuracy. Analytical results of standard sample BCR-2 (basalt) included $^{143}Nd/^{144}Nd = 0.512641 \pm 11$ (2 standard deviation [S.D.]) and $^{87}Sr/^{86}Sr = 0.705012 \pm 22$ (2 S.D.; see Zhang and Hu, 2020). Data reduction for analyses of Sr isotope ratios was conducted using Iso-Compass software (Zhang and Hu, 2020). Whole-rock geochemical and Sr-Nd isotopic results are presented in Table S3 and Table S4, respectively.

[1]Supplemental Material. Table S1: LA-ICP-MS results of zircon U-Pb geochronology for this study. Table S2: Zircon Lu-Hf results of the samples collected for this study. Table S3: Whole-rock major and trace elements of the samples collected for this study. Table S4: Whole-rock Sr-Nd isotopes of the samples collected for this study. Table S5: LA-ICP-MS results of zircon U-Pb geochronology and zircon Lu-Hf, whole-rock major- and trace-element, and whole-rock Sr-Nd isotope analyses from previous studies. Please visit https://doi.org/10.1130/GSAB.S.27153996 to access the supplemental material; contact editing@geosociety.org with any questions.

5. ANALYTICAL RESULTS

5.1. Zircon U-Pb Geochronology and Lu-Hf Isotope Geochemistry

Forty zircon grains from gabbro sample QL20220713-18 yielded convergent U-Pb ages ranging from ca. 493 Ma to 463 Ma (Fig. 6A). The weighted mean U-Pb age of 37 concordant analyses is 477 ± 17 Ma (mean square of weighted deviates [MSWD] = 0.016; Fig. 6A). Zircon grains from this gabbro sample have $\varepsilon Hf_{(t)}$ values of −5.0 to −2.9 (depleted mantle model age [T_{DM}] = 1275–1198 Ma, crustal depleted mantle model age [T_{DMC}] = 1762–1638 Ma; Table S2).

Thirty zircon grains from migmatite sample QL20220713-9 yielded diverse U-Pb ages rang-

TABLE 1. SUMMARY OF SAMPLE LOCATIONS AND GEOCHRONOLOGY RESULTS, NORTHERN QAIDAM CONTINENT (NORTHERN TIBET)

Sample number	Rock type	Latitude (°N)	Longitude (°E)	Elevation (m)	Methods	Age (Ma)
QL20220706-2	Granite	37°27′13.80″	97°43′33.16″	3346	Zircon U-Pb/zircon Lu-Hf/whole-rock geochemistry/Sr-Nd isotope	450 ± 5
QL20220708-4	Mylonitic syenogranite pebble	37°26′14.38″	97°42′31.18″	3372	Zircon U-Pb/zircon Lu-Hf	418 ± 4
QL20220713-2	Granite	37°24′25.95″	97°28′15.43″	3282	Zircon U-Pb/zircon Lu-Hf/whole-rock geochemistry/Sr-Nd isotope	426 ± 6
QL20220713-3	Granite	37°24′26.91″	97°28′14.15″	3280	Zircon U-Pb/zircon Lu-Hf/whole-rock geochemistry/Sr-Nd isotope	443 ± 5
QL20220713-4	Granite	37°24′27.10″	97°28′13.76″	3271	Zircon U-Pb/zircon Lu-Hf/whole-rock geochemistry/Sr-Nd isotope	436 ± 5
QL20220713-5	Granite	37°24′26.69″	97°28′13.96″	3288	Zircon U-Pb/zircon Lu-Hf/whole-rock geochemistry/Sr-Nd isotope	439 ± 10
QL20220713-9	Migmatite gneiss	37°25′14.73″	97°28′15.27″	3401	Zircon U-Pb/zircon Lu-Hf	510 ± 6
QL20220713-12	Garnet-bearing plagioclase amphibolite	37°25′15.60″	97°28′15.63″	3413	Zircon U-Pb/zircon Lu-Hf	423 ± 9
QL20220713-13	Garnet-bearing plagioclase amphibolite	37°25′16.27″	97°28′16.11″	3395	Zircon U-Pb/zircon Lu-Hf	431 ± 13
QL20220713-18	Gabbro	37°23′53.18″	97°31′55.08″	3418	Zircon U-Pb/zircon Lu-Hf/whole-rock geochemistry/Sr-Nd isotope	477 ± 17
QL20220713-19	Pegmatite dike	37°23′53.18″	97°31′55.08″	3418	Zircon U-Pb/zircon Lu-Hf/whole-rock geochemistry/Sr-Nd isotope	424 ± 8

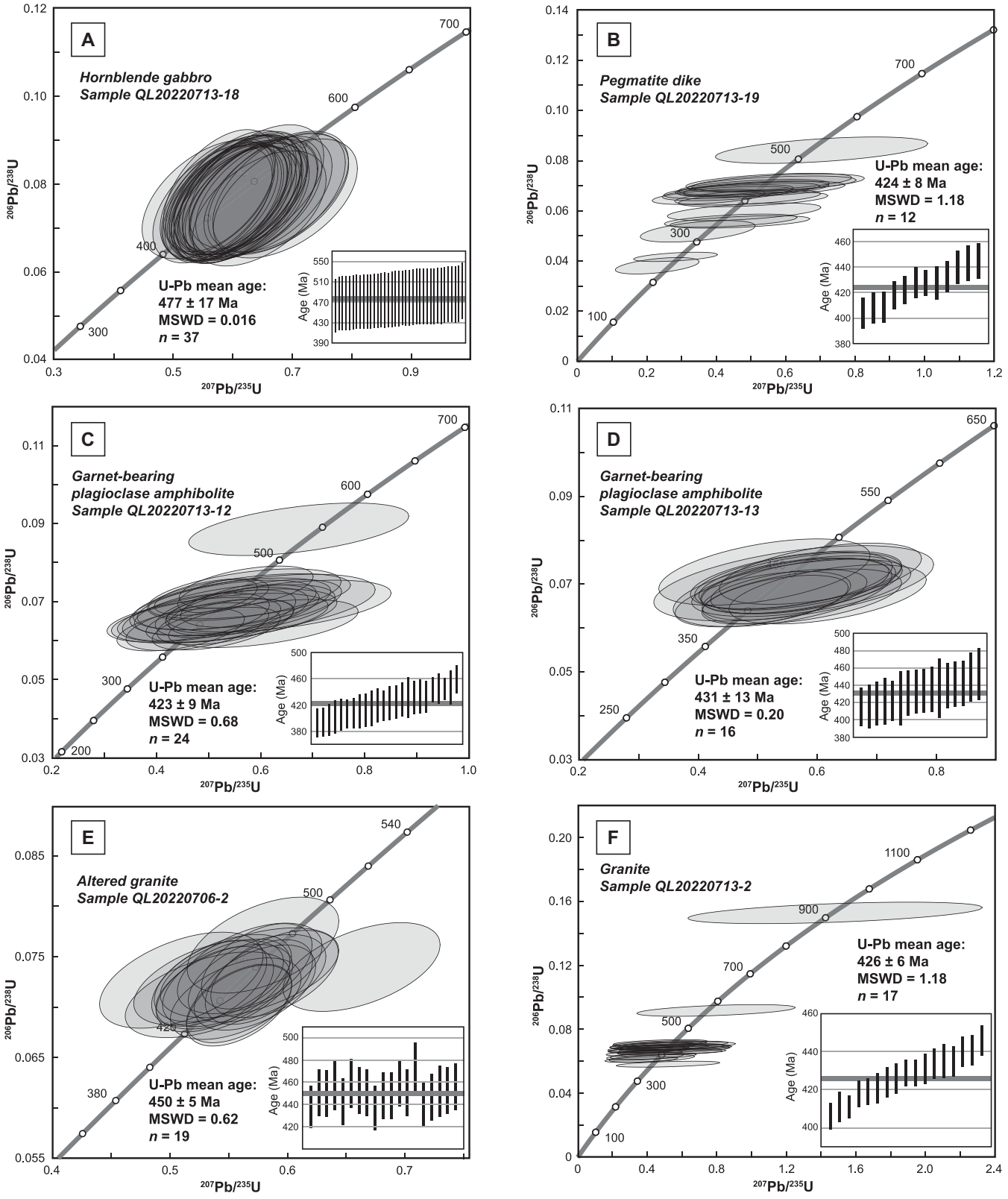

Figure 6. U-Pb concordia diagrams showing results of single-shot zircon analyses. Error ellipses are 2σ. Insets show the weighted mean age for selected zircon grains. (A) Hornblende gabbro sample QL20220713-18. (B) Pegmatite dike sample QL20220713-19. (C, D) Garnet-bearing plagioclase amphibolite samples QL20220713-12 and QL20220713-13. (E–I) Granite samples QL20220706-2, QL20220713-2, QL20220713-3, QL20220713-4, and QL20220713-5. (J) Mylonitic syenogranite pebble sample QL20220708-4. MSWD—mean square of weighted deviates.

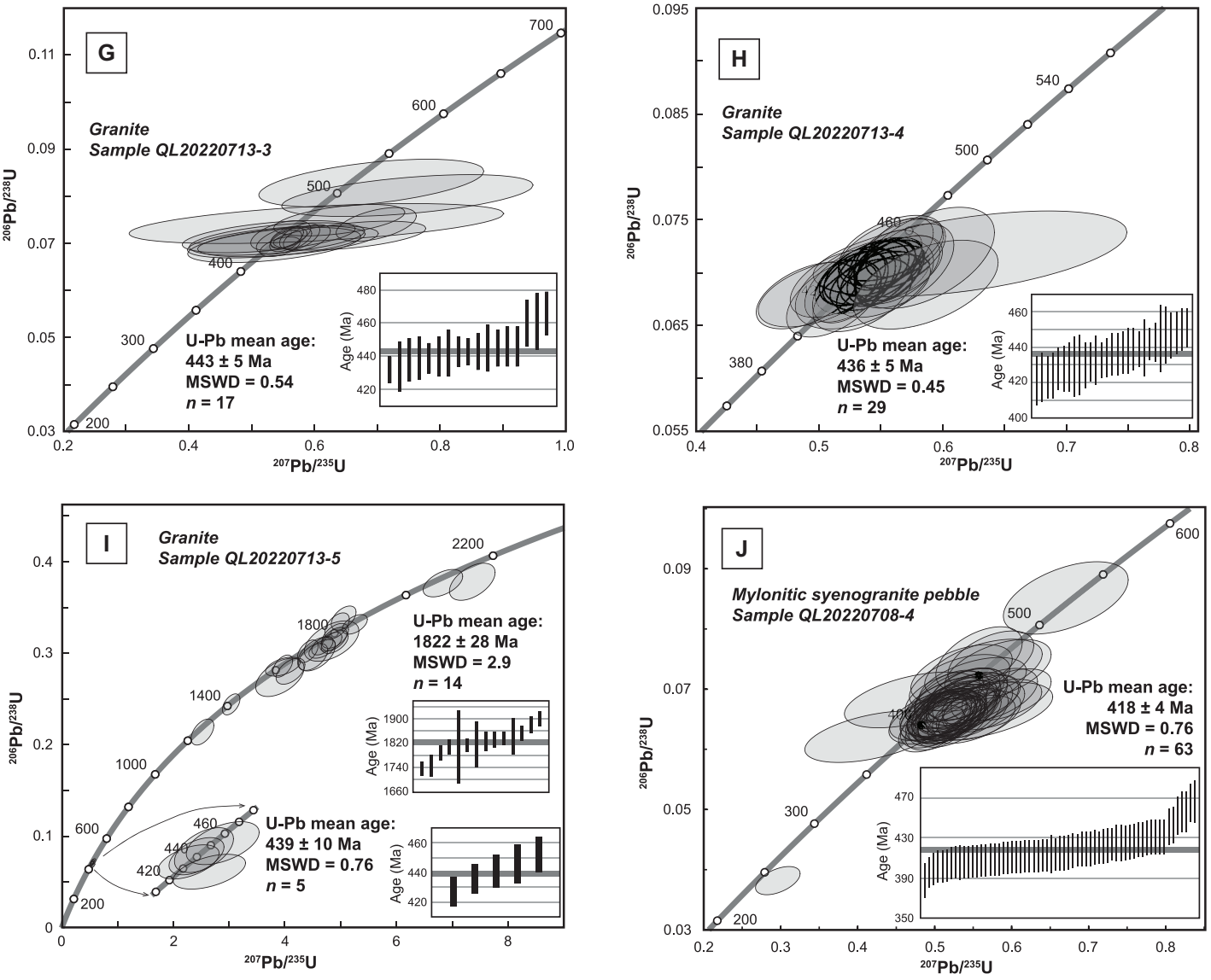

Figure 6. (*Continued*)

ing from ca. 710 Ma to 435 Ma. The weighted mean U-Pb age of 25 concordant analyses is 510 ± 6 Ma (MSWD = 0.39). Zircon grains from this granite sample have $\varepsilon Hf_{(t)}$ values of −10.2 to −2.4 (T_{DM} = 1492–1184 Ma; T_{DMC} = 2101–1613 Ma; Table S2).

Thirty zircon grains of pegmatite dike sample QL20220713-19 yielded convergent U-Pb ages ranging from ca. 695 Ma to 241 Ma (Fig. 6B). The weighted mean U-Pb age of 12 concordant analyses is 424 ± 8 Ma (MSWD = 1.18; Fig. 6B). Zircon grains from this pegmatite dike sample have $\varepsilon Hf_{(t)}$ values of −9.5 to −6.5 (T_{DM} = 2012–1816 Ma; T_{DMC} = 1762–1638 Ma; Table S2).

Thirty zircon grains each from two garnet-bearing plagioclase amphibolite samples, QL20220713-12 and QL20220713-13, yielded convergent U-Pb ages ranging from ca. 547 Ma to 389 Ma and from ca. 501 Ma to 362 Ma, respectively (Figs. 6C and 6D). The weighted mean U-Pb ages of 24 and 16 concordant analyses are 423 ± 9 Ma (MSWD = 0.68) and 431 ± 13 Ma (MSWD = 0.2), respectively (Figs. 6C and 6D). Zircon grains from these garnet-bearing plagioclase amphibolite samples have $\varepsilon Hf_{(t)}$ values of +2.8 to +5.5 (T_{DM} = 918–821 Ma; T_{DMC} = 1223–1062 Ma; Table S2).

Twenty zircon grains from altered granitoid sample QL20220706-2 yielded U-Pb ages ranging from ca. 473 Ma to 437 Ma (Fig. 6E). The weighted mean U-Pb age of 19 concordant analyses is 450 ± 5 Ma (MSWD = 0.62; Fig. 6E). Zircon grains from this granite sample have $\varepsilon Hf_{(t)}$ values of −10.1 to −5.8 (T_{DM} = 1472–1317 Ma; T_{DMC} = 2052–1792 Ma; Table S2).

Thirty zircon grains of granite sample QL20220713-2 yielded diverse U-Pb ages ranging from ca. 917 Ma to 365 Ma (Fig. 6F). The weighted mean U-Pb age of 17 concordant analyses is 426 ± 6 Ma (MSWD = 1.18; Fig. 6F). Zircon grains from this granite sample have $\varepsilon Hf_{(t)}$ values of −11.4 to −6.0 (T_{DM} = 1483–1276 Ma; T_{DMC} = 2119–1774 Ma).

Thirty zircon grains from granite sample QL20220713-3 yielded convergent U-Pb ages ranging from ca. 513 Ma to 432 Ma (Fig. 6G). The weighted mean U-Pb age of 17 concordant analyses is 443 ± 5 Ma (MSWD = 0.54; Fig. 6G). Zircon grains for this granite sample have $\varepsilon Hf_{(t)}$ values of −11.0 to −5.7 (T_{DM} = 1478–1283 Ma; T_{DMC} = 2111–1776 Ma; Table S2).

Thirty zircon grains from granite sample QL20220713-4 yielded convergent U-Pb ages

ranging from ca. 451 Ma to 421 Ma (Fig. 6H). The weighted mean U-Pb age of 29 concordant analyses is 436 ± 5 Ma (MSWD = 0.45; Fig. 6H). Zircon grains for this granite sample have $\varepsilon Hf_{(t)}$ values of −13.1 to −0.3 (T_{DM} = 1445–1056 Ma; T_{DMC} = 2230–1432 Ma; Table S2).

Thirty zircon grains from granite sample QL20220713-5 yielded diverse ages ranging from ca. 2250 Ma (Pb-Pb) to ca. 427 Ma (U-Pb; Fig. 6I). The older population of 14 grains yields a weighted mean age of 1822 ± 28 Ma (MSWD = 2.9) and is interpreted to be inherited. The younger population of five grains yields a weighted mean age of 439 ± 10 Ma (MSWD = 0.76), which is interpreted as the crystallization age of this granite sample (Fig. 6I). Zircon grains from this granite sample have $\varepsilon Hf_{(t)}$ values of −9.9 to −6.8 (T_{DM} = 1447–1313 Ma; T_{DMC} = 2046–1828 Ma; Table S2).

One-hundred zircon grains from mylonitic syenogranite pebble sample QL20220708-4 collected from Permian strata yielded U-Pb ages ranging from ca. 527 Ma to 241 Ma. The weighted mean U-Pb age of 63 concordant analyses is 418 ± 4 Ma (MSWD = 0.76; Fig. 6J).

5.2. Whole-Rock Geochemistry

Early Paleozoic granite samples (ca. 443–426 Ma) have high SiO_2 of 73.98–74.45 wt%, MgO of 0.16–0.34 wt%, Al_2O_3 of 13.27–13.84 wt%, TiO_2 of 0.07–0.28 wt%, and $K_2O + Na_2O$ of 7.89–9.51 wt%. Circa 450 Ma granite sample QL20220706-2 has higher SiO_2 of 81.74 wt%, $K_2O + Na_2O$ of 0.76 wt%, Al_2O_3 of 1.33 wt%, CaO of 5.79 wt%, and ablation (loss on ignition [LOI] = 7.06). We interpret that this sample was likely altered, given the observed calcite veining. The early Paleozoic granite samples are classified as granite on the ($K_2O + Na_2O$) versus SiO_2 plot (Fig. 7A; Middlemost, 1994). In the K_2O versus SiO_2 plot (Le Maitre et al., 1989; Rickwood, 1989), most samples plot within the shoshonitic series field, with the exception of altered granite sample QL20220706-2, which falls within the tholeiitic series field (Fig. 7B). These early Paleozoic samples are peraluminous, as indicated by molar A/CNK of 1.11–1.18 (where A/CNK = molar ratio of $Al_2O_3/[CaO + K_2O + Na_2O]$) and A/NK of 1.19–1.34 (where A/NK = molar ratio of $Al_2O_3/[K_2O + Na_2O]$; Fig. 7C; Maniar and Piccoli, 1989). In Harker diagrams, MgO, CaO, TiO_2, TFe_2O_3, and Al_2O_3 contents decrease with increasing SiO_2 contents (Figs. 7D–7I). Altered granite sample QL20220713-2 (ca. 426 Ma) falls within the A-type granite field (Figs. 7J–7L), which is generally associated with extension regardless of the magma source (e.g., Whalen et al., 1987; Eby, 1990, 1992; Turner et al., 1992). Trace-element discrimination diagrams allow further refinement of the assigned tectonic environments of these four granite samples (ca. 443–426 Ma), which plot in the syncollisional granite field (Figs. 7M–7O). Chondrite-normalized, rare earth element (REE) patterns of these granite samples are characterized by significant light rare earth element (LREE) enrichment and heavy rare earth element (HREE) depletion trends (Fig. 8A). These samples have strongly negative Eu (Eu/Eu* = 0.59–0.17) anomalies, with the exception of early Paleozoic granite sample QL20220713-5 (ca. 439 Ma), which has a slightly positive Eu anomaly (Eu/Eu* = 1.14) (Fig. 8A). In primitive mantle–normalized spider diagrams, these granitoid samples are enriched in large ion lithophile elements (LILES) and depleted in high field strength elements (HFSEs). These granitoid samples display no distinct Ce anomalies (Fig. 8B).

Circa 477 Ma gabbro sample QL20220713-18 has lower SiO_2 of 51.39 wt%, higher MgO of 7.92 wt%, Al_2O_3 of 16.27 wt%, TiO_2 of 0.61 wt%, and lower $K_2O + Na_2O$ of 3.70 wt%, and Ni of 151.25 ppm. The chondrite-normalized REE pattern of this gabbro sample is characterized by moderate LREE enrichment and HREE depletion (La_N/Yb_N = 14.04), with a slightly negative Eu anomaly (Eu/Eu* = 0.79; Fig. 8A). In primitive mantle–normalized spider diagrams, this gabbro sample is depleted in LILES (e.g., Th, U, K) and enriched in HFSEs (e.g., Nb and Ta; Fig. 8B). The gabbro sample is metaluminous, as indicated by molar A/CNK of 0.66 and A/NK of 2.90 (Fig. 7C; Maniar and Piccoli, 1989). The ca. 424 Ma pegmatite dike sample QL20220713-19 has SiO_2 of 60.81 wt%, MgO of 7.92 wt%, Al_2O_3 of 10.61 wt%, TiO_2 of 0.02 wt%, and $K_2O + Na_2O$ of 8.07 wt%. The chondrite-normalized REE pattern of this pegmatite dike sample is characterized by significant LREE enrichment and HREE depletion, with a negative Eu (Eu/Eu* = 0.62) anomaly (Fig. 8A). In the primitive mantle–normalized spider diagram, this pegmatite dike sample is enriched in LILEs and depleted in HFSEs (Fig. 8B). This pegmatite dike sample is classified as monzonite on the ($K_2O + Na_2O$) versus SiO_2 plot (Fig. 7A; Middlemost, 1994) and as calc-alkaline series in the K_2O versus SiO_2 plot (Fig. 7B; Le Maitre et al., 1989; Rickwood, 1989), and it is peraluminous as indicated by molar A/CNK of 0.35 and A/NK of 1.05 (Fig. 7C; Maniar and Piccoli, 1989). High-ablation LOI contents of 2.26% for the gabbro sample and 8.07% for the pegmatite dike sample were measured, indicating potential postmagmatic alteration (Polat et al., 2009).

The ca. 477 Ma gabbro sample QL20220713-18 has an initial $^{87}Sr/^{86}Sr$ ratio of 0.71214108 and $\varepsilon Nd_{(t)}$ value of −5.96837, whereas the ca. 424 Ma pegmatite dike sample QL20220713-19 has an initial $^{87}Sr/^{86}Sr$ ratio of 0.71468586 and $\varepsilon Nd_{(t)}$ value of −7.50694 (Fig. 8C). Five early Paleozoic granite samples (ca. 450–426 Ma) have varied initial $^{87}Sr/^{86}Sr$ ratios of 0.71786482–0.75683854 and consistent $\varepsilon Nd_{(t)}$ values of −10.3556 to −8.83168 (Fig. 8C).

6. DISCUSSION

6.1. Paleozoic–Mesozoic Magmatism in the North Qaidam Continent

The oldest reported intrusion of the northern Qaidam continent is ca. 510 Ma migmatite gneiss from this study. Early Paleozoic granitoids and gabbros (ca. 490–410 Ma) are widespread in the northern Qaidam continent. Geochemistry results indicate that the ca. 493–460 Ma granitoids and ca. 490–485 oceanic-island basalt (OIB)–like gabbros were likely

Figure 7. (A) SiO_2 versus ($K_2O + Na_2O$) total alkali-silica (TAS) diagram for intrusive rocks. Normalization values are from Middlemost (1994). (B) K_2O versus SiO_2 diagram for intrusive rocks. Normalization values are from Le Maitre et al. (1989) and Rickwood (1989). (C) A/CNK versus A/NK diagram for intrusive rocks, where A/CNK = molar ratio of $Al_2O_3/(CaO + K_2O + Na_2O)$ and A/NK = molar ratio of $Al_2O_3/(K_2O + Na_2O)$. (D–I) Harker diagrams of selected major elements showing content variation of major elements. (J–O) Geochemical discrimination diagrams based on Pearce et al. (1984), Pearce (1996), and Whalen et al. (1987) for plutonic samples. syn-COLG—syncollisional granite; WPG—within-plate granite; ORG—orogenic granite; VAG—volcanic-arc granite. Data sources: Li et al. (2022, 2023b); Gao et al. (2018, 2021, 2022); Zhao et al. (2017); Wang et al. (2014, 2017, 2018); Zhu et al. (2014); Wu et al. (2001, 2004, 2006b, 2007, 2009b, 2014, 2019c); Zha et al. (2016); Zhang et al. (2015, 2018); Yang et al. (2015); Yu et al. (2012, 2015, 2019a); Song et al. (2014b); Cao et al. (2017); Zhou et al. (2014, 2015, 2021); Jiang et al. (2016); Shao et al. (2018); Meng et al. (2005); Meng and Zhang (2008); Chen et al. (2012a); Lu et al. (2007); Kou et al. (2017); Qian et al. (2018a); Qiu et al. (2015); Gu et al. (2018); Dong et al. (2014, 2015); Peng et al. (2016); Wang and Zhou (2016); Niu et al. (2018); this study.

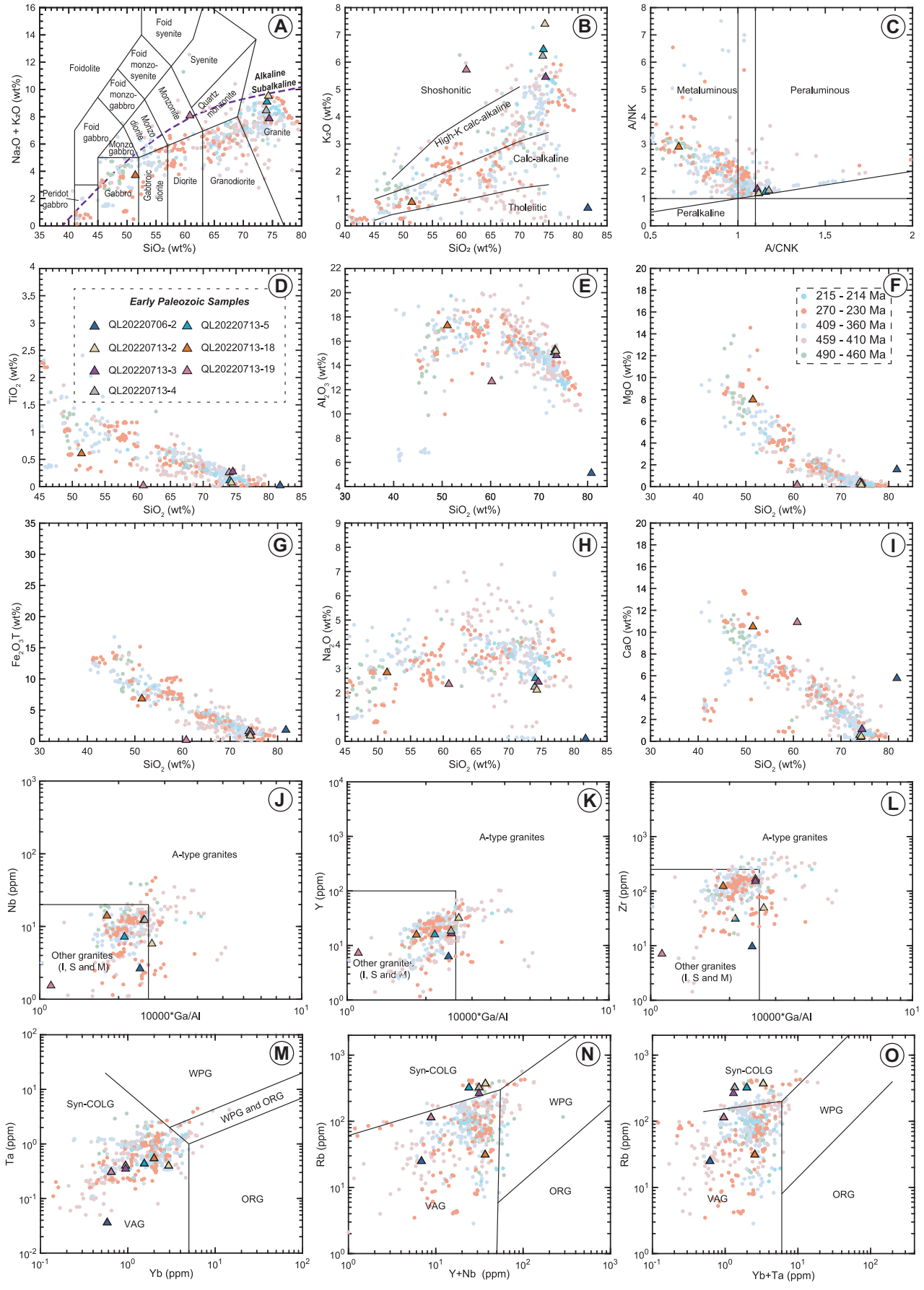

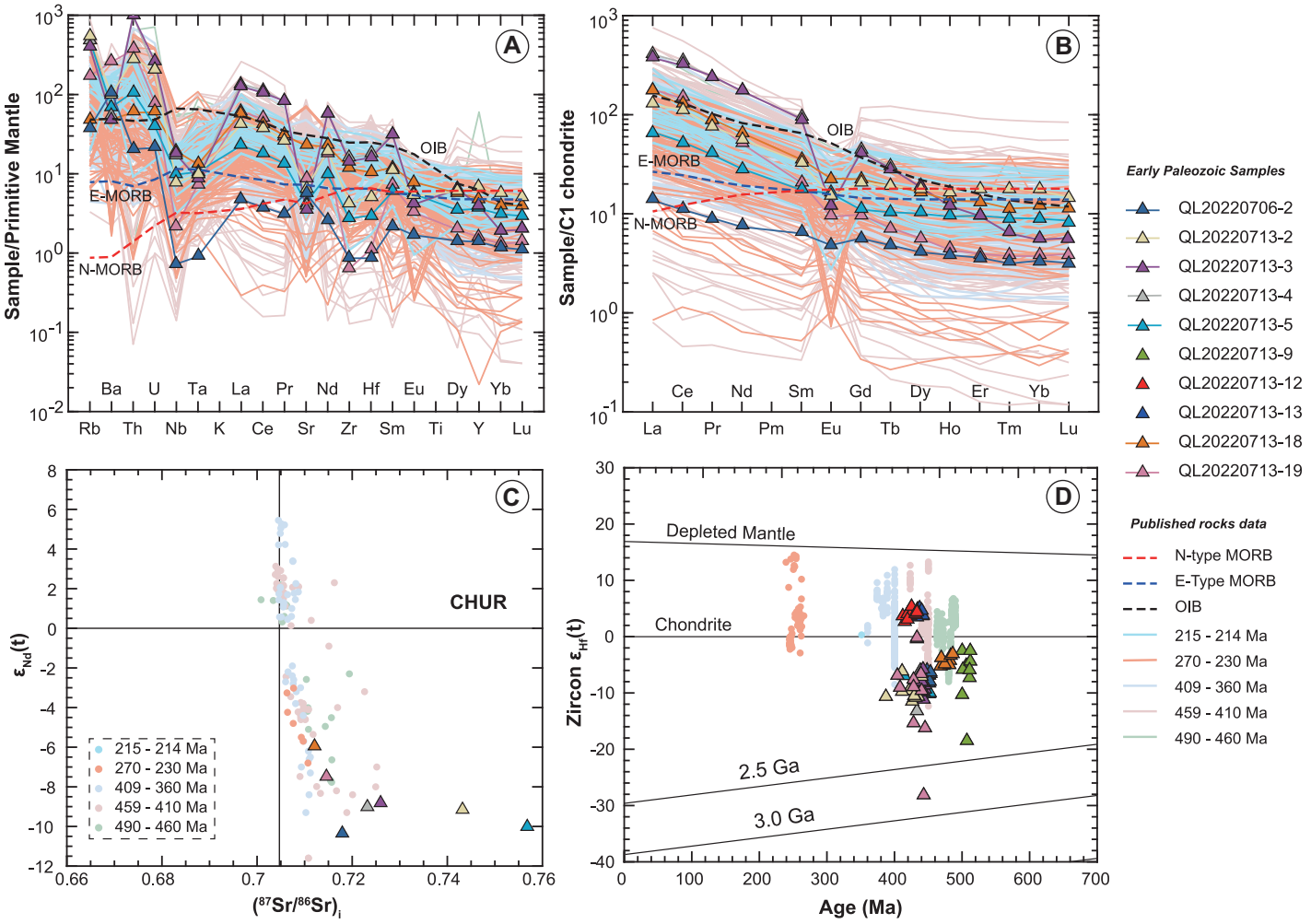

Figure 8. (A, B) Chondrite-normalized rare earth element and primitive mantle–normalized multielement patterns (Boynton, 1984; Sun and McDonough, 1989). (C) Whole-rock $(^{87}Sr/^{86}Sr)_i$ values versus $\varepsilon Nd_{(t)}$ values. (D) Plots of zircon $\varepsilon Hf_{(t)}$ values versus U-Pb ages. E/N-MORB—enriched/normal mid-ocean-ridge basalt; OIB—oceanic-island basalt; CHUR—chondritic uniform reservoir. Data sources: Li et al. (2022, 2023b); Wu et al. (2001, 2004, 2006b, 2007, 2009b, 2014, 2019c, 2022b); Peng et al. (2016); Niu et al. (2018); Gu et al. (2018); Dong et al. (2014, 2015); Wang et al. (2014, 2017, 2018); Wang and Zhou (2016); Qian et al. (2018a); Qiu et al. (2015); Jiang et al. (2016); Zhou et al. (2014, 2015, 2021); Shao et al. (2018); Yu et al. (2012, 2019a); Kou et al. (2017); Sun et al. (2020); Zhang et al. (2008, 2009a, 2015, 2016, 2018); Song et al. (2014b); Meng and Zhang (2008, 2009); Cao et al. (2017); Meng et al. (2005); Chen et al. (2012b); Xiong et al. (2011); Lu et al. (2007); Liu et al. (2012); Zhao et al. (2017); Ren et al. (2016); Gao et al. (2018, 2021, 2022, 2023); Zhu et al. (2014); Yang et al. (2015).

generated in a subduction environment (e.g., Gao et al., 2021). The geochemistry of the ca. 477 Ma gabbro sample from this study, including its positive $\varepsilon Hf_{(t)}$ and negative $\varepsilon Nd_{(t)}$ values (Figs. 8C and 8D), metaluminous composition, low SiO_2 and high MgO and Ni contents, and REE patterns (Figs. 8A and 8B), suggest generation in a suprasubduction zone or mid-ocean-ridge setting. This ca. 477 Ma gabbro shows subduction-related characteristics, which are consistent with the results of ca. 478 Ma plagiogranites and ca. 480–465 Ma mafic rocks from Gao et al. (2023). Zhang et al. (2008) argued that ca. 450 Ma high-pressure, granulite-facies metamorphism recorded in the western part of the northern Qaidam continent may have occurred in thickened lower crust during early Paleozoic continental collision. Records of ca. 446–428 Ma high-pressure granulite-facies metamorphism are synchronous with ca. 446–430 Ma metamorphism of eclogites, ca. 465–450 Ma migmatization, and ca. 470 Ma adakitic magmatism in the northern Qaidam continent. This coeval activity suggests that adakitic melts were derived from anatexis of thickened mafic lower crust during collision (Yu et al., 2012, 2019b). In addition, the occurrences of ca. 458–457 Ma ultrahigh-pressure eclogites related to deep continental subduction and paragneiss with ca. 460–455 Ma metamorphic ages suggest that continental collision in the northern Qaidam continent commenced by ca. 460 Ma (e.g., Zhang et al., 2019b; Yu et al., 2021). In general, we suggest that the age of ultrahigh-pressure eclogites must be older than the timing of the arc-continent collision, whereas continental ultrahigh-pressure eclogites must be younger than initial collision. This study and previous research show that the ca. 460–436 Ma, syncollisional I- and S-type granitoids are widespread in the northern Qaidam continent (Figs. 7M–7O). The ca. 426 Ma, A-type granites and ca. 424 Ma pegmatite dike from this study suggest a postcollisional, extensional setting in the northern Qaidam continent at that time

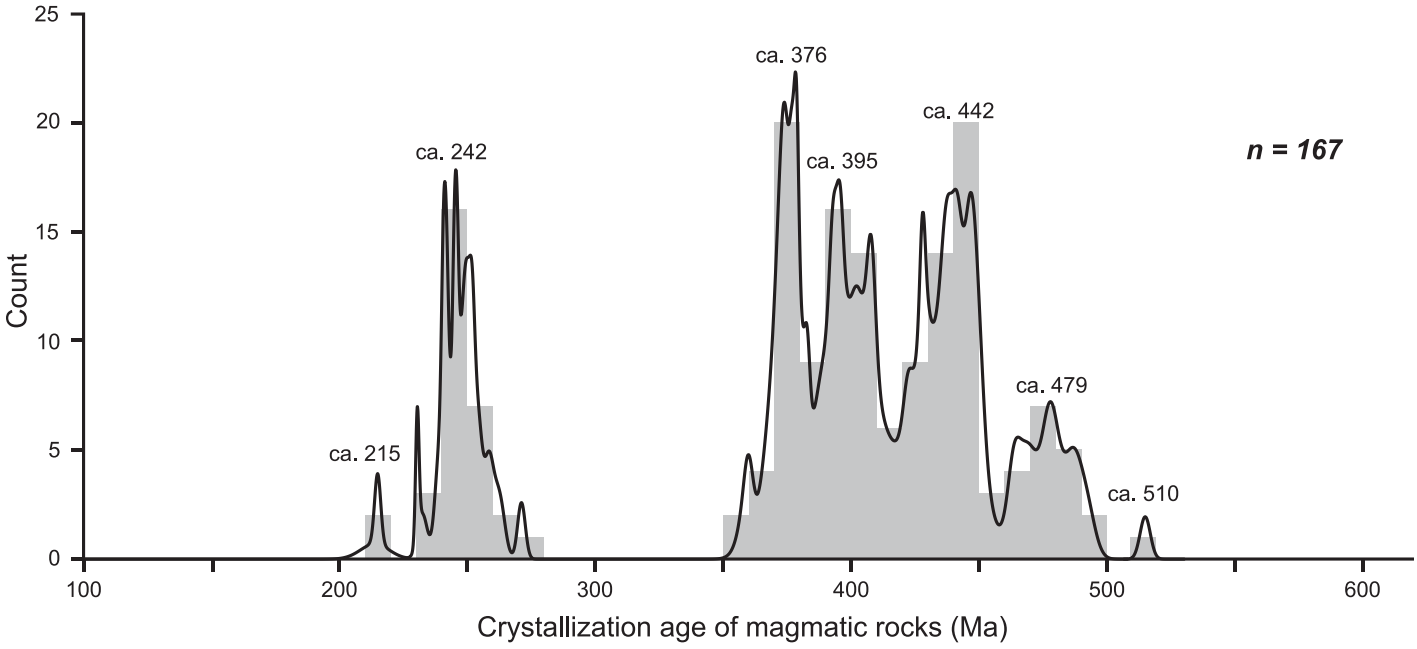

Figure 9. Probability distribution plot of all Paleozoic–Mesozoic U-Pb ages of intrusive rocks in the northern Qaidam continent (n = 167). Data sources: Wu et al. (2001, 2004, 2006a, 2007, 2009a, 2014, 2019c, 2022b); Li et al. (2022, 2023a); Peng et al. (2016); Niu et al. (2018); Gu et al. (2018); Dong et al. (2014, 2015); Qian et al. (2018a); Qiu et al. (2015); Jiang et al. (2016); Yu et al. (2012, 2019b); Shao et al. (2018); Kou et al. (2017); Sun et al. (2020); Song et al. (2014b); Zhou et al. (2014, 2015, 2016, 2021); Meng et al. (2005); Meng and Zhang (2008, 2009); Xiong et al. (2011); Cao et al. (2017); Lu et al. (2007); Ren et al. (2016); Wang et al. (2014, 2017, 2018); Wang and Zhou (2016); Gao et al. (2018, 2021, 2022, 2023); Zhu et al. (2014); Yang et al. (2015); Zhang et al. (2008, 2009a, 2015, 2016, 2018); Chen et al. (2012a); Liu et al. (2012).

(Figs. 7J–7L; e.g., Whalen et al., 1987; Eby, 1990, 1992; Turner et al., 1992). Late Paleozoic extension-related granitoids and volcanic rocks (ca. 409–360 Ma) also occur in the northern Qaidam continent (e.g., Li et al., 2023b). A magmatic lull occurred in the northern Qaidam continent from ca. 360 Ma to 270 Ma (Fig. 9). Furthermore, Permian–Triassic, subduction-related granitoids (ca. 271–230 Ma) and extension-related granitoids (ca. 215–214 Ma) occur in the northern Qaidam continent.

Zircon U-Pb ages of igneous rocks in the northern Qaidam continent fall into two age groups at ca. 493–360 Ma, with an oldest age of ca. 510 Ma, and ca. 271–214 Ma (Figs. 9 and 10). In northern Tibet, zircon U-Pb ages of Paleozoic intrusive rocks in the Qilian Shan have ages of ca. 520–402 Ma with ca. 445 Ma peaks (Fig. 9; Liu et al., 2019; Wu et al., 2022a). Late Devonian, postorogenic granitoids (ca. 392–372 Ma) and Permian–Triassic arc granitoids (ca. 269–235 Ma) occur in the South Qilian orogen and northern Qaidam continent (Fig. 10; e.g., Xie et al., 2014; Hu et al., 2016; Li et al., 2021; Jia et al., 2017; Wu et al., 2004, 2007, 2009a; Cheng et al., 2017; Zhou et al., 2021; this study). In addition, the youngest leucogranite in northern Tibet, dated at ca. 341 Ma, occurs in the central Qilian Shan (e.g., Wu et al., 2021). Circa 550–529 Ma gabbro interpreted to represent Qilian oceanic crust and/or suprasubduction ophiolite occurs in the northern Qilian continent (e.g., Shi et al., 2004; Song et al., 2013). In contrast to the magmatic record of the Qilian Shan, zircon U-Pb ages of Paleozoic–Mesozoic granitoids in the Eastern Kunlun Range fall within two main age groups at ca. 503–357 Ma and ca. 263–194 Ma (Fig. 9; e.g., Wu et al., 2016, 2019a, 2022a). Numerous early Paleozoic (ca. 500–405 Ma) granitoid plutons are exposed throughout the northern Altyn Tagh Range (e.g., Qi et al., 2005; Wu et al., 2006b, 2009b; Kang et al., 2011; Liu et al., 2024a; Hao et al., 2006; Chen et al., 2003). Late Cambrian–Silurian granitic plutons (ca. 491–414 Ma) sporadically occur in the southern Altyn-Tagh Range (e.g., Sobel and Arnaud, 1999; Xinjiang BGMR, 2003; Dong et al., 2011b; Liu et al., 2024a). The timing of Phanerozoic arc magmatism allows us to reinterpret the tectonic evolution of the Tethyan orogenic system.

6.2. Phanerozoic Tectonostratigraphic Evolution of the Qaidam Continent

Cambrian–Ordovician flysch strata in the northern Qaidam continent are dominated by massive carbonate successions interbedded with sandstone (e.g., Sun et al., 2020; Chen et al., 2022). Cambrian strata overlie Neoproterozoic metasedimentary rocks along a parallel unconformity. These Cambrian strata have detrital zircon U-Pb ages of ca. 2688–517 Ma, with two major age peaks at ca. 520 Ma and ca. 990 Ma and a minor age peak at ca. 2400 Ma (Fig. 11; Sun et al., 2020; Chen et al., 2022). Detrital zircon ages of Upper Ordovician strata have two major age peaks of ca. 520 Ma and ca. 940 Ma and yield a maximum depositional age of ca. 480 Ma. Two minor age groups peak at ca. 1640 Ma and ca. 2500 Ma (Fig. 11; Sun et al., 2020). Fu et al. (2014) reported 69 detrital zircon ages ranging from ca. 2636 Ma to 429 Ma for the late Silurian to earliest Devonian molasse strata. These rocks have a major ca. 430 Ma age peak and two minor age peaks at ca. 900 Ma and ca. 1830 Ma (Fig. 11). The age spectra of the early Paleozoic strata suggest that their source was the adjacent Kunlun-Qaidam terrane and linked South Tarim continent.

A regional angular unconformity occurs between Devonian and older strata within the combined Kunlun-Qaidam continent, which suggests a phase of Silurian uplift and orogeny, followed by Devonian postorogenic extension and deposition of volcano-sedimentary rocks. Detrital zircon U-Pb ages of the Devonian lower

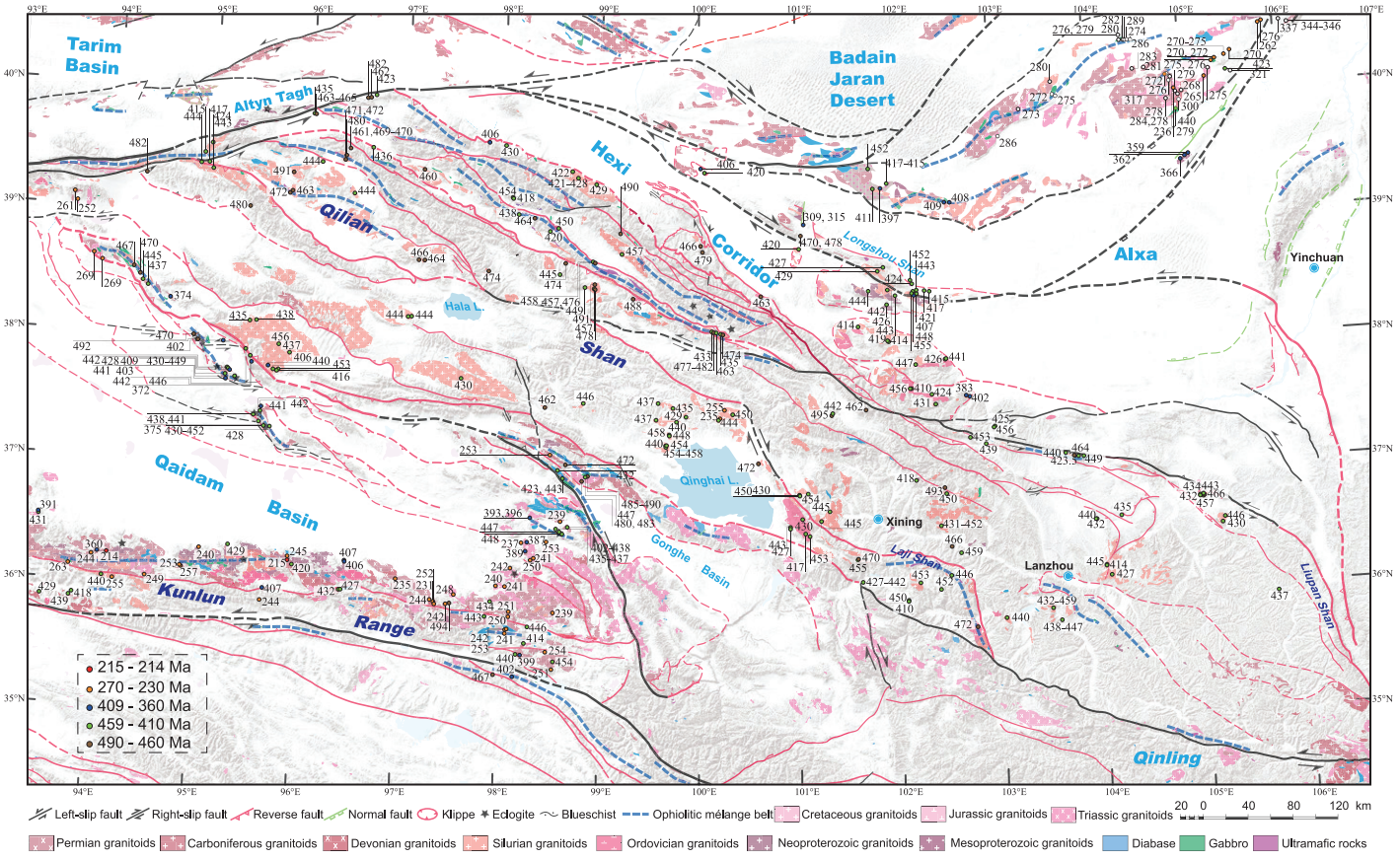

Figure 10. Simplified tectonic map of northern Tibet showing new and existing magmatic ages (in Ma). Data are compiled from Liu et al. (2024b), Wu et al. (2019a, 2022a) and references therein, and this study.

molasse are ca. 3300–408 Ma, with three major age peaks at ca. 420 Ma, ca. 920 Ma, and ca. 2480 Ma (Fig. 11; e.g., Qian et al., 2018b, 2021b; Feng et al., 2015; Zhang et al., 2019a). These strata were also likely sourced from the adjacent Kunlun-Qaidam continent. Rhyolites within the Devonian section yield crystallization ages of ca. 392–375 Ma (Fig. 11; Kou et al., 2017), and the youngest detrital zircon U-Pb age is ca. 365 Ma from the Upper Devonian section (Zhang et al., 2019a). Upper Devonian strata in the northern Qaidam continent have major zircon age peaks at ca. 380 Ma, ca. 925 Ma, ca. 1000 Ma, and ca. 2350 Ma (Fig. 11; Zhang et al. 2019a), which suggest that the central Qilian terrane was a sediment source in addition to the Kunlun-Qaidam continent. Given that the deposition of the Devonian strata was broadly coeval with the emplacement of extension-related, A-type granites in the region (e.g., Wu et al., 2016), we interpret that the Devonian strata were deposited in an intra-arc, extensional basin. We note that all of the pre-Devonian metamorphic rocks in the northern Qaidam continent are bounded by north-dipping Cenozoic thrust faults, and that exposures of the epidote-amphibolite–facies and ultrahigh-pressure metamorphic rocks are controlled by Cenozoic deformation (Yin et al., 2007b; Menold et al., 2009, 2016). Carboniferous strata above a regional unconformity yield detrital zircon U-Pb ages with five major age peaks at ca. 430 Ma, ca. 820 Ma, ca. 935 Ma, ca. 1925 Ma, and ca. 2350 Ma and a maximum depositional age of ca. 335 Ma (Fig. 11; e.g., Sun et al., 2022). These Carboniferous rocks may have been sourced from the Qilian orogen in the north and adjacent northern Qaidam continent. Permian strata are dominated by ca. 300 Ma and ca. 440 Ma age peaks and have a maximum depositional age of ca. 275 Ma (Fig. 11; e.g., Sun et al., 2022), which indicates that the Kunlun arc in the south was an additional source area.

Triassic strata are thrust over the pre-Mesozoic rocks, which yield an age distribution similar to the Permian strata (Fig. 11; e.g., Peng et al., 2015). Previous workers interpreted that the Permian–Triassic strata were deposited in an intra-arc setting (Sun et al., 2022). During the Jurassic, the Qaidam continent experienced extension. The stratigraphy, U-Pb ages, and Hf isotope results, along with detrital provenance constraints, suggest that the sediments of the Lower Jurassic section (i.e., age peaks at ca. 266 Ma, ca. 420 Ma, ca. 850 Ma, and ca. 2430 Ma; Fig. 11) were mainly derived from the adjacent northern Qaidam continent and Altyn Tagh, Qilian, and Eastern Kunlun orogens (e.g., Yu et al., 2017, 2019b; Liu et al., 2017; Wu et al., 2019a; Zhao et al., 2020a, 2020b; Qian et al., 2018b, 2021b; Lu et al., 2019). During the Middle to Late Jurassic, the primary source areas were the Qilian and Eastern Kunlun orogens (i.e., age peaks of ca. 240 Ma, ca. 450 Ma, ca. 930 Ma, ca. 2440 Ma; age peaks of ca. 230 Ma, ca. 420 Ma, ca. 940 Ma, and ca. 2500 Ma; Fig. 11; e.g., Yu et al., 2017, 2019b; Liu et al., 2017; Wu et al., 2019b; Zhao et al., 2020a, 2020b; Qian et al., 2018b, 2021b; Lu et al., 2019; Zhang et al., 2020). From this, we interpret that the Jurassic depositional environment evolved from a series of small-scale, scattered rifts during the Early Jurassic to a larger, unified rift basin during the Middle Jurassic (e.g., Qian et al., 2021a). A disconformity or angular unconformity exists between the Jurassic and overlying Cretaceous strata, and Upper Cretaceous strata are absent (Wu et al., 2011; Zhang et al., 2020). The Lower Cretaceous strata in the Qaidam continent mainly consist of deltaic, fluvial, and allu-

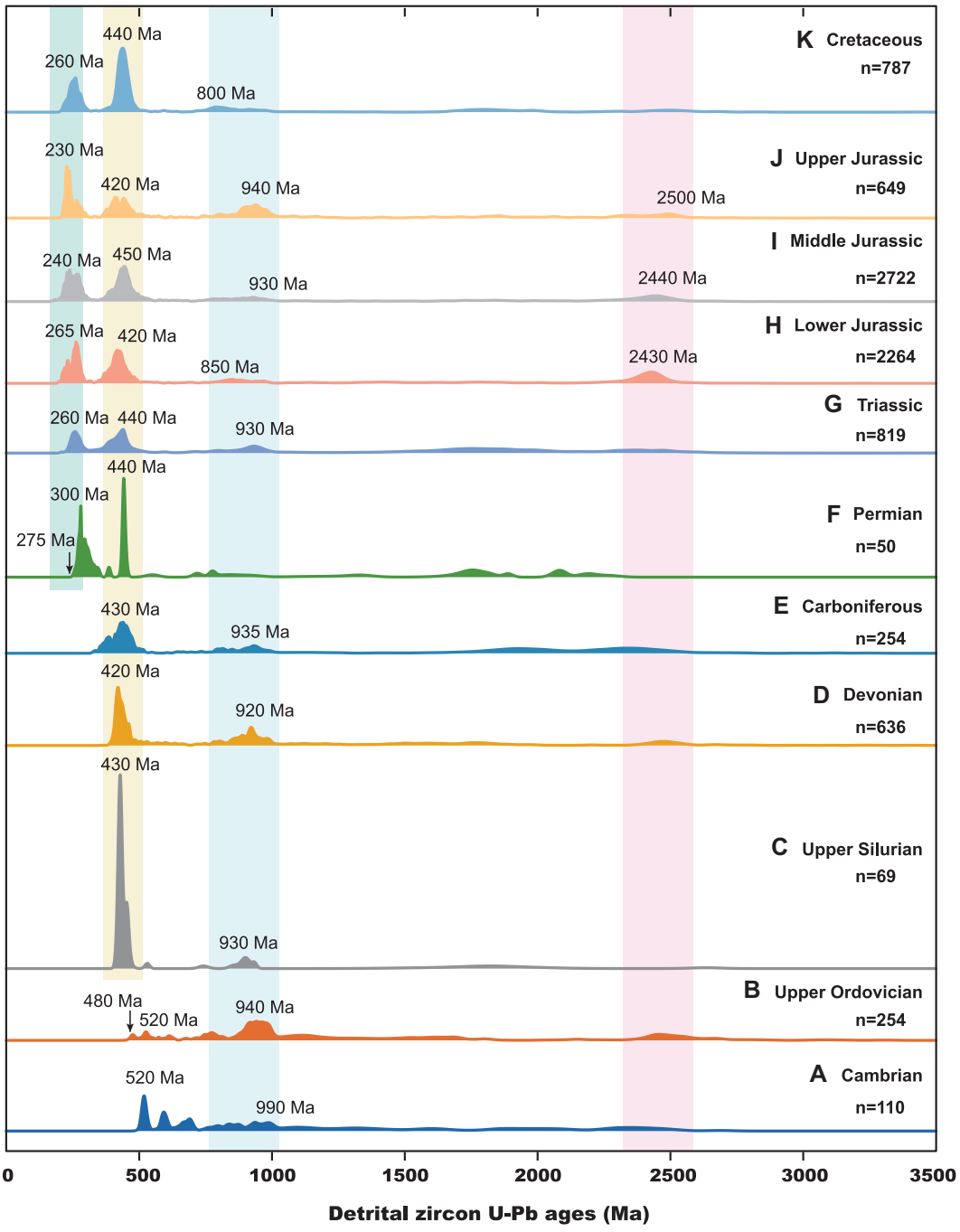

Figure 11. Normalized probability plot of detrital zircon ages from Paleozoic–Mesozoic strata in the northern Qaidam continent: (A) Cambrian strata; (B) Upper Ordovician strata; (C) Upper Silurian strata; (D) Devonian strata; (E) Carboniferous strata; (F) Permian strata; (G) Triassic strata; (H) Lower Jurassic strata; (I) Middle Jurassic strata; (J) Upper Jurassic strata; (K) Cretaceous strata. Data sources: Sun et al. (2020, 2022); Qin et al. (2018); Feng et al. (2015); Fu et al. (2014); Qian et al. (2021a, 2021b); Peng et al. (2015); Zhao et al. (2020a, 2020b); Yu et al. (2017, 2019c); Zhang et al. (2020); Liu et al. (2017); Lu et al. (2019); this study.

vial sandstone and conglomerate, representing orogeny-related molasse deposits with possible provenance in the nearby Qilian orogen to the north, based on southward paleocurrent observations (i.e., age peaks at ca. 260 Ma and ca. 440 Ma, minor ca. 800 Ma, ca. 1780 Ma, and ca. 2500 Ma; Fig. 11; e.g., Lu et al., 2019; Yu et al., 2019b; Zhang et al., 2020). However, the Lower Cretaceous strata yield a large number of Permian–Triassic zircon grains (Fig. 11), which must have been sourced from the nearby Kunlun magmatic arc and Permian–Triassic magmatic arc of the northern Qaidam continent. We also note that Cretaceous strata contain ca. 800–700 Ma zircon grains (Fig. 11), which are similar to the basement rock ages of the western South China craton. Although the source areas for the Lower Cretaceous strata are generally similar to those of the Triassic strata in the Qaidam continent, the Cretaceous landscape must have been much more subdued compared to that in the Triassic (e.g., Wu et al., 2016).

The Cenozoic Qaidam Basin is the largest topographic depression inside Tibet (e.g., Yin et al., 2002; Rieser et al., 2005; Chen et al., 2011; Wang et al., 2017; Wu et al., 2019b), formed as a broad synclinorium bounded by active thrust faults that initiated at ca. 50 Ma in the north and ca. 30–20 Ma in the south (Yin et al., 2008b). The south-directed North Qaidam thrust system juxtaposes Jurassic and older rocks atop Cenozoic strata in the northern Qaidam continent (Yin et al., 2008a). The Cenozoic Qaidam Basin experienced a continuous tectonic history during which sedimentary rock types changed in response to basin-margin deformation. Detrital

zircon results clearly distinguish middle Eocene sandstone of the lower and upper Xiaganchaigou Formation from late Oligocene–Pliocene sandstone (e.g., Wu et al., 2019b; McRivette et al., 2019). Age characteristics of the Songpan-Ganzi terrane to the south are recognized in Paleogene Qaidam strata but are absent in younger Qaidam strata. This suggests the emergence of a topographic barrier in the Neogene (e.g., Wu et al., 2019b; McRivette et al., 2019).

6.3. Paleozoic–Mesozoic Tectonic Evolution of the Qaidam Continent

The Paleozoic–Mesozoic geologic history of the Qaidam continent is closely associated with the tectonic evolution of the early Paleozoic Qilian and Altyn Tagh orogens and late Paleozoic to early Mesozoic Eastern Kunlun orogen. Wu et al. (2020, 2022a) reviewed the magmatic records, paleocrustal thickness, tectonostratigraphy, and detrital zircon age populations of these orogens and suggested that the rocks northwest of the Altyn Tagh fault in the northern Qaidam continent were located adjacent to the Qilian Shan prior to slip along the Altyn Tagh fault. Based on new and previous field observations and analytical results for the northern Qaidam continent, we present a revised, comprehensive model of the Paleozoic–Mesozoic tectonic evolution of northern Tibet. In many reconstructions of the northern Qaidam continent, exposures of discontinuous ultrahigh-pressure metamorphic rocks, rare and undefined mélange complexes, and plutons have been used as evidence for continental collision in the early Paleozoic and/or early Mesozoic. However, any viable model for the tectonic evolution of the northern Qaidam continent must explain the following key observations. First, the original configuration of the northern Qaidam continent was modified by Ordovician arc magmatism, protracted Silurian–Devonian continental collision, Mesozoic extension, and Cenozoic intracontinental deformation. Second, early Paleozoic arc magmatism overlaps spatially and temporally with ophiolite ultrahigh-pressure metamorphism. In addition, the eclogite-bearing rocks experienced ultrahigh-pressure metamorphism followed by amphibolite-facies overprinting, but the ophiolite rocks do not show evidence of higher metamorphic conditions than epidote-amphibolite facies (Menold et al., 2009). These dispersed ophiolites are observed throughout the Qilian Shan and northern Qaidam continent. Third, Paleozoic ultrahigh-pressure continental and oceanic rocks in the Altyn-Tagh Range correlate with those in the northern Qaidam continent and Qilian Shan. Specifically, metamorphic rocks exposed at Jianggelesayi and Bashiwake in the Altyn-Tagh Range are correlative to (1) ultrahigh-pressure rocks in the northern Qaidam continent (Mattinson et al., 2007; Zhang et al., 2001; Yang et al., 2001; Yin and Harrison, 2000); (2) early Paleozoic magmatic arc granitoids throughout northern Tibet; (3) Cambrian ophiolites, including suprasubduction zone ophiolites (Song et al., 2013); (4) ophiolitic mélange in the Qilian Shan; and (5) early Paleozoic blueschist and eclogite in the northern Qilian Shan and Altyn-Tagh Range (e.g., Wu et al., 1993; Liu et al., 2006; Song et al., 2006, 2007; Zhang et al., 2007; Xiao et al., 2009). Fourth, a regional angular unconformity occurs between Devonian and older strata in the combined Kunlun-Qaidam continent. Fifth, a Carboniferous magmatic lull occurred in northern Tibet, and a Carboniferous rift sequence was deposited in the Kunlun-Qaidam continent. Sixth, Permian–Triassic (ca. 270–195 Ma) arc magmatism across the Kunlun-Qaidam terrane lasted until at least ca. 195 Ma in the Eastern Kunlun Range and ceased by ca. 214 Ma in the northern Qaidam continent. Below, we summarize key events of the Paleozoic–Mesozoic tectonic evolution of northern Tibet that support our present understanding of the Qaidam continent.

One or two potentially connected seaways, referred to as the Qilian Ocean(s), existed from ca. 550 Ma to 445 Ma, as evidenced by the distribution of suprasubduction zone ophiolites (ca. 540–500 Ma) within the North China craton, central Qilian terrane, and Kunlun-Qaidam continent (Fig. 12A; e.g., Shi et al., 2004; Smith, 2006; Xiang et al., 2007; Tseng et al., 2007, 2009b; Zhang et al., 2007; Xia and Song, 2010; Song et al., 2013; Zuza et al., 2018; Fu et al., 2018, 2019, 2020b, 2022a, 2022b, 2023). These oceans were formed within and along the margin of the Laurasia supercontinent. The oceans reached their maximum extent in the Cambrian, prior to subduction initiation in the latest Cambrian (e.g., Zuza et al., 2018; Wu et al., 2022a). The distribution of Cambrian ophiolites and marine strata exposed throughout the Qilian Shan and northern Qaidam continent may be the result of early Paleozoic complex mélange/ophiolite obduction, ophiolite underthrusting, or strike-slip duplication, which was supported by a trench-parallel, right-lateral shear zone within the Qilian magmatic arc (e.g., Şengör and Natal'in, 1996; Wu et al., 2017, 2024; Zuza et al., 2018; Allen et al., 2023). Such distributions may have been further modified by later Mesozoic and Cenozoic deformation (e.g., Zuza et al., 2018).

The consumption and closure of the Qilian Ocean basin(s) may have been accommodated by either a single south-dipping subduction zone or a bidirectional north- and south-dipping subduction system. The bidirectional north- and south-dipping subduction model for the closure of the Qilian Ocean is supported by evidence from a magnetotelluric sounding profile across northern Tibet and observations from the Sunan-Laohushan and Yushigou-Yieniugou-Qingshuigou ophiolitic mélange complexes and Ordovician–Silurian arc belt in the Qilian Shan and North China craton (Fig. 12A; e.g., Wu et al., 2022a; Li et al., 2021). The alternative model is that a single south-dipping subduction zone was formed while the Qilian oceanic lithosphere subducted southward beneath the northern margin of the Qaidam continent (Fig. 12B; e.g., Gehrels et al., 2003; Wu et al., 2016, 2022a; Zuza et al., 2018). Arc magmatism, subduction, and continental collision occurred from ca. 500 Ma to 400 Ma, as evidenced by the distribution of arc-related and syncollisional plutons (Fig. 12A; Qian et al., 1998; Cowgill et al., 2003; Gehrels et al., 2003a; Su et al., 2004; Wu et al., 2004, 2006a, 2016; Hu et al., 2005; Liu et al., 2006; Quan et al., 2006; He et al., 2008; Tseng et al., 2009a; Dang, 2011; Xia et al., 2012; Xiao et al., 2012; Xiong et al., 2012; Song et al., 2013; Allen et al., 2023). The closure of one or two Qilian oceans followed counterclockwise rotation of a peninsular Qaidam continent toward the North China craton. This interpretation is supported by the intra-arc, strike-slip fault and westward-tapering, map-view geometry of Silurian flysch basins in the Qilian Shan and northern Qaidam continent (Figs. 12A and 12B; Zuza et al., 2018; Wu et al., 2024). Continental collision occurred at ca. 445–440 Ma (Wu et al., 2016; Zuza et al., 2018), and postcollisional extension terminated by ca. 360 Ma. Silurian strata have been classified as flysch deposits that transition to Devonian molasse rocks. Based on similar lithologic assemblages, the South Qilian suture in the Qilian orogen probably connects with the Erlangping Group in the Qinling orogen suture in the southeast (e.g., Ratschbacher et al., 2003; Xu et al., 2008; Tseng et al., 2009a; Dong et al., 2011a; Wu et al., 2016) and Altyn Tagh suture in the Altyn-Tagh Range in the southwest. This connection forms a >1000-km-long, laterally continuous, early Paleozoic orogenic belt. In this context, the Paleozoic magmatic evolution of the northern Qaidam continent from ca. 490 Ma to 360 Ma was associated with southward subduction of South Qilian oceanic lithosphere, collision between the Central Qilian terrane and Qaidam continent, and postcollisional extension (e.g., Wu et al., 2016; Zuza et al., 2018).

The early Paleozoic magmatic arc sequence and tectonic setting in the northern Qaidam continent support this interpreted tectonic history.

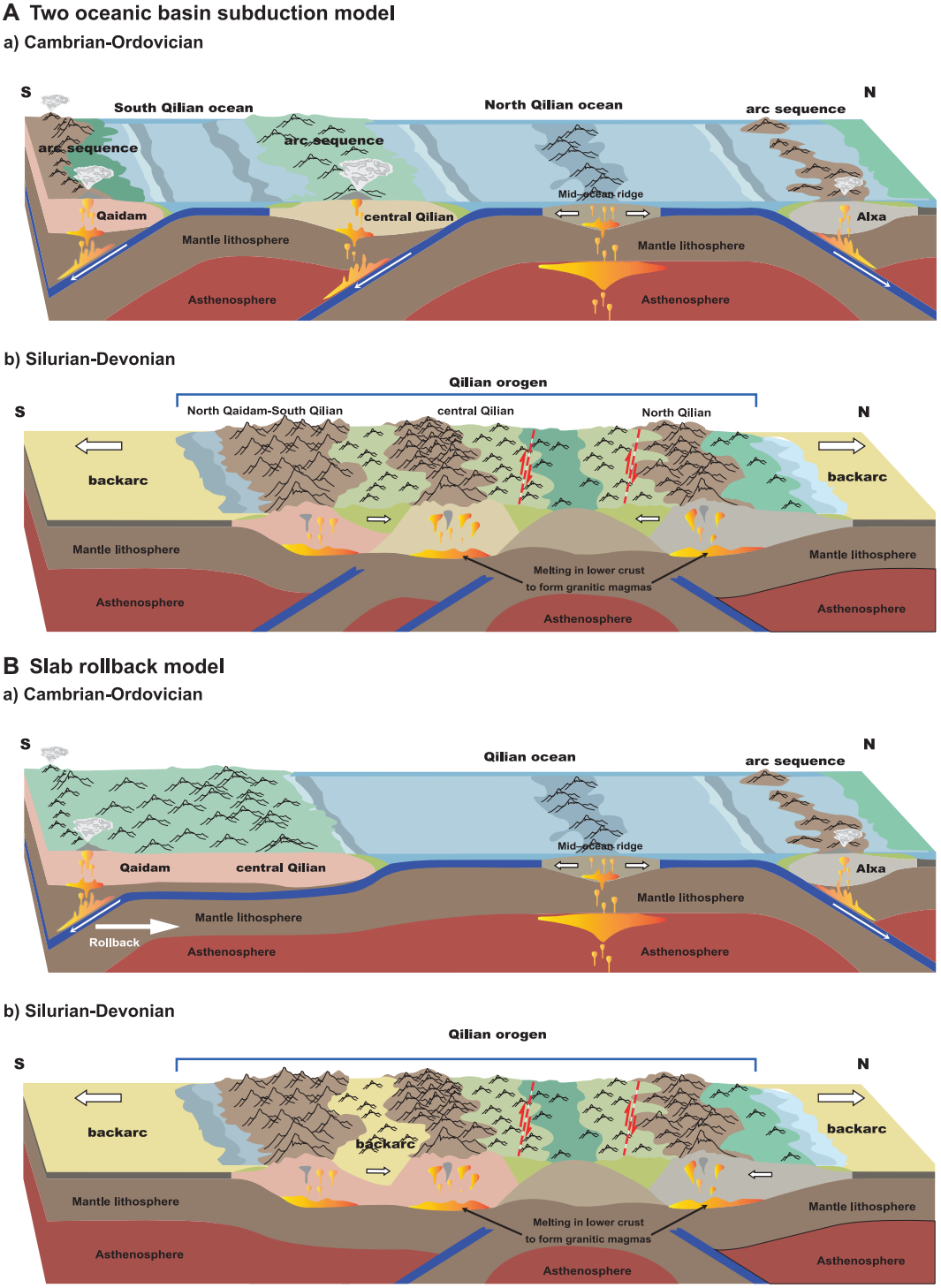

Figure 12. Schematic block diagrams showing the Cambrian–Devonian tectonomagmatic evolution of the northern Qaidam continent and Qilian Shan, northern Tibet. (A) Two oceanic basin subduction model involving (a) Cambrian–Ordovician oceanic subduction and (b) Silurian–Devonian continental collision. (B) Slab rollback model involving (a) Cambrian–Ordovician oceanic slab subduction and rollback and (b) Silurian–Devonian continental collision.

We calculated paleocrustal thickness estimates from exposed plutonic rocks using their trace-element geochemistry. Specifically, the ratio between light and heavy rare earth elements (LREE/HREE) in these rocks can be used to track changes in crustal thickness based on varying stabilities of garnet and/or plagioclase in the residual melts (e.g., Profeta et al., 2015). We determined paleocrustal thicknesses using the calibration of Sundell et al. (2021) plotted against granitoid crystallization ages for the northern Qaidam continent and Qilian Shan. These plots show substantial scatter, similar to other applications of this method (e.g., Chapman et al., 2015; Sundell et al., 2021), but there are clear trends of crustal thickening during the Ordovician–Silurian (Fig. 13A). Crustal thickening during this time is consistent with observed Phanerozoic unconformities that would have resulted during uplift-related erosion. In addition, both regions display a subtle thinning trend from the early Silurian to Devonian–early Carboniferous (Fig. 13A), which may reflect postorogenic extension.

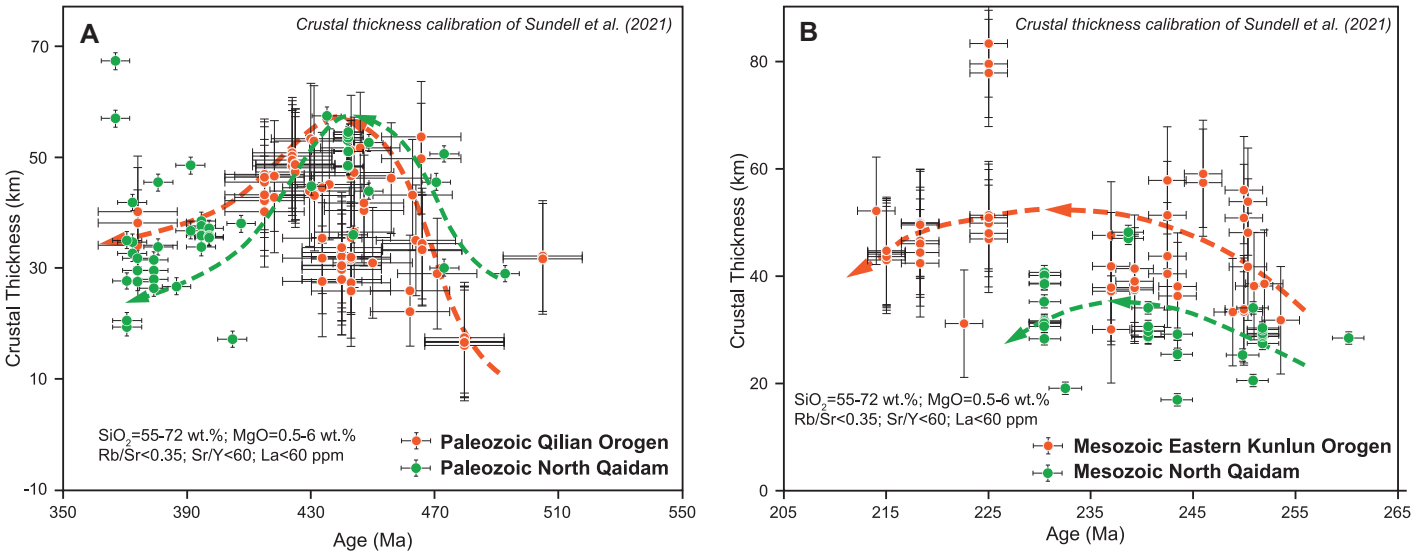

Figure 13. Plots of age versus crustal thickness for the (A) the Paleozoic northern Qaidam continent and Qilian Shan and (B) Mesozoic Eastern Kunlun orogen and northern Qaidam continent, based on the La/Yb(n) calibration of Sundell et al. (2021). Geochemical data are listed in Table S5 (see text footnote 1). Data sources: Li et al. (2023b); Peng et al. (2016); Wu et al. (2004, 2009b, 2014, 2019c); Gu et al. (2018); Wang et al. (2014, 2017); Shao et al. (2018); Meng et al. (2005); Meng and Zhang (2008); Zhao et al. (2017); Gao et al. (2022); Zhu et al. (2014).

The Carboniferous magmatic lull in the combined Kunlun-Qaidam continent was accompanied by passive-margin sedimentation following continental rifting of the Songpan-Ganzi terrane in the south (i.e., Wu et al., 2016; Tang et al., 2023). This rifting opened the Neo-Kunlun Ocean, which has been assigned as part of the Paleo-Tethys domain by Şengör (1984). The development of the wide (>800 km) Permian–Triassic magmatic arc (ca. 270–195 Ma) across the Kunlun-Qaidam continent was induced by flat northward subduction, followed by rapid slab rollback and collision between the Qaidam continent and Songpan-Ganzi terrane (Fig. 14; e.g., Wu et al., 2016, 2019a, 2022a). We interpret that the southward-younging trend of magmatic cessation ages was the result of southward steepening of the subducting Neo-Kunlun oceanic slab

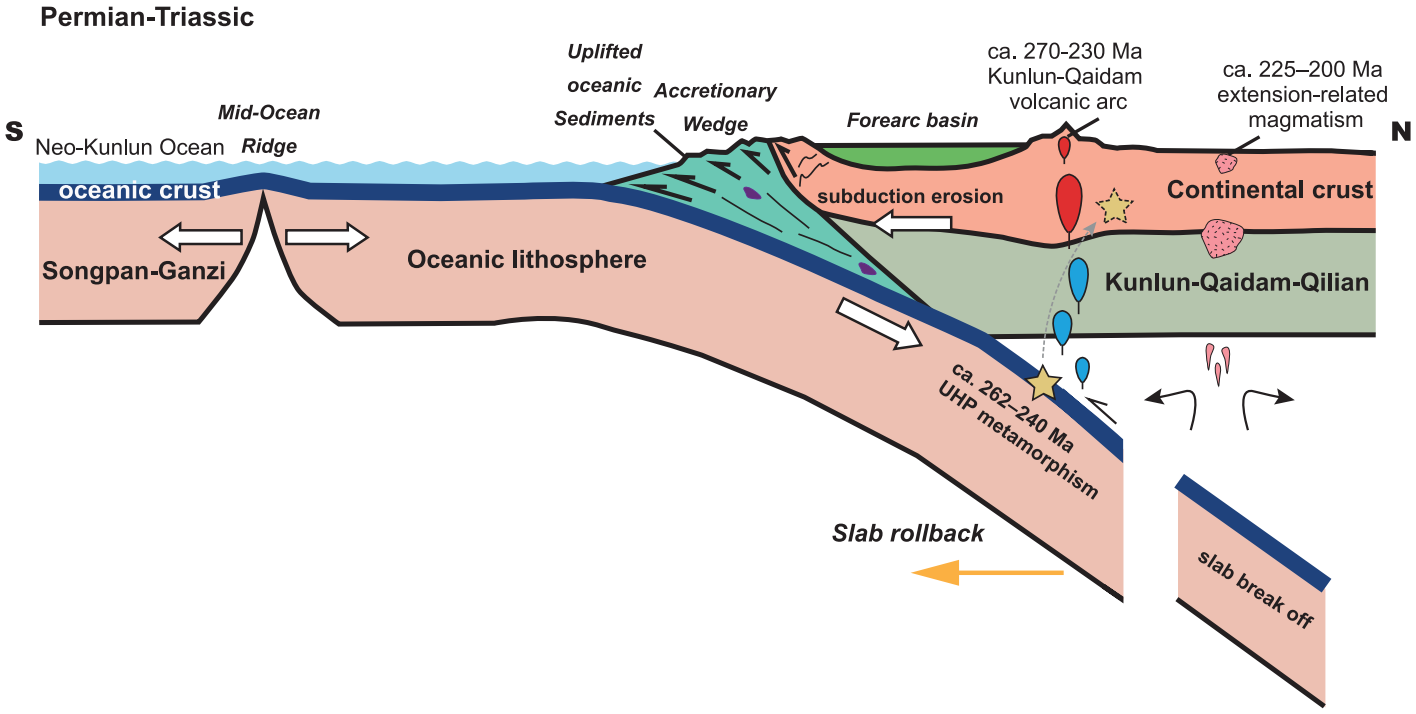

Figure 14. Schematic cross section showing the Permian–Triassic tectonomagmatic setting of the northern Qaidam continent and Eastern Kunlun Range, northern Tibet. UHP—ultrahigh pressure.

(i.e., Wu et al., 2016). In this model, Permian–Triassic subduction-related arc magmatism (ca. 270–230 Ma) and emplacement of extension-related granitoids (ca. 215–214 Ma) occurred in the northern Qaidam continent (Fig. 9) associated with Neo-Kunlun subduction and slab rollback, respectively (e.g., Wu et al., 2016, 2019a).

As discussed above, slab rollback probably occurred from ca. 225 Ma in the South Qilian Shan to ca. 195 Ma in the Eastern Kunlun Range (Fig. 14), as indicated by the late Permian and Early Jurassic younging trend of magmatic arc rocks (Wu et al., 2016, 2019a). The ca. 262–240 Ma Dulan eclogite is located ~100 km north of the Permian–Triassic Kunlun magmatic arc and suture zone, which suggests that the mid-crustal emplacement of ultrahigh-pressure rocks far within the plate interior was controlled by northward flat subduction and subsequent rollback of the Neo-Kunlun oceanic slab and upper-plate extension (Wu et al., 2023). This interpreted tectonic history is supported by records of subtle late Permian–Middle Triassic paleocrustal thickening trends and Late Triassic rapid thinning in the northern Qaidam continent and Eastern Kunlun Range (Fig. 13B). Based on similar lithologic assemblages and ultrahigh-pressure metamorphic events (Fig. 14), the Neo-Kunlun suture in the Eastern Kunlun orogen probably connects with the Mianlue suture in the Qinling orogen and Dabie orogen to the east (e.g., Ratschbacher et al., 2003; Lu et al., 2009; Dong and Santosh, 2016; Wu et al., 2016, 2023), forming an ~3000-km-long late Paleozoic to early Mesozoic orogenic belt. To the south, the triangular-shaped Songpan-Ganzi terrane exposes a Triassic turbidite sequence. The stability of its source areas throughout the Triassic suggests the presence of a long-lived marine basin with pre-Triassic oceanic/continental basement rocks trapped between converging continental blocks (e.g., Ding et al., 2013; Tang et al., 2023). Northern Tibet experienced postcollisional extension and intracontinental deformation since the Jurassic (e.g., Yin and Harrison, 2000; Wu et al., 2019b). Jurassic extension resulted in the exhumation of older strata, and regional extension continued during the Cretaceous.

7. CONCLUSIONS

The Qaidam continent in northern Tibet experienced two major Phanerozoic magmatic and collisional events in the early Paleozoic and late Paleozoic–Mesozoic. By integrating new and previous magmatic and tectonostratigraphic records of the northern Qaidam continent together with other records across northern Tibet, we developed a comprehensive model for the Paleozoic–Mesozoic tectonic evolution of the Tarim–North China craton, including the role of the Qaidam continent. Circa 490–360 Ma magmatism in the northern Qaidam continent was associated with southward subduction of South Qilian oceanic lithosphere (ca. 490–460 Ma), continental collision (ca. 460–410 Ma), and postcollisional extension (ca. 410–360 Ma). The northern Qaidam continent contains a regional angular unconformity between Devonian and older strata, and all pre-Devonian metamorphic rocks are bounded by a north-dipping Cenozoic thrust. Furthermore, the present-day exposure of epidote-amphibolite–facies and ultrahigh-pressure metamorphic rocks in the northern Qaidam continent was controlled by Cenozoic deformation. Early Paleozoic arc magmatism overlaps spatially and temporally with ultrahigh-pressure metamorphism and the emplacement of an ophiolite complex in the northern Qaidam continent. A Carboniferous magmatic lull occurred coeval with the development of a passive margin following extension. Permian–Triassic subduction-related arc magmatism (ca. 270–230 Ma) and the emplacement of granitoids during extension (ca. 215–214 Ma) were associated with subduction and slab rollback of Neo-Kunlun oceanic lithosphere, respectively. In this tectonic evolution, the northern Qaidam continent did not develop during a distinct orogenic cycle as previously interpreted.

ACKNOWLEDGMENTS

We appreciate the efficient editorial handling of science editor Mihai Ducea, associate editor Tim Kusky, and two constructive reviews. This research and the ideas presented within this paper benefited from discussions with the late An Yin over the past decade. This research was supported by grants from the National Natural Science Foundation of China (project no. 42372256), the Basic Science Center for Tibetan Plateau Earth System (grant 41988101), the Second Tibetan Plateau Scientific Expedition and Research Program (grant 2019QZKK0708), and the Tectonics Program of the U.S. National Science Foundation (grants EAR 1914503 and EAR 1914501).

REFERENCES CITED

Allen, M.B., Song, S., Wang, C., Zeng, R., and Wen, T., 2023, An oblique subduction model for closure of the Proto-Tethys and Palaeo-Tethys oceans and creation of the Central China orogenic belt: Earth-Science Reviews, v. 240, https://doi.org/10.1016/j.earscirev.2023.104385.

Andersen, T., 2002, Correction of common lead in U-Pb analyses that do not report ^{204}Pb: Chemical Geology, v. 192, p. 59–79, https://doi.org/10.1016/S0009-2541(02)00195-X.

Badarch, G., Cunningham, W.D., and Windley, B.F., 2002, A new terrane subdivision for Mongolia: Implications for the Phanerozoic crustal growth of Central Asia: Journal of Asian Earth Sciences, v. 21, no. 1, p. 87–110, https://doi.org/10.1016/S1367-9120(02)00017-2.

Bian, Q.T., Li, D.H., Pospelov, I., Yin, L.M., Li, H.S., Zhao, D.S., Chang, C.F., Luo, X.Q., Gao, S.L., Astrakhantsev, O., and Chamov, N., 2004, Age, geochemistry and tectonic setting of Buqingshan ophiolites, north Qinghai-Tibet Plateau, China: Journal of Asian Earth Sciences, v. 23, no. 4, p. 577–596, https://doi.org/10.1016/j.jseaes.2003.09.003.

Biske, Y.S., and Seltmann, R., 2010, Paleozoic Tian-Shan as a transitional region between the Rheic and Urals-Turkestan oceans: Gondwana Research, v. 17, no. 2–3, p. 602–613, https://doi.org/10.1016/j.gr.2009.11.014.

Bovet, P.M., Ritts, B.D., Gehrels, G., Abbink, A.O., Darby, B., and Hourigan, J., 2009, Evidence of Miocene crustal shortening in the north Qilian Shan from Cenozoic stratigraphy of the western Hexi Corridor, Gansu Province, China: American Journal of Science, v. 309, p. 290–329, https://doi.org/10.2475/00.4009.02.

Boynton, W.V., 1984, Cosmochemistry of the rare earth elements: Meteorite studies, *in* Henderson, P., ed., Rare Earth Element Geochemistry: Amsterdam, Elsevier, p. 63–114, https://doi.org/10.1016/B978-0-444-42148-7.50008-3.

Bush, M.A., Saylor, J.E., Horton, B.K., and Nie, J., 2016, Growth of the Qaidam Basin during Cenozoic exhumation in the northern Tibetan Plateau: Inferences from depositional patterns and multiproxy detrital provenance signatures: Lithosphere, v. 8, no. 1, p. 58–82, https://doi.org/10.1130/L449.1.

Cao, Y.T., Liu, L., Chen, D.L., Wang, C., Yang, W.Q., Kang, L., and Zhu, X.H., 2017, Partial melting during exhumation of Paleozoic retrograde eclogite in North Qaidam, western China: Journal of Asian Earth Sciences, v. 148, p. 223–240, https://doi.org/10.1016/j.jseaes.2017.09.009.

Chapman, J.B., Ducea, M.N., DeCelles, P.G., and Profeta, L., 2015, Tracking changes in crustal thickness during orogenic evolution with Sr/Y: An example from the North American Cordillera: Geology, v. 43, p. 919–922, https://doi.org/10.1130/G36996.1.

Che, Z.C., and Sun, Y., 1996, The age of the Altun granulite facies complex and the basement of the Tarim basin: Regional Geology of China, v. 56, p. 51–57 [in Chinese with English abstract].

Chen, D.L., Liu, L., Sun, Y., Sun, W.D., Zhu, X.H., Liu, X.M., and Guo, C.L., 2012a, Felsic veins within UHP eclogite at Xitieshan in North Qaidam, NW China: Partial melting during exhumation: Lithos, v. 136–139, p. 187–200, https://doi.org/10.1016/j.lithos.2011.11.006.

Chen, L., Yan, Z., and Fu, C.L., 2022, Sedimentary environment and tectonic setting of the clastic formation of the Tanjianshan Group in the Tuomoerrite area, North Qaidam: Acta Petrologica Sinica (Yanshi Xuebao), v. 38, no. 3, p. 777–792, https://doi.org/10.18654/1000-0569/2022.03.11 [in Chinese with English abstract].

Chen, X.H., Yin, A., Gehrels, G.E., Cowgill, E.S., Grove, M., Harrison, T.M., and Wang, X.F., 2003, Two phases of Mesozoic north-south extension in the eastern Altyn Tagh range, northern Tibetan Plateau: Tectonics, v. 22, 1053, https://doi.org/10.1029/2001TC001336.

Chen, X.H., Gehrels, G., Yin, A., Li, L., and Jiang, R.B., 2012b, Paleozoic and Mesozoic basement magmatisms of eastern Qaidam Basin, northern Qinghai-Tibet Plateau: LA-ICP-MS zircon U-Pb geochronology and its geological significance: Acta Geologica Sinica, v. 86, no. 2, p. 350–369, https://doi.org/10.1111/j.1755-6724.2012.00665.x.

Chen, X.H., Gehrels, G.E., Yin, A., Zhou, Q., and Huang, P.H., 2015, Geochemical and Nd-Sr-Pb-O isotopic constraints on Permo–Triassic magmatism in eastern Qaidam Basin, northern Qinghai–Tibetan Plateau: Implications for the evolution of the Paleo-Tethys: Journal of Asian Earth Sciences, v. 114, p. 674–692, https://doi.org/10.1016/j.jseaes.2014.11.013.

Chen, Y.X., et al., 2011, Zircon U-Pb age of Xiaomiao Formation of Proterozoic in the eastern section of the East Kunlun orogenic belt: Geoscience (Xiandai Dizhi), v. 25, p. 510–521 [in Chinese with English abstract].

Cheng, F., Fu, S.T., Jolivet, M., Zhang, C.H., and Guo, Z.J., 2016, Source to sink relation between the Eastern Kunlun Range and the Qaidam Basin, northern Tibetan Plateau, during the Cenozoic: Geological Society of America Bulletin, v. 128, p. 258–283, https://doi.org/10.1130/B31260.1.

Cheng, F., Jolivet, M., Hallot, E., Zhang, D., Zhang, C., and Guo, Z., 2017, Tectono-magmatic rejuvenation of the Qaidam craton, northern Tibet: Gondwana Research, v. 49, p. 248–263, https://doi.org/10.1016/j.gr.2017.06.004.

Cowgill, E., Yin, A., Harrison, T.M., and Wang, X.F., 2003, Reconstruction of the Altyn Tagh fault based on U-Pb

geochronology: Role of back thrusts, mantle sutures, and heterogeneous crustal strength in forming the Tibetan Plateau: Journal of Geophysical Research: Solid Earth, v. 108, no. B7, https://doi.org/10.1029/2002JB002080.

Dang, J.H., 2011, Geochemical characteristics and tectonic implications of Jinfosi granite in north Qilian: Gansu Geology, v. 20, no. 2, p. 40–44 [in Chinese with English abstract].

Dewey, J.F., Shackleton, R.M., Chang, C., and Sun, Y., 1988, The tectonic evolution of the Tibetan Plateau: Philosophical Transactions of the Royal Society of London A: Mathematical, Physical and Engineering Sciences, v. 327, no. 1594, p. 379–413, https://doi.org/10.1098/rsta.1988.0135.

Ding, L., Yang, D., Cai, F.L., Pullen, A., Kapp, P., Gehrels, G.E., Zhang, L.Y., Zhang, Q.H., Lai, Q.Z., Yue, Y.H., and Shi, R.D., 2013, Provenance analysis of the Mesozoic Hoh-Xil-Songpan-Ganzi turbidites in northern Tibet: Implications for the tectonic evolution of the eastern Paleo-Tethys Ocean: Tectonics, v. 32, p. 34–48, https://doi.org/10.1002/tect.20013.

Dong, Y., Zhang, G., Neubauer, F., Liu, X., Genser, J., and Hauzenberger, C., 2011a, Tectonic evolution of the Qinling orogen, China: Review and synthesis: Journal of Asian Earth Sciences, v. 41, no. 3, p. 213–237, https://doi.org/10.1016/j.jseaes.2011.03.002.

Dong, Y., He, D., Sun, S., Liu, X., Zhou, X., Zhang, F., Yang, Z., Cheng, B., Zhao, G.C., and Li, J., 2018, Subduction and accretionary tectonics of the East Kunlun orogen, western segment of the Central China orogenic system: Earth-Science Reviews, v. 186, p. 231–261, https://doi.org/10.1016/j.earscirev.2017.12.006.

Dong, Y.P., and Santosh, M., 2016, Tectonic architecture and multiple orogeny of the Qinling orogenic belt, central China: Gondwana Research, v. 29, no. 1, p. 1–40, https://doi.org/10.1016/j.gr.2015.06.009.

Dong, Z.C., Xiao, P.X., Xi, R.G., Guo, L., and Gao, X.F., 2011b, Geochemical characteristics and isotopic dating of bojites in the tectonic mélange belt on the south margin of Altun: Geological Review (Dizhi Lunping), v. 57, no. 2, p. 207–216.

Dong, Z.C., Xiao, P.X., Gu, P.Y., Zhang, H.D., Chen, R.M., and Zha, X.F., 2014, Geochemistry and chronology of Yanchangbeishan gabbro in Lenghu area at the west segment of the north margin of Qaidam: Chinese Journal of Geology, v. 49, no. 4, p. 1132–1149 [in Chinese with English abstract].

Dong, Z.C., et al., 2015, Geochronology, geochemistry, and Hf isotopes of Yanchangbeishan adamellite of Lenghu area in Qinghai: Earth Science: Journal of China University of Geosciences, v. 40, no. 1, p. 130–144 [in Chinese with English abstract].

Du, Y., Wang, J., Han, X., and Shi, G.R., 2003, From flysch to molasse-sedimentary and tectonic evolution of late Caledonian–early Hercynian foreland basin in North Qilian Mountains: Earth Science: Journal of China University of Geosciences (Diqiu Kexue), v. 14, no. 1, p. 1–7 [in Chinese with English abstract].

Eby, G.N., 1990, The A-type granitoids: A review of their occurrence and chemical characteristics and speculations on their petrogenesis: Lithos, v. 26, p. 115–134, https://doi.org/10.1016/0024-4937(90)90043-Z.

Eby, G.N., 1992, Chemical subdivision of the A-type granitoids: Petrogenetic and tectonic implications: Geology, v. 20, p. 641–644, https://doi.org/10.1130/0091-7613(1992)020<0641:CSOTAT>2.3.CO;2.

Enkelmann, E., Weislogel, A., Ratschbacher, L., Eide, E., Renno, A., and Wooden, J., 2007, How was the Triassic Songpan-Ganzi basin filled?: A provenance study: Tectonics, v. 26, no. 4, TC4007, https://doi.org/10.1029/2006TC002078.

Feng, Q., Qin, Y., Fu, S.T., Liu, Y.Q., Zhou, D.W., Ma, D.D., and Wang, C.Y., 2015, U-Pb age of detrital zircons and its geological significance from Maoniushan Formation in the Wulan County, northern margin of Qaidam Basin: Acta Sedimentologica Sinica (Chenji Xuebao), v. 33, no. 3, p. 486–499 [in Chinese with English abstract].

Fu, C.L., Yan, Z., Wang, Z.Q., Buckman, S., Aitchison, J.C., Niu, M.L., Cao, B., Guo, X., Li, X., and Li, J., 2018, Lajishankou ophiolite complex: Implications for Paleozoic multiple accretionary and collisional events in the South Qilian belt: Tectonics, v. 37, p. 1321–1346, https://doi.org/10.1029/2017TC004740.

Fu, C.L., Yan, Z., Aitchison, J.C., Xiao, W.J., Buckman, S., Wang, B.Z., Li, W.F., Li, Y.S., and Ren, H.D., 2020a, Multiple subduction processes of the Proto-Tethyan Ocean: Implication from Cambrian intrusions along the North Qilian suture zone: Gondwana Research, v. 87, p. 207–223, https://doi.org/10.1016/j.gr.2020.06.007.

Fu, C.L., Yan, Z., Aitchison, J.C., Xiao, W.J., Buckman, S., Wang, B.Z., Zhai, Q.G., and Cao, B., 2022a, Short-lived intra-oceanic arc-trench system in the North Qaidam belt (NW China) reveals complex evolution of the Proto-Tethyan Ocean: Geological Society of America Bulletin, v. 134, p. 1741–1759, https://doi.org/10.1130/B36127.1.

Fu, D., Kusky, T., Wilde, S.A., Polat, A., Huang, B., and Zhou, Z.P., 2019, Early Paleozoic collision-related magmatism in the eastern North Qilian orogen, northern Tibet: A linkage between accretionary and collisional orogenesis: Geological Society of America Bulletin, v. 131, p. 1031–1056, https://doi.org/10.1130/B35009.1.

Fu, D., Kusky, T.M., Wilde, S.A., Windley, B.F., Polat, A., Huang, B., and Zhou, Z., 2020b, Structural anatomy of the early Paleozoic Laohushan ophiolite and subduction complex: Implications for accretionary tectonics of the Proto-Tethyan North Qilian orogenic belt, northeastern Tibet: Geological Society of America Bulletin, v. 132, p. 2175–2201, https://doi.org/10.1130/B35442.1.

Fu, D., Huang, B., Johnson, T.E., Wilde, S.A., Jourdan, F., Polat, A., Windley, B.F., Hu, Z.C., and Kusky, T., 2022b, Boninitic blueschists record subduction initiation and subsequent accretion of an arc-forearc in the northeast Proto-Tethys Ocean: Geology, v. 50, p. 10–15, https://doi.org/10.1130/G49457.1.

Fu, D., Huang, B., Wilde, S.A., Johnson, T.E., Polat, A., Windley, B.F., Hu, Z.C., Zhou, Z.P., and Kusky, T.M., 2023, The tempo of back-arc basin evolution: Insights from the early Paleozoic Proto-Tethyan North Qilian orogenic belt, northeastern Tibet: Earth and Planetary Science Letters, v. 603, https://doi.org/10.1016/j.epsl.2022.117976.

Fu, J., Liang, X., Wang, C., Jiang, Y., Zhou, Y., Pan, C., Zhong, Y., Yang, Y., and Wang, Z., 2014, Timing and characteristic of provenance of the c Formation in the Tanjianshan Group, Xitieshan, North Qaidam: Acta Geologica Sinica, v. 88, p. 1081–1092 [in Chinese with English abstract].

Gansu Bureau of Geology and Mineral Resources, 1974, Regional Geology of Gansu Province: Beijing, Geological Publishing House, 690 p. [in Chinese].

Gao, G.Y., Li, B.L., Yang, B.H., and Liao, Y.B., 2018, Zircon U-Pb geochronology, geochemistry and Hf isotopics of granite porphyry in Xitieshan area of north margin of Qaidam Basin: Global Geology, v. 37, no. 3, p. 747–760 [in Chinese with English abstract].

Gao, X., Xiao, P., Guo, L., Ding, Z.C., and Xi, R.G., 2011, Opening of an early Paleozoic limited oceanic basin in the northern Altyn area: Constraints from plagiogranites in the Hongliugou-Lapeiquan ophiolitic mélange: Science China Earth Sciences, v. 54, p. 1871–1879, https://doi.org/10.1007/s11430-011-4332-9.

Gao, X., Yu, S., Peng, Y., Lv, P., Wang, M., Liu, Y., Li, S., Jiang, X., Ji, W., and Li, C., 2021, Insights into OIB-like magmatism contemporaneous with oceanic subduction: Petrogenetic constraints on the Kendelong metagabbro in the North Qaidam: Lithos, v. 392–393, https://doi.org/10.1016/j.lithos.2021.106130.

Gao, X., Yu, S., Li, S., Santosh, M., Liu, Y., Jiang, X., Peng, Y., Zhao, S., and Lv, P., 2022, Syn-collisional I-type granitoids linked to lateral lithospheric heterogeneity: A case study from the North Qaidam orogen, NW China: Journal of Asian Earth Sciences, v. 237, https://doi.org/10.1016/j.jseaes.2022.105363.

Gao, X., Yu, S., Li, S., Liu, Y., Ji, W., Jiang, X., Lv, P., and Peng, Y., 2023, Consecutive underplating of cognate magmas: Contributions to the enclaves and large-volume plagiogranites in the North Qaidam orogen (NW China): Lithos, v. 442–443, https://doi.org/10.1016/j.lithos.2023.107085.

Gehrels, G.E., Yin, A., and Wang, X.F., 2003a, Detrital zircon geochronology of northeastern Tibet: Geological Society of America Bulletin, v. 115, p. 881–896, https://doi.org/10.1130/0016-7606(2003)115<0881:DGOTNT>2.0.CO;2.

Gehrels, G.E., Yin, A., and Wang, X.F., 2003b, Magmatic history of the northeastern Tibetan Plateau: Journal of Geophysical Research: Solid Earth, v. 108, no. B9, https://doi.org/10.1029/2002JB001876.

Gehrels, G.E., et al., 2011, Detrital zircon geochronology of pre-Tertiary strata in the Tibetan-Himalayan orogen: Tectonics, v. 30, TC5016, https://doi.org/10.1029/2011TC002868.

Gu, P.Y., et al., 2018, The age, petrogenesis and geological significance of quartz diorite on the northwestern margin of Qaidam Basin: Acta Petrologica et Mineralogica, v. 37, no. 1, p. 19–33 [in Chinese with English abstract].

Guo, A.L., Zhang, G.W., Qiang, J., Sun, Y.G., Li, G., and Yao, A.P., 2009, Indosinian Zongwulong orogenic belt on the northeastern margin of the Qinghai-Tibet plateau: Acta Petrologica Sinica (Yanshi Xuebao), v. 25, no. 1, p. 1–12 [in Chinese with English abstract].

Guo, J.C., Xu, X.M., Chen, H.Y., Li, X., Dong, H.K., and Ti, Z.H., 2014, Zircon U-Pb age and geological implications of ultramafic rocks in Changshagou, Altun area, Xinjiang Province: Northwest Geology, v. 47, p. 170–177 [in Chinese with English abstract].

Hao, J., Wang, E.Q., Liu, X.H., and Sang, H.Q., 2006, Jinyanshan collisional orogenic belt of the early Paleozoic in the Altun mountains: Evidence from single zircon U-Pb and $^{40}Ar/^{39}Ar$ isotopic dating for the arc magmatite and ophiolitic mélange: Acta Petrologica Sinica (Yanshi Xuebao), v. 22, no. 11, p. 2743–2752 [in Chinese with English abstract].

He, S.P., Wang, H.L., Chen, J.L., Xu, X.Y., Zhang, H.F., Ren, G.M., and Yu, J.Y., 2008, LA-ICP-MS U-Pb zircon geochronology of basic dikes within Maxianshan rock group in the central Qilian Mountains and its tectonic implications: Earth Science: Journal of China University of Geosciences (Diqiu Kexue), v. 33, no. 1, p. 35–45 [in Chinese with English abstract].

Heubeck, C., 2001, Assembly of central Asia during the middle and late Paleozoic, *in* Hendrix, M.S., and Davis, G.A., eds., Paleozoic and Mesozoic Tectonic Evolution of Central and Eastern Asia: From Continental Assembly to Intracontinental Deformation: Geological Society of America Memoir 194, p. 1–22, https://doi.org/10.1130/0-8137-1194-0.1.

Hsü, K.J., Pan, G., and Sengör, A.M.C., 1995, Tectonic evolution of the Tibetan Plateau: A working hypothesis based on the archipelago model of orogenesis: International Geology Review, v. 37, no. 6, p. 473–508, https://doi.org/10.1080/00206819509465414.

Hu, N.G., Xu, A.D., and Yang, J.X., 2005, Characteristics and tectonic environment of Zhigoumen pluton in Longshoushan area: Journal of Earth Sciences and Environment (Diqiu Kexue Yu Huanjing Xuebao), v. 27, p. 5–11 [in Chinese with English abstract].

Hu, W.L., Jia, Z.L., Wang, J.R., Hou, K.X., and Wang, S.H., 2016, Geochronology and geochemistry characteristics of the granites from the Huashigou area, south Qilian, and their tectonic significance: Geological Journal of China Universities (Gaoxiao Dizhi Xuebao), v. 22, no. 2, p. 242–253 [in Chinese with English abstract].

Jackson, S.E., Pearson, N.J., Griffin, W.L., and Belousova, E.A., 2004, The application of laser ablation–inductively coupled plasma–mass spectrometry to in situ U-Pb zircon geochronology: Chemical Geology, v. 211, p. 47–69, https://doi.org/10.1016/j.chemgeo.2004.06.017.

Jia, Z.L., Chen, W.F., Sha, X., and Wang, J.R., 2017, Discovery of middle Permian adakitic rocks in south Qilian area, Gansu, and implications for tectonics and Cu(Au) mineralization: Geotectonica et Metallogenia (Dadi Gouzao Yu Chengkuangxue), v. 41, no. 1, p. 222–234 [in Chinese with English abstract].

Jiang, C.F., Yang, J.S., Feng, B.G., Zhu, Z.Z., Zhao, M., Chai, Y.C., Shi, X.D., Wang, H.D., and Ha, J.Q., 1992, Opening Closing Tectonics of Kunlun Mountains: Geological Memoirs: Beijing, Geological Publishing House, 224 p. [in Chinese with English abstract].

Jiang, H., Sun, F., Li, L., Li, R., Yu, L., Wang, F., and Shen, D., 2016, Geochronology, geochemistry and Hf isotope of monzogranite in Niubiziliang of Qinghai: Global Geology, v. 19, no. 3, p. 153–163 [in Chinese with English abstract].

Kang, L., Liu, L., Cao, Y.T., Wang, C., Yang, W.Q., and Zhu, X.H., 2011, Geochemistry, zircon LA-ICP-MS U-Pb ages and Hf isotopes of Hongliugou moyite from north Altyn Tagh tectonic belt: Geological Bulletin of China (Dizhi Tongbao), v. 30, p. 1066–1076 [in Chinese with English abstract].

Konstantinovskaia, E.A., Brunel, M., and Malavieille, J., 2003, Discovery of the Paleo-Tethys residual peridotites along the Anyemaqen–KunLun suture zone (North Tibet): Comptes Rendus Geoscience, v. 335, no. 8, p. 709–719, https://doi.org/10.1016/S1631-0713(03)00118-4.

Kou, G.C., Feng, J.W., Luo, B.R., Zhou, W.G., and Liu, S.Q., 2017, Zircon U-Pb dating and geochemistry of the volcanic rocks from Maoniushan Formation in Amunike area, Qinghai Province, and its geological implications: Geological Bulletin of China (Dizhi Tongbao), v. 36, no. 2–3, p. 275–284 [in Chinese with English abstract].

Le Maitre, R.W.B., Dudek, P., Keller, A., Lameyre, J., Le Bas, J., Sabine, M.J., Schmid, P.A., Sorensen, R., Streckeisen, H., Woolley, A., and Zanettin, A.R., 1989, A Classification of Igneous Rocks and Glossary of Terms: Recommendations of the International Union of Geological Sciences, Subcommission on the Systematics of Igneous Rocks (No. 552.3 CLA): International Union of Geological Sciences: Oxford, UK, Blackwell, 193 p.

Li, B., et al., 2021, Pre-Cenozoic evolution of the northern Qilian orogen from zircon geochronology: Framework for early growth of the northern Tibetan Plateau: Palaeogeography, Palaeoclimatology, Palaeoecology, v. 562, https://doi.org/10.1016/j.palaeo.2020.110091.

Li, B., Wang, Y., Zuza, A.V., Chen, X., Shao, Z., Wang, Z.Z., Sun, Y.J., and Wu, C., 2023a, Cenozoic deformation in the eastern domain of the North Qaidam thrust belt, northern Tibetan Plateau: Geological Society of America Bulletin, v. 135, p. 331–350, https://doi.org/10.1130/B36215.1.

Li, B., Qi, B., Chen, X., Zuza, A.V., Hu, D., Sun, Y., Wang, Z.Z., and Zhang, Y., 2024, Two-phase kinematic evolution of the Qilian Shan, northern Tibetan Plateau: Initial Eocene–Oligocene deformation that accelerated in the mid-Miocene: Geological Society of America Bulletin, v. 136, p. 2389–2406, https://doi.org/10.1130/B37159.1.

Li, H.R., Qian, Y., Sun, F.Y., and Wang, Y.Z., 2023b, Paleozoic to Mesozoic magmatism in North Qaidam, Qinghai Province, NW China: Implications for tectonic evolution: Gondwana Research, v. 115, p. 37–56, https://doi.org/10.1016/j.gr.2022.11.011.

Li, S., Zhao, S., Liu, X., Cao, H., Yu, S., Li, X., and Suo, Y., 2018, Closure of the Proto-Tethys Ocean and early Paleozoic amalgamation of microcontinental blocks in East Asia: Earth-Science Reviews, v. 186, p. 37–75, https://doi.org/10.1016/j.earscirev.2017.01.011.

Li, X., Niu, M., Yan, Z., Yakymchuk, C., Fu, C., Li, C., Sun, Y., Wu, Q., and He, J., 2022, Early Paleozoic continental arc mafic magmatism in the North Qaidam tectonic belt: Implications for subduction of the Proto-Tethyan oceanic lithosphere: Lithosphere, v. 2022, https://doi.org/10.2113/2022/3011662.

Li, Y.L., and Yang, J.C., 1998, Tectonic geomorphology in the Hexi Corridor, north-west China: Basin Research, v. 10, p. 345–352, https://doi.org/10.1046/j.1365-2117.1998.00070.x.

Liu, C.F., Wu, C., Zhou, Z.G., Zhu, Y., Jiang, T., Song, Z.J., Liu, W.C., Yang, X., and Zhang, H., 2018, U-Pb detrital zircon geochronology from the basement of the Central Qilian terrane: Implications for tectonic evolution of northeastern Tibetan Plateau: International Journal of Earth Sciences, v. 107, p. 673–686, https://doi.org/10.1007/s00531-017-1522-5.

Liu, C.F., Wu, C., Song, Z., Liu, W., and Zhang, H., 2019, Petrogenesis and tectonic significance of early Paleozoic magmatism in the northern margin of the Qilian block, northeastern Tibetan Plateau: Lithosphere, v. 11, no. 3, p. 365–385, https://doi.org/10.1130/L1047.1.

Liu, C.F., Liu, W.C., Ye, B.Y., Zhao, Z.X., Su, H., and Xu, X., 2024a, Munabulake ophiolitic mélange: Implication for the evolution history of the north branch of the Proto-Tethys ocean: Geoscience Frontiers, v. 15, https://doi.org/10.1016/j.gsf.2023.101731.

Liu, L., Che, Z.C., Wang, Y., Luo, J.H., Wang, J.Q., and Gao, Z.J., 1998, The evidence of Sm-Nd isochron age for the early Paleozoic ophiolite in Mangya area, Altun Mountains: Chinese Science Bulletin, v. 43, p. 754–756, https://doi.org/10.1007/BF02898953 [in Chinese with English abstract].

Liu, Q., Tsunogae, T., Zhao, G.C., Li, J.H., Yao, J.L., Han, Y.G., and Wang, P., 2021, Multiphase ophiolite formation in the northern Altyn Tagh orogen, southeastern Tarim: American Journal of Science, v. 321, p. 788–821, https://doi.org/10.2475/06.2021.05.

Liu, W.M., Sun, G.Q., Xie, M., Xian, Y.W., Guo, J.J., Chen, B., and Shi, J.A., 2017, The detrital zircon U-Pb dating and its geological significance of the Lower Jurassic in No. 445 Lenghu, northern margin of Qaidam Basin: Natural Gas Geoscience, v. 28, no. 9, p. 1312–1321 [in Chinese with English abstract].

Liu, W.Y., Wu, C., Li, J., Zhang, C.H., Jiang, T., Zuza, A.V., Haproff, P.J., Chen, X.H., and Yue, Y.H., 2024b, Structure and provenance of the Cretaceous Pingshanhu Basin in the Hexi Corridor: Implications for Mesozoic tectonics in the northern Tibetan Plateau: Geosphere, v. 20, p. 421–450, https://doi.org/10.1130/GES02695.1.

Liu, X., Wu, Y., Gao, S., Liu, Q., Wang, H., Qin, Z., Li, Q., Li, X.H., and Gong, H., 2012, First record and timing of UHP metamorphism from zircon in the Xitieshan terrane: Implications for the evolution of the entire North Qaidam metamorphic belt: The American Mineralogist, v. 97, no. 7, p. 1083–1093, https://doi.org/10.2138/am.2012.4048.

Liu, Y., Genser, J., Neubauer, F., Jin, W., Ge, X., Handler, R., and Takasu, A., 2005, $^{40}Ar/^{39}Ar$ mineral ages from basement rocks in the Eastern Kunlun Mountains, NW China, and their tectonic implications: Tectonophysics, v. 398, no. 3–4, p. 199–224, https://doi.org/10.1016/j.tecto.2005.02.007.

Liu, Y.J., Neubauer, F., Genser, J., Takasu, A., Ge, X.H., and Handler, R., 2006, $^{40}Ar/^{39}Ar$ ages of blueschist facies pelitic schists from Qingshuigou in the northern Qilian Mountains, western China: The Island Arc, v. 15, no. 1, p. 187–198, https://doi.org/10.1111/j.1440-1738.2006.00508.x.

Liu, Z.F., and Wang, C.S., 2001, Facies analysis and depositional systems of Cenozoic sediments in the Hoh Xil basin, northern Tibet: Sedimentary Geology, v. 140, p. 251–270, https://doi.org/10.1016/S0037-0738(00)00188-3.

Long, X., Yuan, C., Sun, M., Kröner, A., and Zhao, G., 2014, New geochemical and combined zircon U-Pb and Lu-Hf isotopic data of orthogneisses in the northern Altyn Tagh, northern margin of the Tibetan Plateau: Implication for Archean evolution of the Dunhuang block and crust formation in NW China: Lithos, v. 200–201, p. 418–431, https://doi.org/10.1016/j.lithos.2014.05.008.

Lu, H., Ye, J., Guo, L., Pan, J., Xiong, S., and Li, H., 2019, Towards a clarification of the provenance of Cenozoic sediments in the northern Qaidam Basin: Lithosphere, v. 11, p. 252–272, https://doi.org/10.1130/L1037.1.

Lu, L., Wu, Z.H., Hu, D.G., Barosh, P.J., Hao, S., and Zhou, C.J., 2010, Zircon U-Pb age for rhyolite of the Maoniushan Formation and its tectonic significance in the East Kunlun Mountains: Acta Petrologica Sinica (Yanshi Xuebao), v. 26, no. 4, p. 1150–1158 [in Chinese with English abstract].

Lu, S.N., Wang, H.C., and Li, H.K., 2002, Redefinition of the "Dakendaban Group" on the northern margin of the Qaidam Basin: Geological Bulletin of China (Dizhi Tongbao), v. 21, p. 19–23 [in Chinese with English abstract].

Lu, S.N., Li, H.K., Wang, H.C., Chen, Z.H., Zheng, J.K., and Xiang, Z.Q., 2009, Detrital zircon population of Proterozoic metasedimentary strata in the Qinling-Qilian-Kunlun orogen: Acta Petrologica Sinica (Yanshi Xuebao), v. 25, p. 2195–2208 [Chinese with English abstract].

Lu, X.X., et al., 2007, The SHRIMP age of Tatalin rapakivi granite at the north margin of Qaidam Basin: Acta Geologica Sinica, v. 5, no. 81, p. 626–634 [in Chinese with English abstract].

Ludwig, K.R., 2003, User's Manual for Isoplot 3.00: A Geochronological Toolkit for Microsoft Excel: Berkeley, California, Berkeley Geochronology Center Special Publication 4, 70 p.

Ma, Z.P., Li, X.M., Sun, J.M., Xu, X.Y., Wang, L.S., and Duan, X.X., 2009, Discovery of layered mafic-ultramafic intrusion in Changshagou, Altyn Tagh, and its geological implication: A pilot study on its petrological and geochemical characteristics: Acta Petrologica Sinica (Yanshi Xuebao), v. 25, p. 793–804 [in Chinese with English abstract].

Maniar, P.D., and Piccoli, P.M., 1989, Tectonic discrimination of granitoids: Geological Society of America Bulletin, v. 101, p. 635–643, https://doi.org/10.1130/0016-7606(1989)101<0635:TDOG>2.3.CO;2.

Mao, J., Zhang, Z., Yang, J., Song, B., Wu, M., and Zuo, G., 1998, Single-zircon dating of Precambrian strata in the west sector of the northern Qilian Mountains and its geological significance: Chinese Science Bulletin, v. 43, no. 15, p. 1289–1294, https://doi.org/10.1007/BF02884144.

Mattinson, C.G., Menold, C.A., Zhang, J.X., and Bird, D.K., 2007, High- and ultrahigh-pressure metamorphism in the North Qaidam and South Altyn terranes, western China: International Geology Review, v. 49, no. 11, p. 969–995, https://doi.org/10.2747/0020-6814.49.11.969.

McRivette, M.W., Yin, A., Chen, X., and Gehrels, G.E., 2019, Cenozoic basin evolution of the central Tibetan Plateau as constrained by U-Pb detrital zircon geochronology, sandstone petrology, and fission-track thermochronology: Tectonophysics, v. 751, p. 150–179, https://doi.org/10.1016/j.tecto.2018.12.015.

Meng, F.C., and Zhang, J.X., 2008, Contemporaneous early Palaeozoic granite and high temperature metamorphism, North Qaidam Mountains, western China: Acta Petrologica Sinica (Yanshi Xuebao), v. 24, no. 7, p. 1585–1594 [in Chinese with English abstract].

Meng, F.C., and Zhang, J.X., 2009, Genesis of the megacrystal zircons in the dunite veins of North Qaidam Mountains, northwestern China: Chinese Science Bulletin, v. 54, p. 4688–4696, https://doi.org/10.1007/s11434-009-0205-4.

Meng, F.C., Zhang, J.X., and Yang, J.S., 2005, Tectonothermal event of post HP/UHP metamorphism in the Xitieshan area of the North Qaidam Mountains, western China: Isotopic and geochemical evidence of granite and gneiss: Acta Petrologica Sinica (Yanshi Xuebao), v. 21, no. 1, p. 45–56 [in Chinese with English abstract].

Menold, C.A., Manning, C.E., Yin, A., Tropper, P., Chen, X.H., and Wang, X.F., 2009, Metamorphic evolution, mineral chemistry and thermobarometry of orthogneiss hosting ultrahigh-pressure eclogites in the North Qaidam metamorphic belt, western China: Journal of Asian Earth Sciences, v. 35, no. 3–4, p. 273–284, https://doi.org/10.1016/j.jseaes.2008.12.008.

Menold, C.A., Grove, M., Sievers, N.E., Manning, C.E., Yin, A., Young, E.D., and Ziegler, K., 2016, Argon, oxygen, and boron isotopic evidence documenting $^{40}Ar_E$ accumulation in phengite during water-rich high-pressure subduction metasomatism of continental crust: Earth and Planetary Science Letters, v. 446, p. 56–67, https://doi.org/10.1016/j.epsl.2016.04.010.

Middlemost, E.A.K., 1994, Naming materials in the magma/igneous rock system: Earth-Science Reviews, v. 37, p. 215–224, https://doi.org/10.1016/0012-8252(94)90029-9.

Molnar, P., 1988, Continental tectonics in the aftermath of plate tectonics: Nature, v. 335, no. 6186, p. 131–137, https://doi.org/10.1038/335131a0.

Nie, S., Yin, A., Rowley, D.B., and Jin, Y., 1994, Exhumation of the Dabie Shan ultra-high-pressure rocks and accumulation of the Songpan-Ganzi flysch sequence, central China: Geology, v. 22, p. 999–1002, https://doi.org/10.1130/0091-7613(1994)022%3C0999:EOTDSU%3E2.3.CO;2.

Niu, M.L., Zhao, Q.Q., Wu, Q., Li, X.C., Yan, Z., Li, J.L., Sun, Y., and Yuan, X.Y., 2018, Magma mixing identified in the Guokeshan pluton, northern margin of the Qaidam basin: Evidences from petrography, mineral chemistry, and whole-rock geochemistry: Acta Petrologica Sinica (Yanshi Xuebao), v. 34, no. 7, p. 1991–2016 [in Chinese with English abstract].

Pan, G., Wang, L., Li, R., Yuan, S., Ji, W., Yin, F., Zhang, W.P., and Wang, B.D., 2012, Tectonic evolution of the Qinghai-Tibet Plateau: Journal of Asian Earth Sciences, v. 53, p. 3–14, https://doi.org/10.1016/j.jseaes.2011.12.018.

Pan, G.T., Ding, J., Yao, D., and Wang, L., 2004, Geological Map of Qinghai-Xiang (Tibet) Plateau and Adjacent Areas: Chengdu Institute of Geology and Mineral Resources and China Geological Survey: Chengdu, China, Chengdu Cartographic Publishing House, scale 1:1,500,000 [in Chinese].

Pearce, J.A., 1996, Sources and settings of granitic rocks: Episodes, v. 19, p. 120–125, https://doi.org/10.18814/epiiugs/1996/v19i4/005.

Pearce, J.A., Harris, N.B.W., and Tindle, A.G., 1984, Trace element discrimination diagrams for the tectonic interpretation of granitic rocks: Journal of Petrology, v. 25, no. 4, p. 956–983, https://doi.org/10.1093/petrology/25.4.956.

Peng, Y., Ma, Y.S., Liu, C.L., Sun, J.P., Cheng, H.Y., Dai, K., and Zheng, C., 2015, The late Hercynian-Indosinian structural characteristics of the Zongwulong tectonic belt in North Qaidam Basin: Acta Geoscientica Sinica, v. 36, no. 1, p. 51–59 [in Chinese with English abstract].

Peng, Y., et al., 2016, Geological characteristics and tectonic significance of the Indosinian granodiorites from the Zongwulong tectonic belt in North Qaidam: Earth Science Frontiers, v. 23, no. 2, p. 206–221 [in Chinese with English abstract].

Polat, A., Kerrich, R., and Windley, B., 2009, Archaean crustal growth processes in southern West Greenland and the southern Superior Province: Geodynamic and magmatic constraints, *in* Cawood, P.A., and Kröner, A., eds., Earth Accretionary Systems in Space and Time: Geological Society, London, Special Publication 318, p. 155–191, https://doi.org/10.1144/SP318.6.

Profeta, L., Ducea, M.N., Chapman, J.B., Paterson, S.R., Gonzales, S.M., Kirsch, M., Petrescu, L., and DeCelles, P.G., 2015, Quantifying crustal thickness over time in magmatic arcs: Scientific Reports, v. 5, https://doi.org/10.1038/srep17786.

Qi, X.X., Li, H.B., and Wu, C.L., 2005, SHRIMP U-Pb zircon dating for Qiashikansayi granodiorite in the northern Altyn Tagh Mountains and its geological implications: Chinese Science Bulletin, v. 50, p. 440–445, https://doi.org/10.1007/BF02897460 [in Chinese with English abstract].

Qian, B., Zhang, Z.W., Li, W.Y., Jing, Z.C., and Shao, J., 2018a, Magma evolution and Ni-Cu sulfide mineralization potentiality of the Yanchangbeishan mafic-ultramafic intrusion in the western North Qaidam orogenic belt: Acta Petrologica Sinica, v. 34, no. 8, p. 2275–2294 [in Chinese with English abstract].

Qian, Q., Wang, Y.M., Li, H.M., Jia, X.Q., Han, S., and Zhang, Q., 1998, Geochemical characteristics and genesis of diorites from Laohushan, Gansu Province: Acta Petrolei Sinica, v. 14, p. 520–528 [in Chinese with English abstract].

Qian, T., Wang, Z.X., Wang, Y., Liu, S.F., Gao, W.L., and Li, W.P., 2021a, Jurassic evolution of the Qaidam Basin in western China: Constrained by stratigraphic succession, detrital zircon U-Pb geochronology and Hf isotope analysis: Geological Society of America Bulletin, v. 133, p. 2291–2318, https://doi.org/10.1130/B35757.1.

Qian, T., Li, W.P., Gao, W.L., and Jiang, W., 2021b, A preliminary study on post-orogenesis of the North Qaidam tectonic belt during the early Paleozoic by provenance analysis of the Devonian sediments: Acta Geologica Sinica, v. 97, p. 672–687 [in Chinese with English abstract].

Qian, T., Wang, Z.X., Liu, Y.Q., Liu, S.F., Gao, W., Li, W.P., Hu, J.J., and Li, L.L., 2018b, Provenance analysis of the Jurassic northern Qaidam Basin: Stratigraphic succession and LA-ICP-MS geochronology: Scientia Sinica Terrae, v. 48, p. 224–242 [in Chinese with English abstract].

Qin, Y., Feng, Q., Chen, G., Chen, Y., Zou, K., Liu, Q., Jiao, Q., Zhou, D., Pan, L., and Gao, J., 2018, Devonian post-orogenic extension-related volcano-sedimentary rocks in the northern margin of the Tibetan Plateau, NW China: Implications for the Paleozoic tectonic transition in the North Qaidam orogen: Journal of Asian Earth Sciences, v. 156, p. 145–166, https://doi.org/10.1016/j.jseaes.2018.01.009.

Qinghai BGMR (Qinghai Bureau of Geology and Mineral Resources), 1978, Geological Map of Delingha Sheet, People's Republic of China: Xining, China, Qinghai BGMR, scale 1:200,000 [in Chinese].

Qinghai BGMR (Qinghai Bureau of Geology and Mineral Resources), 1991, Regional Geology of Qinghai Province: Beijing, Geological Publishing House, 662 p.

Qinghai BGMR (Qinghai Bureau of Geology and Mineral Resources), 1997, Stratigraphy (lithostratic) of Qinghai Province: Wuhan, China University of Geosciences Press, 340 p. [in Chinese].

Qiu, S.D., Dong, Z.C., and Gu, P.Y., 2015, The discovery of adakitic granite in the west segment of the north margin of Qaidam and its geological significance: Acta Geologica Sinica, v. 89, no. 7, p. 1231–1243 [in Chinese with English abstract].

Quan, S., Jia, Q., Guo, Z., and Wang, W., 2006, Basic characteristics of granitoids related to tungsten mineralization in the Qilian Mountains: Mineralium Deposita, v. 25, p. 143–146.

Ratschbacher, L., Hacker, B.R., Calvert, A., Webb, L.E., Grimmer, J.C., McWilliams, M.O., Dong, S.W., and Hu, J., 2003, Tectonics of the Qinling (central China): Tectonostratigraphy, geochronology, and deformation history: Tectonophysics, v. 366, p. 1–53, https://doi.org/10.1016/S0040-1951(03)00053-2.

Ren, E.F., Zhang, G.L., Qiu, W., Li, H.X., and Sun, Z.H., 2012, Characteristics of geochemistry and tectonic significance of Caledonian granite in the Maerzheng region in the south area of East Kunlun: Geosciences, v. 26, no. 1, p. 36–44 [in Chinese with English abstract].

Ren, J.H., Liu, Y.Q., Zhou, D.W., Feng, Q., Zhang, K., Dong, Z.L., and Qin, P.L., 2010, Geochemical characteristics and LA-ICP-MS zircon U-Pb dating of basic dykes in the Xiaomian area: Eastern Kunlun: Journal of Jilin University: Earth Science Edition (Jilin Daxue Xuebao: Diqiu Kexue Ban), v. 40, p. 856–868 [in Chinese with English abstract].

Ren, Y., Chen, D., Hauzenberger, C., Liu, L., Liu, X., and Zhu, X., 2016, Petrology and geochronology of ultrahigh-pressure granitic gneiss from South Dulan, North Qaidam belt, NW China: International Geology Review, v. 58, no. 2, p. 171–195, https://doi.org/10.1080/00206814.2015.1058729.

Rickwood, P.C., 1989, Boundary lines within petrologic diagrams which use oxides of major and minor elements: Lithos, v. 22, p. 247–263, https://doi.org/10.1016/0024-4937(89)90028-5.

Rieser, A.B., Neubauer, F., Liu, Y., and Ge, X., 2005, Sandstone provenance of northwestern sectors of the intracontinental Cenozoic Qaidam basin, western China: Tectonic vs. climatic control: Sedimentary Geology, v. 177, p. 1–18, https://doi.org/10.1016/j.sedgeo.2005.01.012.

Scotese, C.R., and McKerrow, W.S., 1990, Revised world maps and introduction, *in* McKerrow, W.S., and Scotese, C.R., eds., Palaeozoic Palaeogeography and Biogeography: Geological Society, London, Memoir 12, p. 1–21, https://doi.org/10.1144/GSL.MEM.1990.012.01.01.

Şengör, A.M.C., 1984, The Cimmeride Orogenic System and the Tectonics of Eurasia: Geological Society of America Special Paper 195, 74 p.

Şengör, A.M.C., and Natal'in, B.A., 1996, Turkic-type orogeny and its role in the making of the continental crust: Annual Review of Earth and Planetary Sciences, v. 24, p. 263–337, https://doi.org/10.1146/annurev.earth.24.1.263.

Şengör, A.M.C., Altıner, D., Cin, A., Ustaömer, T., and Hsü, K.J., 1988, Origin and assembly of the Tethyside orogenic collage at the expense of Gondwana Land, *in* Audley-Charles, M.G., and Hallam, A., eds., Gondwana and Tethys: Geological Society, London, Special Publication 37, p. 119–181, https://doi.org/10.1144/GSL.SP.1988.037.01.09.

Shao, P.C., Chen, S.Y., Sun, J.P., Ma, S., Liu, J., and Wang, F., 2018, SHRIMP zircon U-Pb dating and petro-geochemistry of Aolaoshan gabbro-diorite in the western north margin of Qaidam basin: Acta Geologica Sinica, v. 92, no. 9, p. 1888–1903 [in Chinese with English abstract].

She, Z., Ma, C., Mason, R., Li, J., Wang, G., and Lei, Y., 2006, Provenance of the Triassic Songpan-Ganzi flysch, west China: Chemical Geology, v. 231, no. 1–2, p. 159–175, https://doi.org/10.1016/j.chemgeo.2006.01.001.

Shi, R.D., Yang, J.S., and Wu, C.L., 2004, First SHRIMP dating for the formation of the late Sinian Yushigou ophiolite, North Qilian Mountains: Acta Geologica Sinica, v. 78, p. 649–657 [in Chinese with English abstract].

Sláma, J., Košler, J., Condon, D.J., Crowley, J.L., Gerdes, A., Hanchar, J.M., and Schaltegger, U., 2008, Plešovice zircon—A new natural reference material for U-Pb and Hf isotopic microanalysis: Chemical Geology, v. 249, no. 1–2, p. 1–35, https://doi.org/10.1016/j.chemgeo.2007.11.005.

Smith, A.D., 2006, The geochemistry and age of ophiolitic strata of the Xinglongshan Group: Implications for the amalgamation of the Central Qilian belt: Journal of Asian Earth Sciences, v. 28, p. 133–142, https://doi.org/10.1016/j.jseaes.2005.09.014.

Sobel, E.R., and Arnaud, N., 1999, A possible middle Paleozoic suture in the Altyn Tagh, NW China: Tectonics, v. 18, no. 1, p. 64–74, https://doi.org/10.1029/1998TC900023.

Song, S.G., Yang, J.S., Liou, J.G., Wu, C.L., Shi, R.D., and Xu, Z.Q., 2003, Petrology, geochemistry and isotopic ages of eclogites from the Dulan UHPM terrane, the North Qaidam, NW China: Lithos, v. 70, no. 3–4, p. 195–211, https://doi.org/10.1016/S0024-4937(03)00099-9.

Song, S.G., Zhang, L.F., and Niu, Y.L., 2004, Ultra-deep origin of garnet peridotite from the North Qaidam ultrahigh-pressure belt, northern Tibetan Plateau, NW China: The American Mineralogist, v. 89, no. 8–9, p. 1330–1336, https://doi.org/10.2138/am-2004-8-922.

Song, S.G., Zhang, L.F., Niu, Y.L., Su, L., Jian, P., and Liu, D.Y., 2005, Geochronology of diamond-bearing zircons from garnet peridotite in the North Qaidam UHPM belt, northern Tibetan Plateau: A record of complex histories from oceanic lithosphere subduction to continental collision: Earth and Planetary Science Letters, v. 234, no. 1–2, p. 99–118, https://doi.org/10.1016/j.epsl.2005.02.036.

Song, S.G., Zhang, L., Niu, Y., Su, L., Song, B., and Liu, D., 2006, Evolution from oceanic subduction to continental collision: A case study from the northern Tibetan Plateau based on geochemical and geochronological data: Journal of Petrology, v. 47, no. 3, p. 435–455, https://doi.org/10.1093/petrology/egi080.

Song, S.G., Zhang, L.F., Niu, Y., Wei, C.J., Liou, J.G., and Shu, G.M., 2007, Eclogite and carpholite-bearing metasedimentary rocks in the north Qilian suture zone, NW China: Implications for early Palaeozoic cold oceanic subduction and water transport into mantle: Journal of Metamorphic Geology, v. 25, no. 5, p. 547–563, https://doi.org/10.1111/j.1525-1314.2007.00713.x.

Song, S.G., Niu, Y., Su, L., and Xia, X., 2013, Tectonics of the North Qilian orogen, NW China: Gondwana Research, v. 23, no. 4, p. 1378–1401, https://doi.org/10.1016/j.gr.2012.02.004.

Song, S.G., Niu, Y., Su, L., Zhang, C., and Zhang, L.F., 2014a, Continental orogenesis from ocean subduction, continent collision/subduction, to orogen collapse, and orogen recycling: The example of the North Qaidam UHPM belt, NW China: Earth-Science Reviews, v. 129, p. 59–84, https://doi.org/10.1016/j.earscirev.2013.11.010.

Song, S.G., Niu, Y., Su, L., Wei, C., and Zhang, L., 2014b, Adakitic (tonalitic-trondhjemitic) magmas resulting from eclogite decompression and dehydration melting during exhumation in response to continental collision: Geochimica et Cosmochimica Acta, v. 130, p. 42–62, https://doi.org/10.1016/j.gca.2014.01.008.

Song, S.G., Wu, Z.Z., Yang, L.M., Su, L., Xia, X.H., Wang, C., Dong, J.L., Zhou, C.A., and Bi, H.Z., 2019, Ophiolite belts and evolution of the Proto-Tethys ocean in the Qilian orogen: Acta Petrologica Sinica (Yanshi Xuebao), v. 35, no. 10, p. 2948–2970 [in Chinese with English abstract].

Stacey, J.S., and Kramers, J.T., 1975, Approximation of terrestrial lead isotope evolution by a two-stage model: Earth and Planetary Science Letters, v. 26, no. 2, p. 207–221, https://doi.org/10.1016/0012-821X(75)90088-6.

Stampfli, G.M., and Borel, G.D., 2002, A plate tectonic model for the Paleozoic and Mesozoic constrained by dynamic plate boundaries and restored synthetic oceanic isochrons: Earth and Planetary Science Letters, v. 196, p. 17–33, https://doi.org/10.1016/S0012-821X(01)00588-X.

Su, J., Zhang, X., Hu, N., Fu, G., and Zhang, H., 2004, Geochemical characteristics and genesis of adakite-like

granites at Yema Nanshan in the western segment of the Central Qilian Mountains: China Geology, v. 31, p. 365–371 [in Chinese with English abstract].

Sun, J., Dong, Y., Jiang, W., Ma, L., Chen, S., Du, J., and Peng, Y., 2020, Reconstructing the Olongbuluke terrane (northern Tibet) in the end-Neoproterozoic to Ordovician Indian margin of Gondwana: Precambrian Research, v. 348, https://doi.org/10.1016/j.precamres.2020.105865.

Sun, J., Dong, Y., Ma, L., Chen, S., and Jiang, W., 2022, Devonian to Triassic tectonic evolution and basin transition in the East Kunlun–Qaidam area, northern Tibetan Plateau: Constraints from stratigraphy and detrital zircon U-Pb geochronology: Geological Society of America Bulletin, v. 134, p. 1967–1993, https://doi.org/10.1130/B36147.1.

Sun, S.-s., and McDonough, W.F., 1989, Chemical and isotopic systematics of oceanic basalts: Implications for mantle composition and processes, *in* Saunders, A.D., and Norry, M.J., eds., Magmatism in the Ocean Basins: Geological Society, London, Special Publication 42, p. 313–345, https://doi.org/10.1144/GSL.SP.1989.042.01.19.

Sun, Z., Yang, Z., Pei, J., Yang, T., and Wang, X., 2006, New Early Cretaceous paleomagnetic data from volcanic and red beds of the eastern Qaidam block and its implications for tectonics of Central Asia: Earth and Planetary Science Letters, v. 243, p. 268–281, https://doi.org/10.1016/j.epsl.2005.12.016.

Sundell, K.E., Laskowski, A.K., Kapp, P.A., Ducea, M.N., and Chapman, J.B., 2021, Jurassic to Neogene quantitative crustal thickness estimates in southern Tibet: GSA Today, v. 31, no. 6, p. 4–10, https://doi.org/10.1130/GSATG461A.1.

Tang, Y., Yin, A., Xu, X., An, K., and Zhang, Y., 2023, Tectonic evolution of the Triassic Songpan-Ganzi basin as constrained by a synthesis of multi-proxy provenance data: Basin Research, v. 35, no. 1, p. 28–60, https://doi.org/10.1111/bre.12703.

Tong, H.K., Wang, S.L., Song, S.C., Tan, S.X., Ma, X.L., and Huang, Q.H., 2004, Study on volcanic rocks and their structural environment of Late Triassic Epoch in Chachaxiangka area in Qinghai province: Earthquake Research Plateau, v. 116, p. 38–48 [in Chinese with English abstract].

Tseng, C.Y., Yang, H.J., Yang, H.Y., Liu, D., Tsai, C.L., Wu, H., and Zuo, G., 2007, The Dongcaohe ophiolite from the North Qilian Mountains: A fossil oceanic crust of the Paleo-Qilian ocean: Chinese Science Bulletin, v. 52, p. 2390–2401, https://doi.org/10.1007/s11434-007-0300-3.

Tseng, C.Y., Yang, H.J., Yang, H.Y., Liu, D., Wu, C., Cheng, C.K., Chen, C.H., and Ker, C.M., 2009a, Continuity of the North Qilian and North Qinling orogenic belts, Central orogenic system of China: Evidence from newly discovered Paleozoic adakitic rocks: Gondwana Research, v. 16, p. 285–293, https://doi.org/10.1016/j.gr.2009.04.003.

Tseng, C.Y., Zuo, G.C., Yang, H.J., Yang, H.Y., Tung, K.A., Liu, D.Y., and Wu, H.Q., 2009b, Occurrence of Alaskan-type mafic-ultramafic intrusions in the North Qilian Mountains, northwest China: Evidence of Cambrian arc magmatism on the Qilian block: The Island Arc, v. 18, p. 526–549, https://doi.org/10.1111/j.1440-1738.2009.00675.x.

Tung, K., Yang, H.-J., Yang, H.-Y., Liu, D., Zhang, J., Wan, Y., and Tseng, C.-Y., 2007, SHRIMP U-Pb geochronology of the zircons from the Precambrian basement of the Qilian block and its geological significances: Chinese Science Bulletin, v. 52, no. 19, p. 2687–2701, https://doi.org/10.1007/s11434-007-0356-0.

Turner, S.P., Foden, J.D., and Morrison, R.S., 1992, Derivation of some A-type magmas by fractionation of basaltic magma—An example from the Padthaway Ridge, South Australia: Lithos, v. 28, p. 151–179, https://doi.org/10.1016/0024-4937(92)90029-X.

Vincent, S.J., and Allen, M.B., 1999, Evolution of the Minle and Chaoshui Basins, China: Implications for Mesozoic strike-slip basin formation in Central Asia: Geological Society of America Bulletin, v. 111, p. 725–742, https://doi.org/10.1130/0016-7606(1999)111<0725:EOTMAC>2.3.CO;2.

Wan, Y.S., Xu, Z.Q., and Yang, J.S., 2001, Ages and compositions of the Precambrian high grade basement of the Qilian terrane and its adjacent areas: Acta Geologica Sinica, v. 75, p. 375–384, https://doi.org/10.1111/j.1755-6724.2001.tb00055.x.

Wang, F., Wang, L., Sun, F.Y., Li, L., Liu, J.L., and Tian, X.C., 2017, Zircon U-Pb geochronology and geochemistry of Niubiziliang granodiorite in northern margin of Qaidam Basin: Global Geology, v. 36, no. 1, p. 93–104 [in Chinese with English abstract].

Wang, L.Q., Pan, G.T., Ding, J., and Yao, D.S., compilers, 2013, Geological Map of the Tibetan Plateau at a scale of 1:1.5 M with Explanations: Beijing, Geological Publishing House, 288 p., scale 1:1,500,000 [in Chinese].

Wang, M., Song, S., Niu, Y., and Su, L., 2014, Post-collisional magmatism: Consequences of UHPM terrane exhumation and orogen collapse, N. Qaidam UHPM belt, NW China: Lithos, v. 210–211, p. 181–198, https://doi.org/10.1016/j.lithos.2014.10.006.

Wang, Q., Dong, Y., Pan, Y., Liao, F., and Guo, X., 2018, Early Paleozoic granulite-facies metamorphism and magmatism in the northern Wulan terrane of the Quanji Massif: Implications for the evolution of the Proto-Tethys Ocean in northwestern China: Journal of Earth Science, v. 29, p. 1081–1101, https://doi.org/10.1007/s12583-018-0881-6.

Wang, S., and Zhou, L.F., 2016, LA-ICP-MS zircon U-Pb dating, geochemistry and tectonic implication of the bojite in the Zongwulong Mountain: Journal of Northwest University: Natural Science Edition, v. 46, no. 5, p. 716–724 [in Chinese with English abstract].

Wang, Y., Chen, X.H., Zhang, Y.Y., Yin, Z., Zuza, A.V., Yin, A., Wang, Y.C., Ding, W.C., Xu, S.L., Zhang, Y.P., Li, B., and Shao, Z.G., 2022, Superposition of Cretaceous and Cenozoic deformation in northern Tibet: A far-field response to the tectonic evolution of the Tethyan orogenic system: Geological Society of America Bulletin, v. 134, p. 501–525, https://doi.org/10.1130/B35944.1.

Wang, Z.M., Han, C.M., Xiao, W.J., and Sakyi, P.A., 2020, Paleoproterozoic multiphase magmatism and metamorphism recorded in metamorphic basement rocks of the northern Altyn Tagh, southeastern Tarim craton: Precambrian Research, v. 346, https://doi.org/10.1016/j.precamres.2020.105827.

Weislogel, A.L., 2008, Tectonostratigraphic and geochronologic constraints on evolution of the northeast Paleotethys from the Songpan-Ganzi complex, central China: Tectonophysics, v. 451, no. 1–4, p. 331–345, https://doi.org/10.1016/j.tecto.2007.11.053.

Weislogel, A.L., Graham, S.A., Chang, E.Z., Wooden, J.L., Gehrels, G.E., and Yang, H., 2006, Detrital zircon provenance of the Late Triassic Songpan-Ganzi complex: Sedimentary record of collision of the North and South China blocks: Geology, v. 34, p. 97–100, https://doi.org/10.1130/G21929.1.

Whalen, J.B., Currie, K.L., and Chappell, B.W., 1987, A-type granites: Geochemical characteristics, discrimination and petrogenesis: Contributions to Mineralogy and Petrology, v. 95, p. 407–419, https://doi.org/10.1007/BF00402202.

Wiedenbeck, M., et al., 1995, Three natural zircon standards for U-Th-Pb, Lu-Hf, trace element and REE analyses: Geostandards Newsletter, v. 19, no. 1, p. 1–23, https://doi.org/10.1111/j.1751-908X.1995.tb00147.x.

Wu, C., Yin, A., Zuza, A.V., Zhang, J.Y., Liu, W.C., and Ding, L., 2016, Pre-Cenozoic geologic history of the central and northern Tibetan Plateau and the role of Wilson cycles in constructing the Tethyan orogenic system: Lithosphere, v. 8, no. 3, p. 254–292, https://doi.org/10.1130/L494.1.

Wu, C., Zuza, A.V., Yin, A., Liu, C.F., Reith, R.C., Zhang, J.Y., Liu, W.C., and Zhou, Z.G., 2017, Geochronology and geochemistry of Neoproterozoic granitoids in the central Qilian Shan of northern Tibet: Reconstructing the amalgamation processes and tectonic history of Asia: Lithosphere, v. 9, no. 4, p. 609–636, https://doi.org/10.1130/L640.1.

Wu, C., Zuza, A.V., Chen, X., Ding, L., Levy, D.A., Liu, C., Liu, W., Jiang, T., and Stockli, D., 2019a, Tectonics of the Eastern Kunlun Range: Cenozoic reactivation of a Paleozoic–early Mesozoic orogen: Tectonics, v. 38, p. 1609–1650, https://doi.org/10.1029/2018TC005370.

Wu, C., Zuza, A.V., Zhou, Z.G., Yin, A., McRivette, M.W., Chen, X.H., Ding, L., and Geng, J.Z., 2019b, Mesozoic–Cenozoic evolution of the Eastern Kunlun Range, central Tibet, and implications for basin evolution during the Indo-Asian collision: Lithosphere, v. 11, no. 4, p. 524–550, https://doi.org/10.1130/L1065.1.

Wu, C., Liu, C.F., Fan, S.F., Zuza, A.V., Ding, L., Liu, W.C., Ye, B.Y., Yang, S.J., and Zhou, Z.G., 2020, Structural analysis and tectonic evolution of the western domain of the Eastern Kunlun Range, northwest Tibet: Geological Society of America Bulletin, v. 132, p. 1291–1315, https://doi.org/10.1130/B35388.1.

Wu, C., Zuza, A.V., Yin, A., Chen, X., Haproff, P.J., Li, J., Li, B., and Ding, L., 2021, Punctuated orogeny during the assembly of Asia: Tectonostratigraphic evolution of the North China craton and the Qilian Shan from the Paleoproterozoic to early Paleozoic: Tectonics, v. 40, https://doi.org/10.1029/2020TC006503.

Wu, C., Li, J., Zuza, A.V., Haproff, P.J., Chen, X., and Ding, L., 2022a, Proterozoic–Phanerozoic tectonic evolution of the Qilian Shan and Eastern Kunlun Range, northern Tibet: Geological Society of America Bulletin, v. 134, p. 2179–2205, https://doi.org/10.1130/B36306.1.

Wu, C., Zuza, A.V., Levy, D.A., Li, J., and Ding, L., 2023, Discovery of Permian–Triassic eclogite in northern Tibet establishes coeval subduction erosion along an ~3000-km-long arc: Geology, v. 51, p. 833–838, https://doi.org/10.1130/G51223.1.

Wu, C.L., Yang, J.S., Li, H.B., and Shi, R.D., 2001, Zircon SHRIMP dating of granite from Aoloshan in the southern margin of Qilian, NW China: Acta Petrologica Sinica (Yanshi Xuebao), v. 17, p. 215–221 [in Chinese with English abstract].

Wu, C.L., Yang, J.S., Xu, Z.Q., and Wooden, J., 2004, Granitic magmatism on the early Paleozoic UHP belt of Northern Qaidam, NW China: Acta Geologica Sinica, v. 78, no. 5, p. 658–674 [in Chinese with English abstract].

Wu, C.L., Wooden, J.L., Yang, J.S., Robinson, P.T., Zheng, L.S., Shi, R.D., and Chen, S.Y., 2006a, Granitic magmatism in the North Qaidam early Paleozoic ultrahigh-pressure metamorphic belt, northwest China: International Geology Review, v. 48, no. 3, p. 223–240, https://doi.org/10.2747/0020-6814.48.3.223.

Wu, C.L., Yao, S.Z., Zeng, L.S., Yang, J.S., Wooden, J.L., Chen, S.Y., and Mazadab, F.K., 2006b, Bashikaogong–Shimierbulake granitic complex, north Altun, NW China: Geochemistry and zircon SHRIMP ages: Science in China Series D: Earth Sciences, v. 49, p. 1233–1251, https://doi.org/10.1007/s11430-006-2041-6.

Wu, C.L., Gao, Y.H., and Wu, S.P., 2007, Zircon SHRIMP dating of granites from Da Qaidam area in the north margin of Qaidam Basin, NW China: Acta Petrologica Sinica (Yanshi Xuebao), v. 23, p. 1861–1875 [in Chinese with English abstract].

Wu, C.L., Wooden, J.L., Robinson, P.T., Gao, Y.H., Wu, S.P., Chen, Q.L., Mazdab, F.K., and Mattinson, C., 2009a, Geochemistry and zircon SHRIMP U-Pb dating of granitoids from the west segment of the North Qaidam: Science China Earth Sciences, v. 52, no. 11, p. 1771–1790, https://doi.org/10.1007/s11430-009-0147-3.

Wu, C.L., Yang, J., Robinson, P.T., Wooden, J.L., Mazdab, F.K., Gao, Y., and Chen, Q., 2009b, Geochemistry, age and tectonic significance of granitic rocks in north Altun, northwest China: Lithos, v. 113, no. 3–4, p. 423–436, https://doi.org/10.1016/j.lithos.2009.05.009.

Wu, C.L., Gao, Y.H., Li, Z.L., Lei, M., Qin, H.P., and Li, M.Z., 2014, Zircon SHRIMP U-Pb dating of granites from Dulan and the chronological framework of the North Qaidam UHP belt, NW China: Science China Earth Sciences, v. 57, no. 12, p. 2945–2965, https://doi.org/10.1007/s11430-014-4958-5.

Wu, C.L., Wu, D., Mattinson, C., Lei, M., and Chen, H.J., 2019c, Petrogenesis of granitoids in the Wulan area: Magmatic activity and tectonic evolution in the North Qaidam, NW China: Gondwana Research, v. 67, p. 147–171, https://doi.org/10.1016/j.gr.2018.09.010.

Wu, F., Zhang, X.J., Zhang, Y.Q., and Zhang, Y.L., 2010, Zircon U-Pb ages for rhyolitic tuffs of the Naocangjiangou

Formation in the East Kulun orogenic belt and their implication: Journal of Geomechanics, v. 16, p. 44–49, https://doi.org/10.3969/j.issn.1006-6616.2010.01.006.

Wu, H.Q., Feng, Y.M., and Song, S.G., 1993, Metamorphism and deformation of blueschist belts and their tectonic implications, North Qilian Mountains, China: Journal of Metamorphic Geology, v. 11, p. 523–536, https://doi.org/10.1111/j.1525-1314.1993.tb00169.x.

Wu, L., Xiao, A., Wang, L., Shen, Z., Zhou, S., Chen, Y., and Guan, J., 2011, Late Jurassic–Early Cretaceous northern Qaidam Basin, NW China: Implications for the earliest Cretaceous intracontinental tectonism: Cretaceous Research, v. 32, no. 4, p. 552–564, https://doi.org/10.1016/j.cretres.2011.04.002.

Wu, Y., Liu, C., Liu, Y., Gong, H., Awan, R.S., Li, G., and Zang, Q., 2022b, Geochemical characteristics and the organic matter enrichment of the Upper Ordovician Tanjianshan Group, Qaidam Basin, China: Journal of Petroleum Science Engineering, v. 208, https://doi.org/10.1016/j.petrol.2021.109383.

Wu, Y.W., Zhang, J.X., Zhang, B., Mao, X.H., Lu, Z., Zhou, G., Teng, X., and Guo, Q., 2024, Early Paleozoic oblique convergence from subduction to collision: Insights from timing and structural style of the transpressional dextral shear zone in the Qilian orogen, northern Tibet of China: Geological Society of America Bulletin, v. 136, p. 1889–1915, https://doi.org/10.1130/B36947.1.

Xia, L., Xia, Z., Zhao, J., Xu, X., Yang, H., and Zhao, D., 1999, Determination of properties of Proterozoic continental flood basalts of western part from North Qilian Mountains: Science in China Series D: Earth Sciences, v. 42, no. 5, p. 506–514, https://doi.org/10.1007/BF02875244.

Xia, L.Q., Xia, Z.C., and Xu, X.Y., 2003, Magmagenesis in the Ordovician backarc basins of the northern Qilian Mountains, China: Geological Society of America Bulletin, v. 115, p. 1510–1522, https://doi.org/10.1130/B25269.1.

Xia, X.H., and Song, S.G., 2010, Forming age and tectonopetrogeneses of the Jiugequan ophiolite in the North Qilian Mountain, NW China: Chinese Science Bulletin, v. 55, p. 1899–1907, https://doi.org/10.1007/s11434-010-3207-3.

Xia, X.H., Song, S., and Niu, Y., 2012, Tholeiite-boninite terrane in the North Qilian suture zone: Implications for subduction initiation and back-arc basin development: Chemical Geology, v. 328, p. 259–277, https://doi.org/10.1016/j.chemgeo.2011.12.001.

Xiang, W.J., Niu, M.L., Yan, Z., Wu, Q., Fu, C.L., and Li, J.L., 2014, Sedimentary facies of the Maoniushan Formation in Maoniushan area along the northern margin of Qaidam terrane: Acta Geologica Sinica, v. 88, no. 5, p. 943–955 [in Chinese with English abstract].

Xiang, Z.Q., Lu, S.N., Li, H.K., Li, H.M., Song, B., and Zheng, J.K., 2007, SHRIMP U-Pb zircon age of gabbro in Aoyougou in the western segment of the North Qilian Mountains, China, and its geological implications: Geological Bulletin of China (Dizhi Tongbao), v. 26, p. 1686–1691.

Xiao, W., Li, S., Santosh, M., and Jahn, B.M., 2012, Orogenic belts in Central Asia: Correlations and connections: Journal of Asian Earth Sciences, v. 49, p. 1–6, https://doi.org/10.1016/j.jseaes.2012.03.001.

Xiao, W.J., Windley, B.F., Yong, Y., Yan, Z., Yuan, C., Liu, C., and Li, J., 2009, Early Paleozoic to Devonian multiple-accretionary model for the Qilian Shan, NW China: Journal of Asian Earth Sciences, v. 35, p. 323–333, https://doi.org/10.1016/j.jseaes.2008.10.001.

Xie, Q.F., Zhou, L.F., and Liu, Y., 2014, LA-ICP-MS zircon U-Pb ages of Gangchadasi granite in Qinghai Province and their geological significance: Geological Bulletin of China (Dizhi Tongbao), v. 33, no. 9, p. 1379–1390 [in Chinese with English abstract].

Xinjiang BGMR (Xinjiang Bureau of Geology and Mineral Resources), 2003, Geological Map of Qiemo, Xinjiang, China, scale 1:25,000: Hubei Autonomous Region Regional Geological Survey Institute: Beijing, Geological Publishing House, 350 p., scale 1:25,000 [in Chinese].

Xiong, Q., Zheng, J., Griffin, W.L., O'Reilly, S.Y., and Zhao, J., 2011, Zircons in the Shenglikou ultrahigh-pressure garnet peridotite massif and its country rocks from the North Qaidam terrane (western China): Meso-Neoproterozoic crust-mantle coupling and early Paleozoic convergent plate-margin processes: Precambrian Research, v. 187, no. 1–2, p. 33–57, https://doi.org/10.1016/j.precamres.2011.02.003.

Xiong, Z.L., Zhang, H.F., and Zhang, J., 2012, Petrogenesis and tectonic implications of the Maozangshi and Huangyanghe granitic intrusions in Lenglongling area, the eastern part of North Qilian Mountains, NW China: Earth Science Frontiers, v. 19, no. 3, p. 214–227 [in Chinese with English abstract].

Xu, X., He, S., Wang, H., Zhang, E., Chen, J., and Sun, J., 2008, Tectonic framework of North Qinling Mountain and North Qilian Mountain conjunction area in early Paleozoic: A study of the evidence from strata and tectonic-magmatic events: Northwest Geology, v. 41, p. 1–21 [in Chinese with English abstract].

Xu, X., Song, S., Su, L., Li, Z., Niu, Y., and Allen, M.B., 2015, The 600–580 Ma continental rift basalts in North Qilian Shan, northwest China: Links between the Qilian-Qaidam block and SE Australia, and the reconstruction of East Gondwana: Precambrian Research, v. 257, p. 47–64, https://doi.org/10.1016/j.precamres.2014.11.017.

Xu, Z., Yang, J., Wu, C., Li, H., Zhang, J., Qi, X., Song, S., and Qiu, H., 2006, Timing and mechanism of formation and exhumation of the northern Qaidam ultrahigh-pressure metamorphic belt: Journal of Asian Earth Sciences, v. 28, p. 160–173, https://doi.org/10.1016/j.jseaes.2005.09.016.

Yan, Z., Xiao, W., Wang, Z., and Li, J., 2007, Integrated analyses constraining the provenance of sandstones, mudstones, and conglomerates: A case study, the Laojunshan conglomerate, Qilian orogen, northwest China: Canadian Journal of Earth Sciences, v. 44, no. 7, p. 961–986, https://doi.org/10.1139/e07-010.

Yan, Z., Aitchison, J., Fu, C., Guo, X., Niu, M., Xia, W., and Li, J., 2015, Hualong Complex, South Qilian terrane: U-Pb and Lu-Hf constraints on Neoproterozoic micro-continental fragments accreted to the northern Proto-Tethyan margin: Precambrian Research, v. 266, p. 65–85, https://doi.org/10.1016/j.precamres.2015.05.001.

Yan, Z., Fu, C., Aitchison, J.C., Buckman, S., Niu, M., Cao, B., Sun, Y., Guo, X.Q., Wang, Z.Q., and Zhou, R., 2019, Retro-foreland basin development in response to Proto-Tethyan Ocean closure, NE Tibet Plateau: Tectonics, v. 38, no. 12, p. 4229–4248, https://doi.org/10.1029/2019TC005560.

Yang, J.S., Robinson, P.T., Jiang, C.F., and Xu, Z.Q., 1996, Ophiolites of the Kunlun Mountains, China, and their tectonic implications: Tectonophysics, v. 258, p. 215–231, https://doi.org/10.1016/0040-1951(95)00199-9.

Yang, J.S., Xu, Z.Q., Song, S.G., Zhang, J.X., Wu, C.L., Shi, R.D., Li, H.B., and Brunel, M., 2001, Discovery of coesite in the North Qaidam early Palaeozoic ultrahigh pressure (UHP) metamorphic belt: NW China: Comptes Rendus de l'Académie des Sciences, Series IIA, Earth and Planetary Sciences, v. 333, no. 11, p. 719–724, https://doi.org/10.1016/S1251-8050(01)01718-9.

Yang, J.Z., Liu, X.C., Wu, Y.B., and Sun, Y.L., 2015, Zircon record of ocean-continent subduction transition process of Dulan UHPM belt, North Qaidam: Journal of Earth Science, v. 26, p. 617–625, https://doi.org/10.1007/s12583-015-0585-0.

Yang, Z.Y., 1983, Triassic of the South Qilian Mountains: Beijing, Geological Publishing, 229 p.

Yao, J.L., Cawood, P.A., Zhao, G.C., Han, Y.G., Xia, X.P., Liu, Q., and Wang, P., 2021, Mariana-type ophiolites constrain the establishment of modern plate tectonic regime during Gondwana assembly: Nature Communications, v. 12, p. 4189, https://doi.org/10.1038/s41467-021-24422-z.

Yin, A., 2010, Cenozoic tectonic evolution of Asia: A preliminary synthesis: Tectonophysics, v. 488, no. 1–4, p. 293–325, https://doi.org/10.1016/j.tecto.2009.06.002.

Yin, A., and Harrison, T.M., 2000, Geologic evolution of the Himalayan-Tibetan orogen: Annual Review of Earth and Planetary Sciences, v. 28, p. 211–280, https://doi.org/10.1146/annurev.earth.28.1.211.

Yin, A., and Nie, S., 1996, A Phanerozoic palinspastic reconstruction of China and its neighboring regions, *in* Yin, A., and Harrison, T.M., eds., The Tectonic Evolution of Asia: New York, Cambridge University Press, p. 442–485.

Yin, A., Rumelhart, P.E., Butler, R., Cowgill, E., Harrison, T.M., Foster, D.A., Ingersoll, R.V., Zhang, Q., Zhou, X.Q., Wang, X.F., Hanson, A., and Raza, A., 2002, Tectonic history of the Altyn Tagh fault system in northern Tibet inferred from Cenozoic sedimentation: Geological Society of America Bulletin, v. 114, p. 1257–1295, https://doi.org/10.1130/0016-7606(2002)114<1257:THOTAT>2.0.CO;2.

Yin, A., Dang, Y., Zhang, M., McRivette, M.W., Burgess, W.P., and Chen, X.H., 2007a, Cenozoic tectonic evolution of Qaidam Basin and its surrounding regions (Part 2): Wedge tectonics in southern Qaidam Basin and the Eastern Kunlun Range, *in* Sears, J.W., et al., eds., Whence the Mountains?: Inquiries into the Evolution of Orogenic Systems: A Volume in Honor of Raymond A. Price: Geological Society of America Special Paper 433, p. 369–390, https://doi.org/10.1130/2007.2433(18).

Yin, A., Manning, C.E., Lovera, O., Menold, C.A., Chen, X., and Gehrels, G.E., 2007b, Early Paleozoic tectonic and thermomechanical evolution of ultrahigh-pressure (UHP) metamorphic rocks in the northern Tibetan Plateau, northwest China: International Geology Review, v. 49, no. 8, p. 681–716, https://doi.org/10.2747/0020-6814.49.8.681.

Yin, A., et al., 2008a, Cenozoic tectonic evolution of Qaidam Basin and its surrounding regions (Part 1): The southern Qilian Shan–Nan Shan thrust belt and northern Qaidam Basin: Geological Society of America Bulletin, v. 120, p. 813–846, https://doi.org/10.1130/B26180.1.

Yin, A., Dang, Y., Zhang, M., Chen, X.H., and McRivette, M.W., 2008b, Cenozoic tectonic evolution of Qaidam Basin and its surrounding regions (Part 3): Structural geology, sedimentation, and regional tectonic reconstruction: Geological Society of America Bulletin, v. 120, p. 847–876, https://doi.org/10.1130/B26232.1.

Yu, L., Xiao, A., Wu, L., Tian, Y., Rittner, M., Lou, Q., and Pan, X., 2017, Provenance evolution of the Jurassic northern Qaidam Basin (West China) and its geological implications: Evidence from detrital zircon geochronology: International Journal of Earth Sciences, v. 106, p. 2713–2726, https://doi.org/10.1007/s00531-017-1455-z.

Yu, L., Sun, F., Li, L., Li, B., Peng, B., Xu, C., Li, R., Wang, F., and Shen, D., 2019a, Geochronology, geochemistry, and Sr-Nd-Hf isotopic compositions of mafic-ultramafic intrusions in the Niubiziliang Ni-(Cu) sulfide deposit, North Qaidam orogenic belt, NW China: Implications for magmatic source, geodynamic setting, and petrogenesis: Lithos, v. 326–327, p. 158–173, https://doi.org/10.1016/j.lithos.2018.12.027.

Yu, S., Li, S., Zhang, J., Peng, Y., Somerville, I., Liu, Y., Wang, Z.Y., Li, Z.F., Yao, Y., and Li, Y., 2019b, Multistage anatexis during tectonic evolution from oceanic subduction to continental collision: A review of the North Qaidam UHP belt, NW China: Earth-Science Reviews, v. 191, p. 190–211, https://doi.org/10.1016/j.earscirev.2019.02.016.

Yu, S., Peng, Y., Zhang, J., Li, S., Santosh, M., Li, Y., Liu, Y.J., Gao, X.Y., Ji, W.T., Lv, P., Li, C.Z., Jiang, X.Z., Qi, L.L., Xie, W.M., and Xu, L.J., 2021, Tectono-thermal evolution of the Qilian orogenic system: Tracing the subduction, accretion and closure of the Proto-Tethys Ocean: Earth-Science Reviews, v. 215, https://doi.org/10.1016/j.earscirev.2021.103547.

Yu, S.Y., Zhang, J., and Del Real, P.G., 2012, Geochemistry and zircon U-Pb ages of adakitic rocks from the Dulan area of the North Qaidam UHP terrane, north Tibet: Constraints on the timing and nature of regional tectonothermal events associated with collisional orogeny: Gondwana Research, v. 21, no. 1, p. 167–179, https://doi.org/10.1016/j.gr.2011.07.024.

Yu, S.Y., Zhang, J.X., Sun, D.Y., Del Real, P.G., Li, Y.S., Zhao, X.L., and Hou, K.J., 2015, Petrology, geochemistry, zircon U-Pb dating and Lu-Hf isotope of granitic leucosomes within felsic gneiss from the North Qaidam UHP terrane: Constraints on the timing and nature of partial melting: Lithos, v. 218, p. 1–21, https://doi.org/10.1016/j.lithos.2015.01.008.

Yu, X., Guo, Z., Guan, S., Du, W., Wang, Z., Bian, Q., and Li, L., 2019c, Landscape and tectonic evolution of Bayin River watershed, northeastern Qaidam Basin, northern Tibetan Plateau: Implications for the role of river morphology in source analysis and low-temperature thermochronology: Journal of Geophysical Research: Earth Surface, v. 124, p. 1701–1719, https://doi.org/10.1029/2018JF004989.

Yu, X., Guo, Z., Guan, S., Du, W., Wang, Z., Wu, J., Yang, Y., Yi, K., and Peng, L., 2023, Buried Jurassic rift system in the middle segment of the northern Qaidam Basin: Implications for Mesozoic landforms of the northern Tibetan Plateau: International Geology Review, v. 65, no. 16, p. 2539–2557, https://doi.org/10.1080/00206814.2022.2148134.

Zha, X., Gu, P., Dong, Z., Chen, R., and Lu, Z., 2016, Geological record of tectono-thermal event at early Paleozoic and its tectonic setting in west segment of the North Qaidam: Earth Science, v. 41, p. 586–604 [in Chinese with English abstract].

Zhang, C., Wu, L., Chen, W., Zhang, Y., Xiao, A., Zhang, J., Chen, S., and Chen, H., 2020, Early Cretaceous foreland-like northeastern Qaidam Basin, Tibetan Plateau, and its tectonic implications: Insights from sedimentary investigations, detrital zircon U-Pb analyses and seismic profiling: Palaeogeography, Palaeoclimatology, Palaeoecology, v. 557, https://doi.org/10.1016/j.palaeo.2020.109912.

Zhang, C.Y., Zhao, Y., Liu, J., Dai, K., and Zheng, C., 2019a, Provenance analysis of the Maoniushan Formation in the North Qaidam Basin and its tectonic significance: Acta Geologica Sinica, v. 93, no. 3, p. 712–723 [in Chinese with English abstract].

Zhang, J., Zhang, Z., Xu, Z., Yang, J., and Cui, J., 2001, Petrology and geochronology of eclogites from the western segment of the Altyn Tagh, northwestern China: Lithos, v. 56, no. 2–3, p. 187–206, https://doi.org/10.1016/S0024-4937(00)00052-9.

Zhang, J.X., Yang, J.S., Mattinson, C.G., Xu, Z.Q., Meng, F.C., and Shi, R.D., 2005, Two contrasting eclogite cooling histories, North Qaidam HP/UHP terrane, western China: Petrological and isotopic constraints: Lithos, v. 84, p. 51–76, https://doi.org/10.1016/j.lithos.2005.02.002.

Zhang, J.X., Meng, F.C., and Wan, Y.S., 2007, A cold early Palaeozoic subduction zone in the North Qilian Mountains, NW China: Petrological and U-Pb geochronological constraints: Journal of Metamorphic Geology, v. 25, p. 285–304, https://doi.org/10.1111/j.1525-1314.2006.00689.x.

Zhang, J.X., Mattinson, C.G., Meng, F.C., Wan, Y.S., and Tung, K., 2008, Polyphase tectonothermal history recorded in granulitized gneisses from the North Qaidam HP/UHP metamorphic terrane, western China: Evidence from zircon U-Pb geochronology: Geological Society of America Bulletin, v. 120, p. 732–749, https://doi.org/10.1130/B26093.1.

Zhang, J.X., Mattinson, C.G., Meng, F.C., Yang, H.J., and Wan, Y.S., 2009a, U-Pb geochronology of paragneisses and metabasite in the Xitieshan area, north Qaidam Mountains, western China: Constraints on the exhumation of HP/UHP metamorphic rocks: Journal of Asian Earth Sciences, v. 35, p. 245–258, https://doi.org/10.1016/j.jseaes.2008.08.008.

Zhang, J.X., Li, H.K., Meng, F.C., Xiang, Z.Q., Yu, S.Y., and Li, J.P., 2011a, Polyphase tectonothermal events recorded in "metamorphic basement" from the Altyn Tagh, the southeastern margin of the Tarim Basin, western China: Constraint from U-Pb zircon geochronology: Acta Petrologica Sinica (Yanshi Xuebao), v. 27, no. 1, p. 23–46.

Zhang, J.X., Mattinson, C., Yu, S., Li, Y., Yu, X., Mao, X., and Peng, Y., 2019b, Two contrasting accretion v. collision orogenies: Insights from early Paleozoic polyphase metamorphism in the Altun–Qilian–North Qaidam orogenic system, NW China, *in* Zhang, L., et al., eds., HP-UHP Metamorphism and Tectonic Evolution of Orogenic Belts: Geological Society, London, Special Publication 474, p. 153–181, https://doi.org/10.1144/SP474.8.

Zhang, L., Chen, R.X., Zheng, Y.F., and Hu, Z., 2015, Partial melting of deeply subducted continental crust during exhumation: Insights from felsic veins and host UHP metamorphic rocks in North Qaidam, northern Tibet: Journal of Metamorphic Geology, v. 33, p. 671–694, https://doi.org/10.1111/jmg.12146.

Zhang, L., Chen, R.X., Zheng, Y.F., Li, W.C., Hu, Z., Yang, Y., and Tang, H., 2016, The tectonic transition from oceanic subduction to continental subduction: Zirconological constraints from two types of eclogites in the North Qaidam orogen, northern Tibet: Lithos, v. 244, p. 122–139, https://doi.org/10.1016/j.lithos.2015.12.003.

Zhang, W., and Hu, Z.C., 2020, Estimation of isotopic reference values for pure materials and geological reference materials: Spectroscopy, v. 41, no. 3, p. 93–102, https://doi.org/10.46770/AS.2020.03.001.

Zhang, Y.L., Hu, D.G., Shi, Y.R., and Lu, L., 2010, SHRIMP zircon U-Pb ages and tectonic significance of Maoniushan Formation volcanic rocks in East Kunlun orogenic belt, China: Dizhi Tongbao, v. 29, no. 11, p. 1614–1618 [in Chinese with English abstract].

Zhang, Y.L., et al., 2018, Zircon U-Pb ages and geological significance of volcanic rocks from Maoniushan Formation in the northern margin of Qaidam Basin: Geoscience (Xiandai Dizhi), v. 32, no. 2, p. 329–334 [in Chinese with English abstract].

Zhang, Z., Klemperer, S., Bai, Z., Chen, Y., and Teng, J., 2011b, Crustal structure of the Paleozoic Kunlun orogeny from an active-source seismic profile between Moba and Guide in East Tibet, China: Gondwana Research, v. 19, no. 4, p. 994–1007, https://doi.org/10.1016/j.gr.2010.09.008.

Zhang, Z.C., Guo, Z.J., and Song, B., 2009b, SHRIMP zircon dating of gabbro from the ophiolite mélange in the northern Altyn Tagh and its geological implications: Acta Petrologica Sinica (Yanshi Xuebao), v. 25, p. 568–576 [in Chinese with English abstract].

Zhao, J., Zeng, X., Tian, J., Hu, C., Wang, D., Yan, Z., Wang, K., and Zhao, X., 2020a, Provenance and paleogeography of the Jurassic northwestern Qaidam Basin (NW China): Evidence from sedimentary records and detrital zircon geochronology: Journal of Asian Earth Sciences, v. 190, https://doi.org/10.1016/j.jseaes.2019.104060.

Zhao, X., Zhao, J., Zeng, X., Tian, J., Guo, Z., Wang, C., Wang, D., and Hu, C., 2020b, Early–Middle Jurassic paleogeography reconstruction in the western Qaidam Basin: Insights from sedimentology and detrital zircon geochronology: Marine and Petroleum Geology, v. 118, https://doi.org/10.1016/j.marpetgeo.2020.104445.

Zhao, Z., Huang, X., Zhang, X., Yang, B., Chen, Z.Q., and Xiong, F., 2016, Permian radiolarians from the A'nyemaqen mélange zone in the Huashixia area of Madoi County, Qinghai Province, Western China, and their implications on regional tectonism: Journal of Earth Science, v. 27, no. 4, p. 623–630, https://doi.org/10.1007/s12583-016-0711-7.

Zhao, Z.X., Wei, J.H., Fu, L.B., Liang, S.N., and Zhao, S.Q., 2017, The Early Paleozoic Xitieshan syn-collisional granite in the North Qaidam ultrahigh-pressure metamorphic belt, NW China: Petrogenesis and implications for continental crust growth: Lithos, v. 278–281, p. 140–152, https://doi.org/10.1016/j.lithos.2017.01.019.

Zhiyi, Z., and Dean, W.T., 1996, Phanerozoic Geology of Northwest China: Beijing, Science Press, 316 p.

Zhou, B., et al., 2014, Zircon dating of early Paleozoic adakitic granite on the northern margin of Qaidam Basin and its geological significance: Geoscience (Xiandai Dizhi), v. 28, no. 5, p. 875–883 [in Chinese with English abstract].

Zhou, C.A., Song, S., Allen, M.B., Wang, C., Su, L., and Wang, M., 2021, Post-collisional mafic magmatism: Insights into orogenic collapse and mantle modification from North Qaidam collisional belt, NW China: Lithos, v. 398–399, https://doi.org/10.1016/j.lithos.2021.106311.

Zhou, D., and Graham, S.A., 1996, Extrusion of the Altyn Tagh wedge: A kinematic model for the Altyn Tagh fault and palinspastic reconstruction of northern China: Geology, v. 24, p. 427–430, https://doi.org/10.1130/0091-7613(1996)024<0427:EOTATW>2.3.CO;2.

Zhou, J.H., Feng, C.Y., Li, D.X., and Li, G.C., 2016, Geological, geochemical, and geochronological characteristics of Caledonian W-Sn mineralization in the Baiganhu orefield, southeastern Xinjiang, China: Ore Geology Reviews, v. 75, p. 125–149, https://doi.org/10.1016/j.oregeorev.2015.12.009.

Zhou, W., Xia, M.Z., Wu, X.H., Du, W., Wang, B.Y., Xia, Z.D., Song, Y.F., and Song, Z.B., 2015, U-Pb dating of zircons from Gaxiuyapingdong and Hongliugoubei mafic-ultramafic intrusions on the northern margin of Qaidam Basin and its geological and prospecting significance: Geological Bulletin of China (Dizhi Tongbao), v. 34, no. 10, p. 1860–1868 [in Chinese with English abstract].

Zhu, X., Chen, D., Liu, L., Zhao, J., and Zhang, L., 2014, Geochronology, geochemistry and significance of the early Paleozoic back-arc type ophiolite in Lvliangshan area, North Qaidam: Acta Petrologica Sinica (Yanshi Xuebao), v. 30, p. 822–834 [in Chinese with English abstract].

Zhuang, G., Hourigan, J.K., Ritts, B.D., and Kent-Corson, M.L., 2011, Cenozoic multiple-phase tectonic evolution of the northern Tibetan Plateau: Constraints from sedimentary records from Qaidam Basin, Hexi Corridor, and Subei Basin, northwest China: American Journal of Science, v. 311, no. 2, p. 116–152, https://doi.org/10.2475/02.2011.02.

Zonenshain, L.P., Kuzmin, M.I., Natapov, L.M., and Page, B.M., eds., 1990, Geology of the USSR: A Plate-Tectonic Synthesis: American Geophysical Union Geodynamics Monograph 21, 242 p., https://doi.org/10.1029/GD021.

Zuza, A.V., and Yin, A., 2017, Balkatach hypothesis: A new model for the evolution of the Pacific, Tethyan, and Paleo-Asian oceanic domains: Geosphere, v. 13, p. 1664–1712, https://doi.org/10.1130/GES01463.1.

Zuza, A.V., Cheng, X., and Yin, A., 2016, Testing models of Tibetan Plateau formation with Cenozoic shortening estimates across the Qilian Shan–Nan Shan thrust belt: Geosphere, v. 12, p. 501–532, https://doi.org/10.1130/GES01254.1.

Zuza, A.V., Wu, C., Reith, R.C., Yin, A., Li, J.H., Zhang, J.Y., Zhang, Y.X., Wu, L., and Liu, W.C., 2018, Tectonic evolution of the Qilian Shan: An early Paleozoic orogen reactivated in the Cenozoic: Geological Society of America Bulletin, v. 130, p. 881–925, https://doi.org/10.1130/B31721.1.

Science Editor: Mihai Ducea
Associate Editor: Timothy Kusky

Manuscript Received 19 July 2024
Revised Manuscript Received 10 September 2024
Manuscript Accepted 2 October 2024